Reply to technical corrections by Dr. Heini Wernli

We thank the editor Heini Wernli for the thoughtful handling of our manuscript and for his final thoughts which further helped to improve the manuscript. The editor comments are given in bold, the answers in plain text, changes to the manuscript are in italics.

1) I am not so sure what an "updraft" is and it is not fully clear to me what you regard as an "updraft" in your study. I typically use this term only for deep convection, for the region with very strong, almost vertical ascent. It seems to me that in your study, "everything that ascends" (also in a dry simulation) is an "updraft". I don't say that this is wrong, but maybe you could better introduce and define how you use the term. It is notable that the term occurs for the first time in line 339 (discussion of Gutwoski et al. paper), then on line 417 (where you seem to define the term as air parcels lifted by 2.5 km in many days - which is clearly not convective) and then it kind of becomes the most frequent word on the final pages of the manuscript. Since you use the term so often in your conclusions, it deserves, I think, a better introduction / definition.
Thanks for pointing this out. We added some more sentences in Section 2.1 in the paragraph when we introduce the passive tracers. We also replaced the term “updrafts” with either “vertically ascending” or “lifted air masses” at some places.
“We want to note here that we will use positive values of Δz as a predictor of vertically ascending air masses. In this study we will also use the term updraft to describe these air masses, independently of the cause of the ascent, e.g., frontal or convective, and of any time period in which this ascent has occurred. The only criteria are that Δz is larger than 2.5 km and that these air masses reach the altitude of the tropopause.”

2) The term "warm conveyor belt" appears on line 412 for the first time without explanation and reference. How should the reader know in Fig. 9 where the WCB is? Maybe some more words here would be justified. As a side remark: the study by Peevey et al. is very fuzzy about the WCB-TIL link.
We added more information on the WCB:
“This airstream originates in the lower troposphere in the region ahead of the trough axis (e.g., Carlson, 1998). In the WCB moist air masses rapidly
ascend within 1-2 days into the upper troposphere, associated with cloud
formation, precipitation, and release of latent heat (e.g., Wernli and Davies (1997) and Madonna et al. (2014)).”

3) Line 421: is this passive tracer also affected by the parameterisation of convection, i.e., does it record the occurrence of convection in the model?
The passive tracers are only subject to advection (see lines 157/158), thus the tracer does not record the occurrence of convection. For BRTC (only convection added) the effect is almost negligible, since the convective activity is still rather low. For BRTCS with stronger convective activity we might miss some of the convective events in the tracer. However, the correlation between Δz and N^2max is still very good, especially during the first hours of the life cycle when the TIL forms. Thus, we think that it is

acceptable that the tracer is in this our case not affected by additional convective transport.

4) Line 143: unit should be K km-1 (check in other places)
Checked and corrected.

5) Line 765: spelling of "Lagrangian"
Corrected. Although we initially followed the notation from QJRMS. See also http://onlinelibrary.wiley.com/doi/10.1002/qj.49712353811/abstract .

Manuscript prepared for Atmos. Chem. Phys.
with version 2015/04/24 7.83 Copernicus papers of the LaTeX class copernicus.cls.
Date: 10 December 2015

The tropopause inversion layer in baroclinic life cycle experiments: the role of diabatic processes

Daniel Kunkel[1], Peter Hoor[1], and Volkmar Wirth[1]

[1]Institute for Atmospheric Physics, Johannes-Gutenberg University Mainz, Germany

Correspondence to: Daniel Kunkel (dkunkel@uni-mainz.de)

Abstract. Recent studies on the formation of a quasi-permanent layer of enhanced static stability above the thermal tropopause revealed the contributions of dynamical and radiative processes. Dry dynamics lead to the evolution of a tropopause inversion layer (TIL) which is, however, too weak compared to observations and thus diabatic contributions are required. In this study we aim to assess the importance of diabatic processes in the understanding of TIL formation at midlatitudes. The non-hydrostatic model COSMO is applied in an idealized mid-latitude channel configuration to simulate baroclinic life cycles. The effect of individual diabatic processes related to humidity, radiation, and turbulence is studied first to estimate the contribution of each of these processes to the TIL formation in addition to dry dynamics. In a second step these processes are stepwise included in the model to increase the complexity and finally estimate the relative importance of each process. The results suggest that including turbulence leads to a weaker TIL than in a dry reference simulation. In contrast, the TIL evolves stronger when radiation is included but the temporal evolution is still comparable to the reference. Using various cloud schemes in the model shows that latent heat release and consecutive increased vertical motions foster an earlier and stronger appearance of the TIL than in all other life cycles. Furthermore, updrafts moisten the upper troposphere and as such increase the radiative effect from water vapor. Particularly, this process becomes more relevant for maintaining the TIL during later stages of the life cycles. Increased convergence of the vertical wind induced by updrafts and by propagating inertia-gravity waves, which potentially dissipate, further contributes to the enhanced stability of the lower stratosphere. Furthermore, radiative feedback of ice clouds reaching up to the tropopause is identified to potentially further affect the strength of the TIL in the region of the clouds.

1 Introduction

The sharpness of the tropopause in the extratropics has gained increased attention in recent years (e.g., Gettelman and Wang, 2015). Local maxima of static stability, usually measured by the squared Brunt–Vaisala frequency $N^2 = g/\Theta \cdot \partial\Theta/\partial z$ with g, the gravitational acceleration, Θ, the potential temperature, and z, the geometric altitude, inferred from radiosonde measurements (e.g., Birner

et al., 2002; Birner, 2006) and Global Positioning System (GPS) radio occultation measurements (Randel et al., 2007), revealed the existence of a quasi-permanent inversion layer above the thermal tropopause. This tropopause inversion layer (TIL) is a distinct feature of the region of the upper troposphere and lower stratosphere (UTLS), from tropical to polar regions (e.g., Grise et al., 2010) and is also evident in general circulation models and climate analysis data sets (e.g., Birner et al., 2006).

Global studies of GPS temperature profiles and reanalysis data sets showed that the TIL is present at all latitudes (Grise et al., 2010; Gettelman and Wang, 2015). In the tropical lower stratosphere two maxima of enhanced static stability are found at about 17 and 19 km altitude. The upper peak shows a seasonal cycle with a winter maximum, while the lower peak has relatively large values all year round (Grise et al., 2010). In polar regions a distinct summer maximum occurs (Randel and Wu, 2010), while the TIL is evident in midlatitudes throughout the entire year with a slightly deeper appearance during winter (Bell and Geller, 2008). Generally, the smallest values of static stability above the thermal tropopause are evident in the region of the subtropical jet (Grise et al., 2010).

In several studies it was shown that a TIL can form from balanced, adiabatic and frictionless dynamics without explicit contributions from radiation in the extratropics. These idealized model simulations span the range from local to global scales, with studies of the dynamics of upper-level anomalies of potential vorticity (further abbreviated with PV) (Wirth, 2003, 2004), of baroclinic life cycles (Erler and Wirth, 2011), and of the dynamical response to a forcing of a Held–Suarez test (Held and Suarez, 1994) in a dry general circulation model (Son and Polvani, 2007). In the latter case, the TIL forms spontaneously under a wide variety of model parameters, such as horizontal and vertical model resolution. From the analysis of positive and negative PV-anomalies it was found that the sharpening of the tropopause was linked to the convergence of the vertical wind. Particularly, this was related to a cross-frontal circulation (Wirth, 2004). Furthermore, the TIL evolved stronger above anti-cyclonic than over cyclonic flow (Wirth, 2003). This result was confirmed in studies of adiabatic baroclinic life cycles, in which the TIL became evident after breaking of baroclinic waves (Erler and Wirth, 2011). Recently, the impact of dissipating inertia-gravity waves was suggested to persistently contribute to the formation and maintenance of the TIL. These waves result from imbalances along the jet and the dissipation may alter the thermal structure through energy dissipation, local heating, and turbulent motions (Kunkel et al., 2014). Moreover, Birner (2010) showed that the vertical structure of the residual circulation in the stratosphere contributes to the sharpening of the tropopause by inducing a dipole forcing of static stability around the tropopause. This process was identified to significantly add to the tropopause sharpening during winter in the midlatitudes.

Balanced dynamics alone, however, can not explain all features related to the TIL (Son and Polvani, 2007) and as has been shown by Randel et al. (2007) radiative processes contribute significantly to the TIL. From fixed dynamical radiative transfer calculations it was concluded that water vapor cooling around the tropopause and heating by ozone in the lower and middle strato-

sphere contribute to a layer of enhanced static stability above the thermal tropopause. Particularly, the water vapor cooling has been identified to be a major process for the summer TIL in polar regions (Randel and Wu, 2010).

Thus, several mechanisms have been identified so far to explain the strength and occurrence of the TIL at all latitudes. Since dry dynamics are not sufficient to fully explain all features of the TIL, processes beyond adiabatic and frictionless dynamics are required to close this gap. Especially in the midlatitude tropopause region, all processes, synoptic-scale and stratospheric dynamics as well as the radiative forcings, need to be considered. With this knowledge we can ask the question which of the before mentioned processes is most important to form and maintain the TIL. In this study we aim to address this question in the framework of idealized baroclinic life cycles with a limited area, non-hydrostatic model. We extend the work of Erler and Wirth (2011) and include diabatic processes, i.e., related to humidity, radiation, or turbulence. These processes can violate material conservation of potential vorticity Q and are further referred to as non-conservative processes in this study. Since we focus on a rather short time scale, we assume that the effect of the stratospheric circulation is rather small and exclude this effect in the interpretation of our results. Thus, we focus mainly on the following questions: (1) How do non-conservative processes, i.e., diabatic processes, alter the TIL evolution in baroclinic life cycles compared to the well-known evolution in the adiabatic and frictionless case? (2) What is the relative importance of individual processes that contribute to the formation the TIL during different stages of the life cycles?

To answer these questions we structured our analysis as follows. In Sect. 2 we introduce the model setup along with the physical parameterizations and a summary of the conducted simulations. We then present results from two sets of simulations of so-called anti-cyclonic life cycles. In Sect. 3 we show results from baroclinic life cycles in which only one individual non-conservative process is turned on separately to address question (1). In a second set of simulations we show results of simulations with a successively increasing number of physical processes to address question (2) (Sect. 4). Before we summarize our results and give further conclusions in Sect. 6, we discuss the evolution of the tropopause inversion layer in experiments of the cyclonic life cycle in Sect. 5.

2 Model formulation and baroclinic life cycle experiments

2.1 Adiabatic model configuration and initial state

We conducted baroclinic life cycle experiments in an idealized, spherical, midlatitude channel configuration of the non-hydrostatic regional model COSMO (COnsortium for Small-scale MOdelling, Steppeler et al., 2003). For the adiabatic model we only use the dynamical core of the model which solves the hydro-thermodynamical equations. Only a fourth order horizontal hyper-diffusion has to be applied to guarantee numerical stability. Physical processes such as microphysics, convection, turbulence, radiation are introduced in more detail further below (see Sect. 2.2). Time integration is

performed with a third order, two-time-level Runge–Kutta scheme, in which fast terms, i.e., sound and gravity waves, are stepped forward in time with a smaller time step. We use a fifth order centered finite difference approximation in the horizontal and a third order scheme in the vertical. Passive tracer advection is done with a fourth order Bott Scheme with Strang splitting (Doms, 2011).

We study baroclinic waves with wavenumber six with a model setup similar to Erler and Wirth (2011) and Kunkel et al. (2014). Our model domain spans over 60° longitude and 70° latitude, from the surface up to a height of $25.0\,\mathrm{km}$ and with a grid spacing of 0.4° ($\sim 44\,\mathrm{km}$) in the horizontal and $110\,\mathrm{m}$ in the vertical in the region of the tropopause. Consequently, we obtain an aspect ratio ($\Delta z/\Delta x$) of about $1/400$ which is considered favorable to study the TIL (Birner et al., 2006; Erler and Wirth, 2011). In the uppermost seven kilometer of the model domain Rayleigh damping is applied to avoid reflection of upward propagating signals and there is no orography at the bottom. In meridional direction the boundary conditions are relaxed towards the initial values to avoid reflection of outgoing signals, while periodic boundary conditions are specified in the zonal direction.

For the initial conditions we follow Olson and Colle (2007) and Schemm et al. (2013) with slight adaptations to account for the spherical geometry of our approach. A background state is obtained for three dimensional fields of temperature, T, and pressure, p, from which a thermally balanced wind is calculated as in Erler and Wirth (2011). The initial vertical wind, w, is zero and the background state is baroclinically unstable by construction. However, to allow a fast evolution of the baroclinic wave, this state is superimposed by perturbation fields for p, T, u, and v which result from an inversion of a specified PV anomaly. This circular anomaly is introduced in the middle of the domain at the altitude of the tropopause. Slight changes in the initial state allow us to study various types of baroclinic life cycles (for details we refer to Olson and Colle, 2007). To obtain a solution of our experiments that is known as LC2 (Thorncroft et al., 1993), an additional cyclonic barotropic shear is added to the background state described above. However, the main focus of this study is on the classical LC1 wave type (Thorncroft et al., 1993), since it produces a stronger TIL in the adiabatic case (Erler and Wirth, 2011). In Section 5 we will present differences in the evolution of the TIL in LC2 experiments. The LC1 type is characterized by a thinning trough which then forms a streamer and later a cut-off cyclone, while the baroclinic wave breaks anti-cyclonically. Thus, the LC1 is also known as the anti-cyclonic case. In contrast, in the LC2 a large cyclonic trough dominates the evolution of the wave with no streamer and no cut-off cyclone being evident. This case is known as the cyclonic case, since the wave breaks cyclonically. More details on the development of these waves and the corresponding evolution of the tropopause inversion layer are generally given in Erler and Wirth (2011) and for the LC1 setup specifically in Kunkel et al. (2014), where the authors used a higher resolution version of this model. It is noted here that the lower resolution model well reproduces the results of Kunkel et al. (2014). For this reason and because of the vast number of conducted model simulations (see Table 1), we decided to use a coarser grid spacing in our simulations.

Figure 1 shows the initial state in the center of our model domain. The zonal wind u has its maximum velocity between the thermal and dynamical tropopause (here defined as the $Q = 2.0\,\mathrm{pvu}$ contour line, with pvu = potential vorticity units, and $1.0\,\mathrm{pvu} = 1.0 \times 10^{-6}\,\mathrm{K\,m^2\,kg^{-1}\,s^{-1}}$). For the thermal tropopause we follow the definition given in *WMO* (1957), where the tropopause is defined as the lowest level where the temperature lapse rate falls below ~~2.0 K/km~~ $2.0\,\mathrm{K\,km^{-1}}$ and its average between this level and all higher levels within two km above this level remains below this value. The thermal tropopause further separates tropospheric ($N^2 < 1.5 \times 10^{-4}\,\mathrm{s^{-2}}$) from the stratospheric ($N^2 > 4.0 \times 10^{-4}\,\mathrm{s^{-2}}$) background values of static stability. The initial zonally symmetric specific humidity field, depicted with the blue lines, has been constructed such that it is comparable in magnitude and distribution to moisture profiles from re-analysis data. For this it is constructed as follows: a constant surface relative humidity ($\mathrm{RH_s}$) is given which decreases linearly with height everywhere. If not specified otherwise, $\mathrm{RH_s}$ is $60\,\%$ and decreases with a gradient of $10\,\%/2\,\mathrm{km}$. Thus, above $12\,\mathrm{km}$ altitude the relative humidity (RH) is zero. The model, however, requires specific humidity q_v as input variable. This quantity is obtained by multiplication of the relative humidity with the saturation specific humidity ($q_\mathrm{vs} : q_\mathrm{v} = \mathrm{RH}/100 \cdot q_\mathrm{vs}$). The latter quantity is computed from the saturation water vapor, which is computed with the parameterization of Magnus (Murray, 1967). A final constraint is given for the initial distribution of q_v, i.e., that $\min(q_\mathrm{v}) = 2.0 \times 10^{-6}\,\mathrm{kg\,kg^{-1}}$. Note that this leads to a constant initial value of $q_\mathrm{v} = 2.0 \times 10^{-6}\,\mathrm{kg\,kg^{-1}}$ in the stratosphere in our simulations.

We further use passive tracers to diagnose particular features of our baroclinic life cycles. These tracers are purely advected and not explicitly mixed vertically or horizontally by a parameterization scheme. However, mixing due to numerical reasons does still affect the tracer distribution. In particular, we use three tracers which carry information of the initial state of the baroclinic life cycles: (1) the initial height of each grid box z_0, (2) the initial static stability N_0^2, and (3) the initial potential vorticity Q_0. With these tracers it is possible to calculate the differences between the current and the initial distribution of these quantities and as such obtain information about whether an air parcel has gained or lost (1) altitude, measured by $\Delta z = z - z_0$, (2) static stability, measured by $\Delta N^2 = N^2 - N_0^2$, and (3) changed their potential vorticity because of non-conservative processes, measured by $\Delta Q = Q - Q_0$, with $Q = \varrho^{-1}\boldsymbol{\eta} \cdot \nabla\Theta$ and ϱ air density, $\boldsymbol{\eta}$ absolute vorticity, and Θ potential temperature. We want to note here that we will use positive values of Δz as a predictor of vertically ascending air masses. In this study we will also use the term updraft to describe these air masses, independently of the cause of the ascent, e.g., frontal or convective, and of any time period in which the ascent has occurred. The only criteria are that Δz is larger than $2.5\,\mathrm{km}$ and that these air masses reach the altitude of the tropopause.

2.2 Formulation of non-conservative processes in COSMO

2.2.1 Turbulence

Turbulence is calculated for the three dimensional wind (u, v, and w), the liquid water potential temperature (Θ_l), and the total water (q_w) which is the sum of specific water vapor q_v and specific cloud water q_c. Budget equations for the second order moments are reduced under application of a closure of level 2.5 (in the notation of Mellor and Yamada, 1982), i.e., local equilibrium is assumed for all moments except for turbulent kinetic energy (TKE), for which advection and turbulent transport is retained. Three dimensional turbulent effects are neglected which is a valid approximation for simulations on the mesoscale, which means that horizontal homogeneity is assumed. Hence, only vertical turbulent fluxes are parameterized under consideration of the Boussinesq approximation. Moreover, the TKE budget equation depends significantly on the vertical shear of the horizontal wind components and the vertical change in Θ_l and q_w. More details are given in Doms (2011).

2.2.2 Cloud microphysics

Cloud microphysics follow a bulk approach using a single moment scheme with five types of water categories being treated prognostically: specific humidity q_v for the gas phase, two non-precipitating cloud types, i.e., cloud water q_c and cloud ice q_i, as well as two precipitating types, i.e., rain q_r and snow q_s. These five water types can interact within various processes such as cloud condensation and evaporation, depositional growth and sublimation of snow, evaporation of snow and rain, melting of snow and cloud ice, homogeneous and heterogeneous nucleation of cloud ice, autoconversion, collection and freezing. More details are given in Doms (2011) and Joos and Wernli (2012).

2.2.3 Radiation

Radiation is parameterized by the δ-2 stream approximation, i.e., separate treatment of solar and terrestrial wavelengths. In total, eight spectral bands are considered, five in the solar range and three infrared bands. Absorbing and scattering gases are water vapor ($\mathrm{H_2O}$) with a variable content as well as $\mathrm{CO_2}$, $\mathrm{O_3}$, $\mathrm{CH_4}$, $\mathrm{N_2O}$, and $\mathrm{O_2}$ with fixed amounts. Aerosols have been totally neglected whereas a cloud radiative feedback can be calculated in all spectral bands. Further details about the general scheme are given in Ritter and Geleyn (1992) and about the implementation in Doms (2011).

2.2.4 Convection

The scheme of Tiedtke (1989) is used to parameterize sub-grid scale convective clouds and their effects on the large scale environment. This approach uses moisture convergence in the boundary layer to estimate the cloud base mass-flux. The convection scheme then affects the large-scale budgets of the environmental dry static energy, the specific humidity, and the potential energy.

2.2.5 Surface fluxes

Instead of using a bottom free-slip boundary condition surface fluxes of momentum and heat are calculated explicitly in one experiment. This results in non-zero turbulent transfer coefficients of momentum and heat and thus affects the roughness length and the fluxes of latent and sensible heat. As we will show later, this has some significant effects on the initiation of convection.

2.3 Simulations of baroclinic life cycles

In total we present the results of 17 different simulations of the anti-cyclonic and of five different simulations of the cyclonic baroclinic life cycle (see Table 1). Variations between the individual simulations are introduced by either the kind or the number of non-conservative processes. Moreover, additional variability is created by changing the initial humidity as well as by the complexity of treating cloud related processes.

In a first set of simulations, we conducted four different baroclinic life cycles. Using the adiabatic and frictionless life cycle as conservative reference simulation (REF), we obtain further results from life cycles additionally including either turbulence, further denoted as TURB, or radiation, RAD, or bulk microphysics, BMP. For these simulations we apply the standard physical parameterizations of COSMO, which were briefly described in the previous section.

We performed further sensitivity simulations for BMP and RAD to test for the impact of initial conditions as well as the model formulation of a diabatic process. For microphysics we conducted in total four additional life cycle experiments. We first tested for the initial specific humidity q_v. In one case we reduced the initial q_v by setting the surface relative humidity to $30\,\%$ and the gradient to $5.0\,\%/2\,\mathrm{km}$ (BMP R30), while we increased the initial q_v by using $\mathrm{RH_s} = 80\,\%$ and a gradient of $13.33\,\%/2\,\mathrm{km}$ in another case (BMP R80). Furthermore, we conducted simulations in which we used different schemes to represent cloud processes. In one simulation only warm phase clouds are considered, excluding cloud ice (BMP NOICE). In another simulation condensation and evaporation between water vapor and cloud water is realized by a saturation adjustment process (BMP SATAD). Since this simulation includes only large scale diabatic effects from latent heating, it has the least additional effects compared to the dry reference (Schemm et al., 2013).

In case of radiation we performed sensitivity simulations with respect to the initial distribution of specific humidity and ozone. These two trace gases are thought to have the largest impact on the thermal structure around the tropopause (e.g., Randel et al., 2007; Riese et al., 2012). We conducted one simulation with reduced initial specific humidity (RAD R30), similar to BMP R30, while we explicitly set the specific humidity to zero above the tropopause in another simulation (RAD woSW). In another case we reduced the amount of ozone (RAD rO3). However, we explicitly note here that ozone is poorly represented in the model. Instead of a three dimensional distribution, only a simple vertical distribution is assumed which has a maximum concentration at altitudes which are close

to our model top at a pressure of $42\,\mathrm{hPa}$ and a total vertically integrated ozone partial pressure of $0.06\,\mathrm{Pa}$. These two parameters are used in the radiation code to calculate the feedback of the solar and thermal extinction by ozone. We reduced the total amount of ozone by one third to estimate whether this has an impact on the strength of the TIL.

In a next step we use a set of simulations with combinations of non-conservative processes to study potential additive effects as well as to assess the relative contribution of individual processes on the TIL formation and maintenance during different stages of the life cycles. For this we compare results from BMP (here as a reference) to results from simulations where we first add radiation (BMP RAD) and turbulence (BMP TURB) individually and then together (abbreviated with BRT for BMP RAD TURB). In further simulations we include convective clouds (BRTC) and surface fluxes (BRTCS). The convective activity is much stronger in the simulation with surface fluxes than in the simulation with the free-slip boundary condition. Hence, BRTCS can be regarded as simulation with strong convection, while BRTC can rather be seen as life cycle with weak to moderate convective activity. A final sensitivity study was conducted in which the cloud radiative forcing has been neglected to study the effect of this feedback in the region of the tropopause (BMP RAD NOCRF).

3 Non-conservative processes and the formation of a TIL in baroclinic life cycles

In a first step we aim to answer the question which non-conservative process, i.e., related to clouds, radiation, or turbulent mixing has the largest impact on the formation of the TIL in baroclinic life cycles. For this we compare first the results of four anti-cyclonic life cycles (REF, TURB, RAD, and BMP), before we discuss the effects of initial conditions and process formulations on the model results.

3.1 Impact of non-conservative processes on the TIL evolution

The baroclinic life cycle 1, also known as LC1, has been discussed under various aspects (e.g., Thorncroft et al., 1993) and also in light of the evolution of the tropopause inversion layer (Erler and Wirth, 2011). Our REF simulation features the same general characteristics of this life cycle and is described in more detail in Kunkel et al. (2014). One dominant feature of the LC1 is the thinning trough, the so-called stratospheric streamer (often also referred to as Θ- or PV-streamer, e.g., Sprenger et al., 2003). In the mature stage of the baroclinic wave this feature is evident for instance in the distribution of potential temperature Θ on an isosurface of potential vorticity, e.g., $Q = 2.0\,\mathrm{pvu}$. The distribution of potential temperature for our four cases is shown in the upper row of Fig. 2. After $120\,\mathrm{h}$ of model integration we see similar structures for REF, TURB, and RAD with minor differences in the exact location of the streamer and the absolute values of Θ in the warm sector (red colors). The most complex distribution occurs in BMP with warmer temperatures than

in the other three simulations at the southern tip of the streamer. These warmer temperatures are associated with cloud processes and the release of latent heat during rapid ascent. Moreover, the entire Θ-field shows a more in-homogeneous appearance compared to the other three simulations.

Our main focus is, however, on the static stability N^2 in the lowermost stratosphere. In particular, we are interested in the regions where the stability increases significantly during the life cycle. This is typically the case within the first kilometer above the thermal tropopause. However, the spatial appearance is not homogeneous, as is evident from the lower panels in Fig. 2. These panels depict the vertical mean of N^2 over the first kilometer above the thermal tropopause. In all four cases large values of N^2 appear in the warm sector west of the streamer, which is in the region of anti-cyclonic flow. This region has been shown to exhibit a stronger TIL in models (Erler and Wirth, 2011; Wirth, 2003) and in observations (Randel et al., 2007). The life cycle with turbulence shows the lowest values of N^2, while the static stability has generally larger values in the case of radiation than in the reference simulation. In the life cycle with cloud processes we additionally see enhanced values of N^2 on smaller scales than in the other cases. As we will show later these enhancements are related to moist dynamics and vertical motions.

The moist life cycle shows the strongest development in terms of minimum surface pressure, p_s, evolution, in contrast to the life cycle with radiation (Fig. 3a). While all other life cycles show still a deepening of p_s, the absolute minimum pressure has already been reached in BMP after $140\,\mathrm{h}$ of model integration. Moreover, by considering two metrics to trace the evolution of the TIL in our life cycles, we infer that the TIL formation differs most significantly from the dry reference case in the moist life cycle. The maximum static stability N^2_max increases rather suddenly in BMP instead of more gradually as in the other three simulations (Fig. 3b). After reaching its absolute maximum value, N^2_max keeps values above $7.0 \times 10^{-4}\,\mathrm{s}^{-2}$ at consecutive times. Only after about $130\,\mathrm{h}$ after model start N^2_max in RAD, and a little bit later in REF and TURB, has reached the same magnitude as in the moist simulation. Furthermore, an earlier increase of N^2_max is evident in RAD than in REF and TURB, while in the latter case N^2_max is smaller than in the reference case at all times. A similar picture is obtained from the metric that is used as a proxy for the spatial extent of the TIL in the life cycles, i.e., the area in which $N^2 > 5.5 \times 10^{-4}\,\mathrm{s}^{-2}$, denoted as $A_{5.5}$ (Fig. 3c). The earliest appearance is evident in BMP, the latest in TURB. Moreover, the temporal evolution of $A_{5.5}$ clearly shows that the TIL covers a larger area when moist or radiative processes are included in the life cycles. We also tested other thresholds for N^2 for this metric with no significant changes with respect to the qualitative interpretation of our results.

So far, we provided a rather descriptive view on the TIL evolution in our life cycles without giving details about the underlying processes. For the case with turbulence the TIL appears weaker due to the tendency of turbulence to reduce strong vertical gradients. Turbulence acts against the effects of dry dynamics which enhance the lower stratospheric stability during the life cycle. Consequently, only a weak TIL forms in this case.

Including radiation results in a stronger TIL than in the reference case. This is related to the radiative feedback of water vapor, which increases over time in the region of the tropopause (Fig. 4a). Since no microphysics is included in RAD, water vapor is transported as a passive tracer in this simulation. Upward motions in the troposphere and tropopause dynamics lead to more water vapor at the altitude of the tropopause, finally changing the water vapor gradient significantly (Fig. 4b). This causes differential cooling by water vapor in the UTLS, which then results in a non-uniform change of the thermal structure (e.g., Zierl and Wirth, 1997). Additionally, recently lifted, moist air is then partly located also in the lower stratosphere, where its residence time is longer and thus can potentially affect the thermal structure over longer time scales. This process further enhances the static stability directly above the tropopause and thus strengthens the TIL which also forms by the dynamics of the baroclinic wave. Thus, a process directly changing the thermal structure alters the appearance of the TIL in the case with radiation.

In the moist case we present evidence that a process at lower tropospheric levels is responsible for the different appearance of the TIL. The spontaneous increase in N^2_{max} is well correlated with the earliest release of latent heat in the model (Fig. 5a and b). Since the same effect is evident from the simulation with the saturation adjustment scheme (BMP SATAD), we can conclude that it is the release of latent heat rather than a microphysical process being responsible for the observed effect. Latent heat release is, however, not only a sign of condensation but also fosters vertical motions in the model. These vertical motions reach in many cases the tropopause and often lift this vertical transport barrier. Consequently, also the air above is slightly lifted, thereby increasing the vertical gradient of potential temperature, resulting in enhanced static stability above the tropopause. This process differs, however, fundamentally from the process related to dry dynamics on spatial and temporal scales. While the latter is rather slow and occurs predominantly in an anti-cyclonic flow region with on average descending air motion, this lifting process is fast, occurs on small scales, and is related to upward motions. Thus taken together, the incorporation of water in the model fosters a stronger TIL development as consequence of enhanced upward motions within the life cycle due to the release of latent heat.Our results agree with those obtained by Gutowski et al. (1992). They compared dry and moist baroclinic life cycles and showed that including moisture leads to stronger updrafts as well as to a faster evolution of the life cycle.

Although the temporal and spatial appearance of the TIL is rather heterogeneous in all four simulations, the TIL becomes also evident in the domain mean vertical profiles of N^2. These averages are obtained between $25°$–$65°$ N in the meridional direction and in the entire zonal direction. ΔN^2 represents the difference between the current N^2 and the passively advected tracer N^2_0 (Fig. 6, left panels) and ΔQ the difference between the current potential vorticity Q and the passively advected initial potential vorticity Q_0 (Fig. 6, right panels), respectively. The vertical profiles of ΔN^2 and ΔQ are given in a tropopause based coordinate system for every $24\,\text{h}$ of the model integration and the thin solid line shows the location of the tropopause. In all four simulations an increase in static

stability forms sooner or later during the life cycles just above the tropopause. While the domain mean TIL appears only during the late stages in REF and TURB, it is much earlier obvious in RAD and BMP. However, PV at the tropopause shows significant positive changes only in the simulation with radiation. The location of the maximum diabatic change in PV correlates temporally and spatially (relative to the thermal tropopause) well with the changing gradient of water vapor (see Fig. 4). Moreover, this change in PV occurs over large areas in the model domain (not explicitly shown) and is thus clearly evident in the mean vertical profile of ΔQ. In simulations of real extratropical cyclones over the North Atlantic, the evolution of a dipole structure with a positive PV anomaly above the tropopause and a negative anomaly below have been reported by Chagnon et al. (2013). They could also show that these anomalies are largely related the radiation scheme in their model. In contrast, only minor changes of PV are found in the simulations with turbulence and cloud processes. In the latter case the largest changes of PV occur rather at low- and mid-tropospheric altitudes where the major release of latent heat occurs. These changes occur, however, on smaller spatial areas, and more specifically not always at the same altitude relative to the tropopause. Thus, compared to RAD ΔQ has no pronounced tendency in the domain mean in case of BMP. In the reference case the minor changes of potential vorticity are solely related to the numerics, especially to the tracer advection scheme (Kunkel et al., 2014). Thus, in case of radiation the formation of the TIL is directly related to a diabatic process in the tropopause region, while the diabatic processes related to clouds have an indirect impact on the TIL, i.e., the diabatic processes and the response of the static stability above the tropopause occur at a different places. Mixing, like radiation, also directly affects the TIL but to a much lesser extent.

3.2 Sensitivity of individual diabatic processes

In the next paragraphs we briefly discuss the impact of initial conditions on the model results, focusing especially on experiments with cloud microphysics and radiation.

For microphysics we tested for the amount of initial specific humidity, comparing BMP to BMP R30, and BMP R80, as well as for the representation of the cloud processes, comparing BMP to BMP NOICE, and BMP SATAD. From the temporal evolution of N^2_{max} (Fig. 7a) we infer that the amount of specific humidity is more important than the model formulation of cloud processes. If more water is initially present, then the TIL appears earlier. In contrast, with less initial water the TIL appears later and the entire appearance approximates towards the adiabatic case. Moreover, the occurrence of the TIL is relatively insensitive to the representation of the cloud processes as long as the initial amount of specific humidity is the same as it is the case in BMP, BMP NOICE, and BMP SATAD.

In case of radiation we tested for the initial amount and distribution of water, comparing RAD to RAD R30, and RAD woSW, as well as for the amount of ozone, comparing RAD to RAD rO3. We find only minor differences in the evolution of N^2_{max} for the various sensitivity simulations (Fig. 7b). Reducing the amount of water leads to a reduced radiative feedback and thus to a less strong TIL.

Changing the amount of ozone has, in our case, no significant effect at all, however, with the caveat of the simple representation of ozone in our model. The largest difference is found if we completely remove the water in the stratosphere. This results in an artificially large water vapor gradient between the troposphere and the stratosphere. As we have seen before (Fig. 4), a strong water vapor gradient results in a sharp tropopause. A similar result has been discussed by Fusina and Spichtinger (2010) who studied amongst many other features the response of the static stability to the sharpness of a gradient between saturated and unsaturated air.

4 Relative importance of dynamical and diabatic processes on the TIL formation

Until here we provided new insights of the isolated effect of individual physical processes on the formation of the tropopause inversion layer in baroclinic life cycles. Now we turn our discussion to the relative importance of these processes, and especially whether the dynamical or the radiative forcing is more important for the TIL formation and maintenance. For this purpose we use our second set of baroclinic life cycle experiments where we successively increase the number of processes and as such increase complexity. The simulation with cloud processes (BMP) serves as reference while we first add radiation (BMP RAD) and turbulence (BMP TURB) separately and then combine all three processes (BRT). We further add convection (BRTC) and then also surface fluxes of momentum and heat (BRTCS).

The six life cycles evolve similar, all forming a Θ-streamer and anti-cyclonic wave breaking. Again the temperature distribution at the southern tip of the streamer varies most between the individual life cycles (Fig. 8). Moreover, in some cases a smooth Θ-distribution is evident, e.g., BMP TURB, BRT, or BRTC, while the distribution is more variable and shows more small scale features in other life cycles, especially in BRTCS. In all six cases the static stability above the tropopause is larger in the anti-cyclonic part of the wave than in the cyclonic part (not explicitly shown). After 120 h at least two regions with enhanced values of N^2 are evident. One is further to the north along the cold front ahead of the cyclonic center. The other is more located at the south-western edge of the streamer. As evident from the time series in Figure 9 both maxima are related to the outflow of the warm conveyor belt (WCB). This airstream ~~lifts moist , low-tropospheric air masses into the tropopause region~~originates in the lower troposphere in the region ahead of the trough axis (e.g., Carlson, 1998) . In the WCB moist air masses rapidly ascend within 1-2 days into the upper troposphere, associated with cloud formation, precipitation, and release of latent heat (e.g., Wernli and Davies, 1997; Madonna et al., 2014) . The existence of a relation between WCB and TIL has been proposed by Peevey et al. (2014) who used HIRDLS satellite and ECMWF model data to obtain their results. Moreover, Figure 9 shows that enhanced values of static stability above the tropopause are closely related to the location of strong updrafts and cirrus clouds at the time of the

first TIL appearance. The cirrus clouds are identified by the cloud ice content below the tropopause. ~~We refer to strong~~ Note again that we refer to updrafts here, when an air mass has been lifted by at least $2.5\,\mathrm{km}$ since model start. This change in altitude of an air parcel is calculated from the difference of the current altitude z of this air parcel and its initial altitude z_0, which is carried by a passive tracer. We further denote this difference as Δz which is positive if an air parcel raised and negative if an air parcel descended since model start. The static stability is enhanced almost at all times in the center of the WCB outflow, where the ice cloud branches towards the north-west and south-east. From $102\,\mathrm{h}$ onward a second maximum is evident in the south-eastern branch of the ice cloud which moves further to the south in subsequent hours. This maximum is located more in the region where inertia-gravity waves are generated and influence the thermal structure of the tropopause (Kunkel et al., 2014). This influence is such that the static stability maximum keeps its large values almost entirely constant at subsequent hours of the simulation. In case of BRTCS a larger area exhibits enhanced static stability values above the tropopause which is the result of convective activity as we will see later in more detail.

In the following we aim to answer the question why the TIL appears earlier in some life cycles and how the TIL is maintained after it has been generated. We first compare the time of first appearance of the TIL between the six life cycles. Figure 10a–e shows the first $80\,\mathrm{h}$ of model integration for various variables. The initial increase of N^2_{max} can be divided into three sections which are related to the physical processes considered in the respective life cycle (Fig. 10a). The latest TIL appearance after about $65\,\mathrm{h}$ is found when considering only cloud processes and turbulence. Including radiation to the model simulations shifts the time of appearance ten hours ahead, while the earliest TIL formation starts already after about $35\,\mathrm{h}$ in case of considering convection and surface fluxes. This division into three time sectors correlates well with the proxy for strong updrafts Δz. Figure 10b depicts the maximum Δz in the layer between the thermal tropopause and $500\,\mathrm{m}$ below this level, from which we infer that there is strong temporal coincidence between the first appearance of N^2_{max} and updrafts originating at low levels. The earlier appearance of ~~updrafts~~ vertically ascending air masses in case with radiation and convection is related to the these processes, since they foster an earlier emerging of updrafts in the model. This finding supports our results from the previous section that moist dynamics including stronger updrafts than in the dry case has a strong impact on the first appearance of the TIL. These ~~updrafts~~ lifted air masses further enhance the local convergence of the vertical wind just above the tropopause as we will see later. Moreover, we find good agreement between the temporal increase of N^2_{max} and two tracers for moisture, specific humidity q_{v} (Fig. 10c) and specific cloud ice content q_{i} (Fig. 10d). Thus, the ~~updrafts~~ ascending air masses moisten the upper troposphere below the tropopause which, as shown before, supports the TIL formation by differential radiative cooling. The gradual increase of N^2_{max} in case of BRTCS can further be related to another tracer for updrafts, which is the cloud base mass flux which is available for the two simulations in which the convective cloud parameterization is switched on (Fig. 10e). This quantity serves as proxy

for convective activity and starts to increase gradually in the case with surface fluxes early during the simulation. Thus, these findings further support our suggestion from Sect. 3 that vertical motions are the essential key parameter for the initial TIL appearance in baroclinic life cycles with moist diabatic processes.

We further provide evidence that there is not only a temporal but also a spatial coincidence between updrafts and TIL occurrence. Figure 11 shows zonal cross-sections of N^2 for the six simulations along 45° N after 120 h of model integration. Indications of increased static stability are found in all cases above the ~~updrafts~~ lifted air masses which reach the tropopause. Clouds often form in the regions of the updrafts and in the lowermost stratosphere we find regions of convergence of the vertical wind. This convergence results from emerging gravity waves from the updrafts, but is also present in regions of propagating inertia-gravity in the eastern most region of the cross-sections. Gravity waves can alter the TIL temporarily during propagation (Otsuka et al., 2014) and possibly permanently by breaking or wave capture (Kunkel et al., 2014). In addition to the effects of dry dynamics, i.e., distribution of cyclonic and anti-cyclonic flow and breaking of the baroclinic wave (see Erler and Wirth, 2011), the effects from updrafts, small-scale convergence, and radiation, contribute most strongly to the TIL formation. Furthermore, note that low-, and mid-tropospheric diabatic heating causes a negative change in PV above the region of maximum heating, thus enhancing the anti-cyclonic flow in the tropopause region above (e.g., Joos and Wernli, 2012; Wernli and Davies, 1997), which further has a positive feedback on the TIL evolution.

To this point we demonstrated that ~~updrafts~~ lifted air masses reaching the tropopause level are initially important to form the TIL. However, this could be a transient effect on the static stability in the stratosphere and as such its contribution could decrease over time with other effects becoming more important. One other potential process might be related to the convergence of the vertical wind $\partial w/\partial z$. If this term becomes negative at or just above the tropopause, the static stability is increased in this region (Wirth, 2004). Convergence can occur on small scales when gravity waves are present or on large scales in anti-cyclonic flow. We introduce here another metric to measure the impact of updrafts and convergent regions on enhanced static stability. For this we calculate the domain mean vertical profile of static stability N^2 as well as the mean vertical profile of static stability in regions with strong updrafts $N^2_{\mathrm{d}z}$, i.e., $\Delta z \geq 2.5\,\mathrm{km}$ below the tropopause, and in regions with strong convergence of the vertical wind $N^2_{\mathrm{w}z}$, i.e., $\partial w/\partial z \leq -5.0\times10^{-5}\,\mathrm{s}^{-1}$. We subtract the domain mean from these values to obtain quantitative measures how strong the TIL is enhanced in the respective regions compared to the TIL in the entire domain. Figure 12 shows the tropopause-based vertical profiles of $N^2_{\mathrm{d}z} - N^2$ (upper panel a) and $N^2_{\mathrm{w}z} - N^2$ (lower panel b) for every 24 h. In $N^2_{\mathrm{d}z} - N^2$ a TIL like vertical profile (i.e., with maximum values just above the tropopause) is evident in all six cases, especially in the first days of the simulations. However, the difference becomes smaller with time, which is partly related to the fact that the TIL becomes more evident in the domain mean N^2. Moreover, the number of grid cells contributing to $N^2_{\mathrm{d}z}$ stagnates at later times, indicating the

decreasing number of new updrafts over time, which reach the tropopause (compare the numbers in the top left corners in each panel of Fig. 12). The differences $N^2_{\mathrm{w}z} - N^2$ also become smaller above the tropopause with time, i.e., the TIL like shape is less evident. However, compared to the relative decreases of the differences $N^2_{\mathrm{d}z} - N^2$, the decreases of $N^2_{\mathrm{w}z} - N^2$ over time are relatively smaller. Moreover, the number of grid cells contributing to $N^2_{\mathrm{w}z}$ becomes significantly larger over time and is in most cases also larger than the number for $N^2_{\mathrm{d}z}$. From this we follow that updrafts might be potentially more important during the initial formation of the TIL. In contrast, the convergence of the vertical wind might become relatively more important in maintaining the TIL during later times of the life cycles.

We already saw that moistening the upper troposphere fosters the evolution of the TIL. Since ice clouds also reach the level of the tropopause, we briefly discuss their potential impact on the thermal structure above the tropopause. We only use cloud processes and radiation in this analysis here and exclude the effects of mixing and convection. We conducted a further simulation in which we turned off the cloud radiative feedback (BMP RAD NOCRF) and compare the results to those from a simulation with feedback (BMP RAD) to assess the impact of ice clouds on TIL in the model. From instantaneous vertical profiles of meteorological and tracer quantities within a region which exhibits a TIL and ice clouds up to the tropopause we infer the following points (Fig. 13): (1) the net heating rate is much more negative in the upper troposphere when the forcing is turned on, with the cooling being strongest just below the thermal tropopause (black solid lines); (2) the temperature profile in the UTLS differs significantly between both cases – while there is a clear minimum in the case with cloud radiative forcing, an almost neutral temperature profile is evident in the first two kilometers above the tropopause in BMP RAD NOCRF (black dashed lines); (3) the upper edge of the ice cloud is located slightly above the tropopause in BMP RAD and slightly below in the other case (blue solid lines); (4) the specific humidity has a local maximum at the top of the ice cloud which is stronger in the case with feedback (blue dashed lines); (5) the static stability is increased in both cases with a slightly higher located and stronger maximum in case with feedback (red solid lines); (6) the height tracer indicates lifted air mass in the troposphere below the maximum of static stability, however, with stronger updrafts in the case with feedback (red dashed lines). From points (1), (2), and (5) we conclude that the tropopause can be sharper due to strong differential cooling in the UTLS, if ice clouds are present. Moreover, from (3), (4), and (6) it follows that the potential to moisten the lower stratosphere is also increased which might in turn enhance the radiative formation process of the TIL. Thus, the results from this sensitivity suggest that there is a larger potential to obtain a stronger TIL when clouds reach up to the level of the tropopause. Moreover, this might be of further interest, since ice clouds, or ice super-saturated regions, have been shown to occur frequently in the lower stratosphere (e.g., Spichtinger et al., 2003; Spang et al., 2015).

So far we mainly focused on radiative and moist effects. In the last paragraph we turn to the effect of mixing and analyze where turbulent mixing occurs at the tropopause and whether this spatially and

temporally coincides with the appearance of the TIL. Turbulent mixing contributes to the process of small scale stratosphere-troposphere exchange (STE). It has been speculated in several studies that TIL and STE are causally related beyond a pure spatial coincidence (e.g., Gettelman and Wang, 2015). Kunz et al. (2009) used airborne measurements and ECMWF analysis data from which they concluded that mixing at the tropopause is a synoptic scale process on rather short time scales which, however, enhances the concentration of radiatively active trace gases in the mixing layer. This then leads to an increase in static stability further downwind of the region of the STE event. Thus, they focused on the long term relation between mixing and N^2. On the other hand we see that values of turbulent kinetic energy (TKE) are often increased in regions where a TIL is present (Fig. 14). These values are smaller than in the boundary layer, but nevertheless increased compared to the background values in the tropopause region at other locations and times in our model simulations. Such exchange events may have only spatial extension of a few tenths of kilometers or even less. Müller et al. (2015) recently reported a comparable event based on airborne in-situ measurements of nitrous oxide, ozone, and ice cloud particles. However, since our model is not capable of resolving this process with sufficient accuracy to conduct a quantitative estimate of STE, we will leave a more detailed analysis open to further studies.

5 The TIL in cyclonic life cycle experiments

So far, the discussion of the results focused on the anti-cyclonic life cycle (LC1, Thorncroft et al., 1993). We will now extend the analysis and show results for five selected cyclonic life cycles (LC2). We obtain this life cycle by adding a cyclonic shear to the background state of the LC1 (see Section 2.1). We briefly compare the results of the LC1 and LC2 and discuss the main difference in the following paragraphs. For this we analyze the results from a dry reference experiment (REF LC2), from three simulations with one additional diabatic process, i.e., with clouds (BMP LC2), with radiation (RAD LC2), and with turbulence (TURB LC2), and from one simulation with a more complex setup including clouds and convection, radiation, and turbulence (BRTC LC2).

Generally, LC2 experiments show a less strong deepening of the minimum surface pressure compared to their LC1 counterparts (Fig. 15a). Similarly to the LC1 waves, the deepening of the surface cyclone is less strong, when radiation is included in the simulations (RAD LC2, BRTC LC2). N^2_{max} above the thermal tropopause shows several differences between LC1 and LC2. In the cases without moisture (REF LC2, RAD LC2, and TURB LC2) the maximum values are always below $7.0 \times 10^{-4}\,\text{s}^{-2}$. Moreover, in contrast to the sudden increase of N^2_{max} in all moist LC1 cases, N^2_{max} increases rather stepwise, in particular in the BMP LC2 case. The absolute maximum is reached only after $110\,\text{h}$ after simulation start and thus much later than in the LC1 BMP case (compare Fig. 3b). Furthermore, at the end of the simulated period N^2_{max} is almost equal in all LC1 cases, which is, however, not the case in the LC2 cases. The TIL area ($A_{5.5}$, see Figure 15c) is largest for BMP LC2

and shows even comparable numbers to its LC1 counterpart. However, in the other cases the $A_{5.5}$ is much smaller in the LC2 cases than in the LC1 cases. Thus, the TIL evolves less strong in amplitude and spatial extent in the LC2 compared to the LC1. Generally, this is in agreement with the results from Erler and Wirth (2011) for dry adiabatic life cycles.

The processes relevant for the TIL formation are rather similar between LC1 and LC2. In the moist cases BMP LC2 and BRTC LC2 N^2_{max} shows a strong correlation to Δz (see Figure 15d) and thus updrafts may be as important in the LC2 as they are in the LC1 to initially form the TIL in the life cycles. This relation is further obvious when the spatial co-occurrence between ~~updrafts~~ lifted air masses and enhanced static stability is studied (Figure 16). The first enhancement of N^2 in the lower stratosphere are again present just above regions which exhibit strong updrafts and also ice clouds just below the tropopause. Thus, except for the difference in the timing of the first vertical ascent patterns, there is no major difference to the LC1 baroclinic life cycle. However, the temporal variability of N^2_{max} in BMP LC2 and BRTC LC2 is slightly larger than in their LC1 counterparts. This might be related to the less strong evolving gravity waves in the LC2 simulations. In particular, gravity waves from the jet-front system are much more evident in LC1 than in LC2 which has been discussed in Kunkel et al. (2014). Thus, the effect of gravity waves on the TIL maintenance might be less strong in case of LC2. Taken together the LC2 cases generally show a less strong developed TIL compared with their LC1 counterparts. Nevertheless, the physical processes leading the TIL formation seem to be similar in LC1 and LC2.

6 Conclusions and summary

By conducting various simulations of baroclinic life cycles we aimed to improve the understanding whether dynamical or diabatic processes are more relevant to form a tropopause inversion layer (TIL). For this we used the non-hydrostatic, limited area model COSMO in a midlatitude channel configuration along with a varying number of physical parameterizations. We first analyzed the effect of individual diabatic processes, i.e., related to clouds, radiation, and mixing processes before we estimated the relative importance of each process.

In a first set of simulations the evolution of the TIL has been compared in baroclinic life cycles. A life cycle experiment with only dry dynamics served as reference case, while three additional life cycle experiments have been performed with individual non-conservative process added. We further assessed the impact of initial conditions and process formulation in the diabatic cases. In a second step we successively increased the number of processes to assess the relative importance of the various dynamical and diabatic processes to the TIL evolution. We further conducted sensitivity experiments to study differences between life cycles of type 1 (LC1) and 2 (LC2).

Most importantly, our experiments highlighted the role of different moisture related processes for the formation and evolution of the TIL with varying relevance and strength in different phases of the baroclinic life cycles. In detail, we derived the following results:

1. A TIL forms in baroclinic life cycles with only dry dynamics as well as in life cycles with additionally either vertical turbulence, cloud processes, or radiation. Compared to the dry reference case the TIL appears weaker with respect to its maximum value as well as to the spatial appearance in the case with turbulence. The opposite is evident in the case with radiation with a larger maximum static stability and larger spatial appearance. The temporal evolution is, however, still similar to the reference case. This is different with cloud processes. The TIL emerges much earlier and shows generally the largest maximum values and spatial extension.

2. The processes forming the TIL in the cases with diabatic processes are as follows. Turbulence acts against the forming process from dynamics, and as such a weaker TIL is the final result. With only radiative processes, the (passive) transport of moisture from low to high levels leads to an increase in the moisture burden in the UTLS and to a change in the moisture gradient in this region. The UTLS is then cooled non-uniformly which finally further enhances the static stability above the tropopause. The important process with clouds is the release of latent heat during condensation. This increases the frequency and strength of vertical motions which locally increase the static stability above the regions of the updrafts. Especially, the TIL forms in the region of the warm conveyor belt. In contrast to the direct diabatic forcing (occurring in the region of the tropopause) in the case with radiation, the enhancement of static stability results from a diabatic forcing at lower levels in the case with clouds.

3. Analysis of initial conditions and process formulations showed that the TIL formation in the model is relatively insensitive to the formulation of the cloud forming process itself and more dependent on the initial amount of specific humidity. For radiation no significant dependency on the initial water or ozone amount is evident. Here, the change of the gradient of specific humidity is the more important process.

4. Further simulations of baroclinic life cycles with varying complexity with respect to the number of incorporated physical processes showed that there is a correlation between the first appearance of the TIL and of updrafts reaching the tropopause. However, the exact timing of this first occurrence further depends on the included physical processes. The TIL emerges latest when only cloud processes and turbulence are considered while it appears earlier when radiation is incorporated and even more with convection. From this result it is concluded that ~~updrafts~~ vertically ascending air masses which reach the tropopause altitude are the key process in the initial formation of the TIL in moist baroclinic life cycles, however, noting that their effect is probably fading with time.

5. The updrafts that reach the tropopause lead to the emission of gravity wave in the lower stratosphere. Such small scale waves have a further source in the jet-front system (inertia-gravity waves). In recent studies (e.g., Kunkel et al., 2014; Otsuka et al., 2014) it has been shown that these small-scale disturbances can alter the thermal structure above the tropopause temporarily as well as permanently and as such affect the TIL during the entire life cycle after their first appearance. At least in parts, the appearance and strength of such gravity waves might explain the weaker appearance of the TIL in the cyclonic life cycles compared to their anti-cyclonic counterparts.

6. Finally, ~~updrafts~~ air masses lifted from moist, low-tropospheric regions enhance the moisture content of the upper troposphere, not only by transporting water vapor to this altitude. Clouds also form within the updrafts and locally alter the thermal structure of the upper troposphere. Especially, at the top of the clouds a strong cooling can occur which further contributes to the formation and maintenance of a strong TIL. In general, radiative impacts become more relevant during later stages of the life cycle.

Thus, the various dynamical and diabatic processes lead to a highly variable temporal and spatial appearance of the TIL on the time-scale of a week. While updrafts are important for the first appearance of the TIL when moisture is included in the baroclinic life cycles, the radiative effects as well as the convergence of the vertical wind are more important in maintaining the TIL during later phases of the life cycles. In reality the TIL in the midlatitudes may be restrengthened by each passing baroclinic wave and the lifted water vapor serves as a cooling agent in the upper troposphere and even in the lower stratosphere over a longer time-scale than a week. Taking into account that baroclinic waves occur relatively frequent at midlatitudes, especially from autumn to spring, might further help to explain the quasi-permanent appearance of a layer of enhanced static stability.

Acknowledgements. D. Kunkel acknowledges funding from the German Science Foundation under grant HO 4225/2-1. The authors thank A. Roches, U. Blahak, and S. Schemm for model support and the HPC team of the university of Mainz for computing time. We further thank P. Spichtinger for valuable comments on an earlier version of the manuscript. The comments on the discussion paper from S. Schemm, G. Craig, and an anonymous referee helped to significantly improve the final manuscript. Further information on data (model code and output) relevant to this paper can be obtained upon request via email to the authors (dkunkel@uni-mainz.de).

References

Bell, S. W. and Geller, M. A.: Tropopause inversion layer: seasonal and latitudinal variations and representation in standard radiosonde data and global models, J. Geophys. Res.-Atmos., 113, D05109, doi:10.1029/2007JD009022, 2008.

Birner, T.: Fine-scale structure of the extratropical tropopause region, J. Geophys. Res., 111, D04104, doi:10.1029/2005JD006301, 2006.

Birner, T.: Residual Circulation and Tropopause Structure, J. Atmos. Sci., 67, 2582–2600, doi:10.1175/2010JAS3287.1, 2010.

Birner, T., Dörnbrack, A., and Schumann, U.: How sharp is the tropopause at midlatitudes?, Geophys. Res. Lett., 29, 1700, doi:10.1029/2002GL015142, 2002.

Birner, T., Sankey, D., and Shepherd, T. G.: The tropopause inversion layer in models and analyses, Geophys. Res. Lett., 33, L14804, doi:10.1029/2006GL026549, 2006.

Carlson, T. N.: Mid-Latitude Weather Systems, Amer. Meteor. Soc., 507 pp., 1998.

Chagnon, J. M. Gray, S. L., and Methven, J.: Diabatic processes modifying potential vorticity in a North Atlantic cyclone, Q. J. Roy. Meteor. Soc., 139, 1270–1282, doi:10.1002/qj.2037, 2013.

Doms, G.: A Description of the Nonhydrostatic Regional COSMO-Model, Part I: Dynamics and Numerics, Tech. rep., Deutscher Wetterdienst, Offenbach, Germany, 2011.

Erler, A. R. and Wirth, V.: The static stability of the tropopause region in adiabatic baroclinic life cycle experiments, J. Atmos. Sci., 68, 1178–1193, doi:10.1175/2010JAS3694.1, 2011.

Fusina, F. and Spichtinger, P.: Cirrus clouds triggered by radiation, a multiscale phenomenon, Atmos. Chem. Phys., 10, 5179–5190, doi:10.5194/acp-10-5179-2010, 2010.

Gettelman, A. and Wang, T.: Structural diagnostics of the tropopause inversion layer and its evolution, J. Geophys. Res.-Atmos., 120, 46–62, doi:10.1002/2014JD021846, 2015.

Grise, K. M., Thompson, D. W. J., and Birner, T.: A global survey of static stability in the stratosphere and upper troposphere, J. Climate, 23, 2275–2292, doi:10.1175/2009JCLI3369.1, 2010.

Gutowski, W. J., Branscome, L. E., and Stewart, D. A.: Life cycles of moist baroclinic eddies, J. Atmos. Sci., 49, 306–319, doi:10.1175/1520-0469(1992)049<0306:LCOMBE>2.0.CO;2, 1992.

Held, I. M. and Suarez, M. J.: A proposal for the intercomparison of the dynamical cores of atmospheric general circulation models, B. Am. Meteorol. Soc., 75, 1825–1830, doi:10.1175/1520-0477(1994)075<1825:APFTIO>2.0.CO;2, 1994.

Joos, H. and Wernli, H.: Influence of microphysical processes on the potential vorticity development in a warm conveyor belt: a case-study with the limited-area model COSMO, Q. J. Roy. Meteor. Soc., 138, 407–418, doi:10.1002/qj.934, 2012.

Kunkel, D., Hoor, P., and Wirth, V.: Can inertia-gravity waves persistently alter the tropopause inversion layer?, Geophys. Res. Lett., 41, 7822–7829, doi:10.1002/2014GL061970, 2014.

Kunz, A., Konopka, P., Müller, R., Pan, L. L., Schiller, C., and Rohrer, F.: High static stability in the mixing layer above the extratropical tropopause, J. Geophys. Res., 114, D16305, doi:10.1029/2009JD011840, 2009.

Madonna, E., Wernli, H., Joos, H. and Martius, O.: Warm conveyor belts in the ERA-Interim data set (1979-2010). Part I: Climatology and potential vorticity evolution, J. Climate, 27, 3-26, 2014

Mellor, G. L. and Yamada, T.: Development of a turbulence closure model for geophysical fluid problems, Rev. Geophys., 20, 851, doi:10.1029/RG020i004p00851, 1982.

Müller, S., Hoor, P., Berkes, F., Bozem, H., Klingebiel, M., Reutter, P., Smit, H. G. J., Wendisch, M., Spichtinger, P., and Borrmann, S.: In situ detection of stratosphere-troposphere exchange of cirrus particles in the midlatitudes, Geophys. Res. Lett., 42, 949–955, doi:10.1002/2014GL062556, 2015.

Murray, F. W.: On the computation of saturation vapor pressure, J. Appl. Meteorol., 6, 203–204, doi:10.1175/1520-0450(1967)006<0203:OTCOSV>2.0.CO;2, 1967.

Olson, J. B. and Colle, B.: A modified approach to initialize an idealized extratropical cyclone within a mesoscale model, Mon. Weather Rev., 135, 1614–1624, doi:10.1175/MWR3364.1, 2007.

Otsuka, S., Takeshita, M., and Yoden, S.: A numerical experiment on the formation of the tropopause inversion layer associated with an explosive cyclogenesis: possible role of gravity waves, Progress in Earth and Planetary Science, 1, 19, doi:10.1186/s40645-014-0019-0, 2014.

Peevey, T. R., Gille, J. C., Homeyer, C. R., and Manney, G. L.: The double tropopause and its dynamical relationship to the tropopause inversion layer in storm track regions, J. Geophys. Res.-Atmos., 119, 10194–10212, doi:10.1002/2014JD021808, 2014.

Randel, W. J. and Wu, F.: The Polar summer tropopause inversion layer, J. Atmos. Sci., 67, 2572–2581, doi:10.1175/2010JAS3430.1, 2010.

Randel, W. J., Wu, F., and Forster, P.: The extratropical tropopause inversion layer: global observations with GPS data, and a radiative forcing mechanism, J. Atmos. Sci., 64, 4489–4496, doi:10.1175/2007JAS2412.1, 2007.

Riese, M., Ploeger, F., Rap, A., Vogel, B., Konopka, P., Dameris, M., and Forster, P.: Impact of uncertainties in atmospheric mixing on simulated UTLS composition and related radiative effects, J. Geophys. Res., 117, D16305, doi:10.1029/2012JD017751, 2012.

Ritter, B. and Geleyn, J.-F.: A comprehensive radiation scheme for numerical weather prediction models with potential applications in climate simulations, Mon. Weather Rev., 120, 303–325, doi:10.1175/1520-0493(1992)120<0303:ACRSFN>2.0.CO;2, 1992.

Schemm, S., Wernli, H., and Papritz, L.: Warm conveyor belts in idealized moist baroclinic wave simulations, J. Atmos. Sci., 70, 627–652, doi:10.1175/JAS-D-12-0147.1, 2013.

Son, S.-W. and Polvani, L. M.: Dynamical formation of an extra-tropical tropopause inversion layer in a relatively simple general circulation model, Geophys. Res. Lett., 34, L17806, doi:10.1029/2007GL030564, 2007.

Spang, R., Günther, G., Riese, M., Hoffmann, L., Müller, R., and Griessbach, S.: Satellite observations of cirrus clouds in the Northern Hemisphere lowermost stratosphere, Atmos. Chem. Phys., 15, 927–950, doi:10.5194/acp-15-927-2015, 2015.

Spichtinger, P., Gierens, K., Leiterer, U., and Dier, H.: Ice supersaturation in the tropopause region over Lindenberg, Germany, Meteorol. Z., 12, 143–156, doi:10.1127/0941-2948/2003/0012-0143, 2003.

Sprenger, M., Croci Maspoli, M., and Wernli, H.: Tropopause folds and cross-tropopause exchange: a global investigation based upon ECMWF analyses for the time period March 2000 to February 2001, J. Geophys. Res.-Atmos., 108, 8518, doi:10.1029/2002JD002587, 2003.

Table 1. Summary of experiment acronyms, description, and water treatment

Experiment	Short description	Water species
REF	adiabatic reference simulation	no water species
BMP	standard cloud microphysics	interactive water
RAD	standard radiation scheme	passive water vapor
TURB	standard turbulence scheme	no water species
BMP R30	BMP sensitivity, reduced specific water vapor	interactive water
BMP R80	BMP sensitivity, increased specific water	interactive water
BMP NOICE	BMP sensitivity, only warm clouds	interactive water, no ice phase
BMP SATAD	BMP sensitivity, saturation adjustment	water vapor and cloud water
RAD woSW	RAD sensitivity, no stratospheric water	passive water vapor
RAD R30	RAD sensitivity, reduced specific water vapor	passive water vapor
RAD rO3	RAD sensitivity, reduced ozone concentration	passive water vapor
BMP RAD	cloud microphysics and radiation	interactive water
BMP RAD NOCRF	cloud microphysics and radiation no cloud radiative feedback	interactive water
BMP TURB	cloud microphysics and turbulence	interactive water
BRT	cloud microphysics, radiation, and turbulence	interactive water
BRTC	cloud microphysics, radiation, turbulence, and convection	interactive water
BRTCS	cloud microphysics, radiation, turbulence, convection, and surface fluxes for momentum and heat	interactive water
REF LC2	adiabatic reference simulation for LC2	no water species
BMP LC2	standard cloud microphysics for LC2	interactive water
RAD LC2	standard radiation scheme for LC2	passive water vapor
TURB LC2	standard turbulence scheme for LC2	no water species
BRTC LC2	cloud microphysics, radiation, turbulence, and convection for LC2	interactive water

Steppeler, J., Doms, G., Schättler, U., Bitzer, H. W., Gassmann, A., Damrath, U., and Gregoric, G.: Meso-gamma scale forecasts using the nonhydrostatic model LM, Meteorol. Atmos. Phys., 82, 75–96, doi:10.1007/s00703-001-0592-9, 2003.

Thorncroft, C. D., Hoskins, B. J., and McIntyre, M. E.: Two paradigms of baroclinic-wave life-cycle behaviour, Q. J. Roy. Meteor. Soc., 119, 17–55, doi:10.1002/qj.49711950903, 1993.

Tiedtke, M.: A comprehensive mass flux scheme for cumulus parameterization in large-scale models, Mon. Weather Rev., 117, 1779–1800, doi:10.1175/1520-0493(1989)117<1779:ACMFSF>2.0.CO;2, 1989.

Wernli, H. and Davies, H. C.: A ~~lagrangian-based~~ Lagrangian-based analysis of extratropical cyclones. I: The method and some applications, Q. J. Roy. Meteor. Soc., 123, 467–489, doi:10.1002/qj.49712353811, 1997.

Wirth, V.: Static stability in the extratropical tropopause region, J. Atmos. Sci., 60, 1395–1409, doi:10.1175/1520-0469(2003)060<1395:SSITET>2.0.CO;2, 2003.

Wirth, V.: A dynamical mechanism for tropopause sharpening, Meteorol. Z., 13, 477–484, 2004.

WMO (1957), Meteorology - a three dimensional science, *WMO Bulletin*, pp. 134–138.

Zierl, B. and Wirth, V.: The influence of radiation on tropopause behavior and stratosphere-troposphere exchange in an upper tropospheric anticyclone, J. Geophys. Res., 102, 23883, doi:10.1029/97JD01667, 1997.

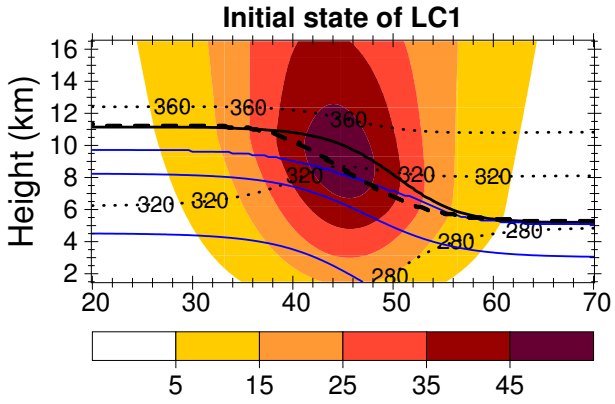

Figure 1. Meridional cross section of the initial state at the center of the model domain: the zonal wind U is color-coded for values of 5, 15, 25, 35, and 45 ms^{-1}; the potential temperature Θ is shown by the black dotted lines for 280, 320, and 360 K (from bottom to top); the water vapor mixing ratio is shown by the blue lines for values of 2.0, 0.2, and $0.02\,\mathrm{gkg}^{-1}$ (from bottom to top); the location of thermal tropopause is indicated by the solid thick black line and separates also the region of tropospheric values ($N^2 < 1.5 \times 10^{-4}\,\mathrm{s}^{-2}$) from stratospheric values ($N^2 \sim 4.0 \times 10^{-4}\,\mathrm{s}^{-2}$) of static stability; the location of the dynamical tropopause, defined as the isosurface of potential vorticity $Q = 2.0\,\mathrm{pvu}$, is shown by the dashed thick line.

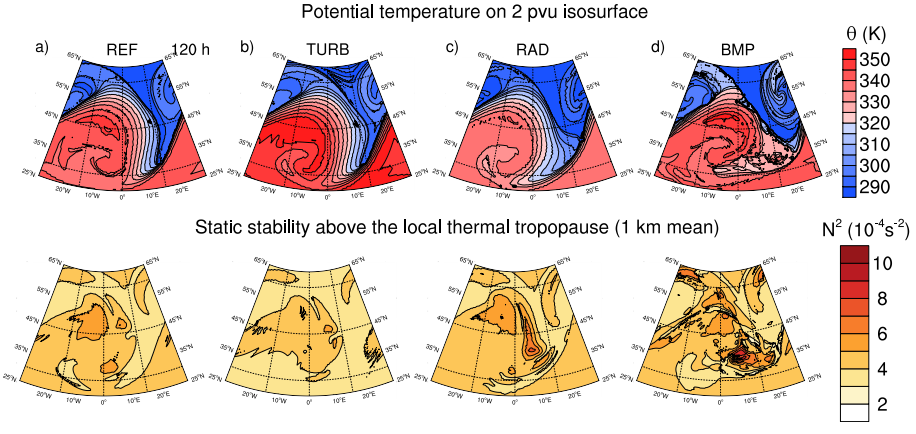

Figure 2. Dynamical and thermodynamical state of the baroclinic life cycles after 120 h of model integration. In the upper row the distribution of potential temperature Θ (in K) on the dynamical tropopause is depicted, while the lower row shows the distribution of static stability N^2 (in $10^{-4}\,\mathrm{s}^{-2}$) averaged over the first kilometer above the thermal tropopause. The four columns show from left to right the following simulations: **(a)** REF, **(b)** TURB, **(c)** RAD, and **(d)** BMP.

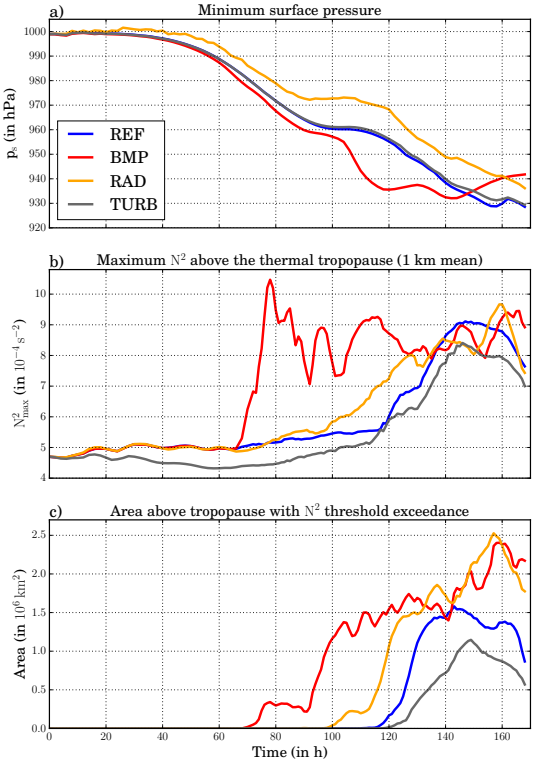

Figure 3. Temporal evolution over the entire simulated life cycles of **(a)** the minimum surface pressure p_{s} (in hPa), **(b)** the maximum static stability N^2_{max} (in $10^{-4}\,\mathrm{s}^{-2}$) above the thermal tropopause, and **(c)** the area $A_{5.5}$ (in $10^6\,\mathrm{km}^2$) of N^2 threshold exceedance above the thermal tropopause (with a threshold of $N^2 = 5.5 \times 10^{-4}\,\mathrm{s}^{-2}$). The colored lines indicate the following simulations: REF (blue), BMP (red), RAD (orange), and TURB (gray).

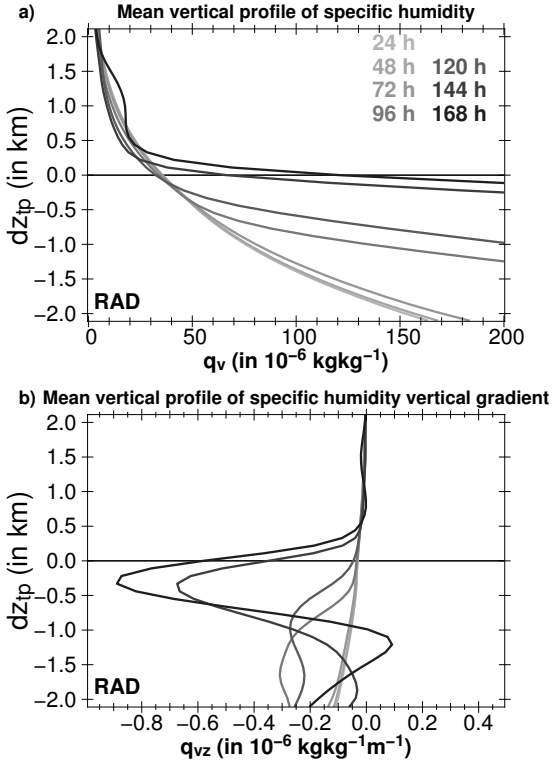

Figure 4. Instantaneous thermal tropopause based domain mean values of **(a)** specific humidity q_{v} (in $10^{-6}\,\mathrm{kg\,kg^{-1}}$) and **(b)** the vertical gradient of specific humidity $\partial q_{\mathrm{v}}/\partial z$ (in $10^{-6}\,\mathrm{kg\,kg^{-1}\,m^{-1}}$) for RAD. The domain mean is calculated within 25–65° latitude and the entire zonal domain. dz_{tp} is the distance to the height of the thermal tropopause. The intensity of the gray colors indicates the time since model start in 24 h intervals.

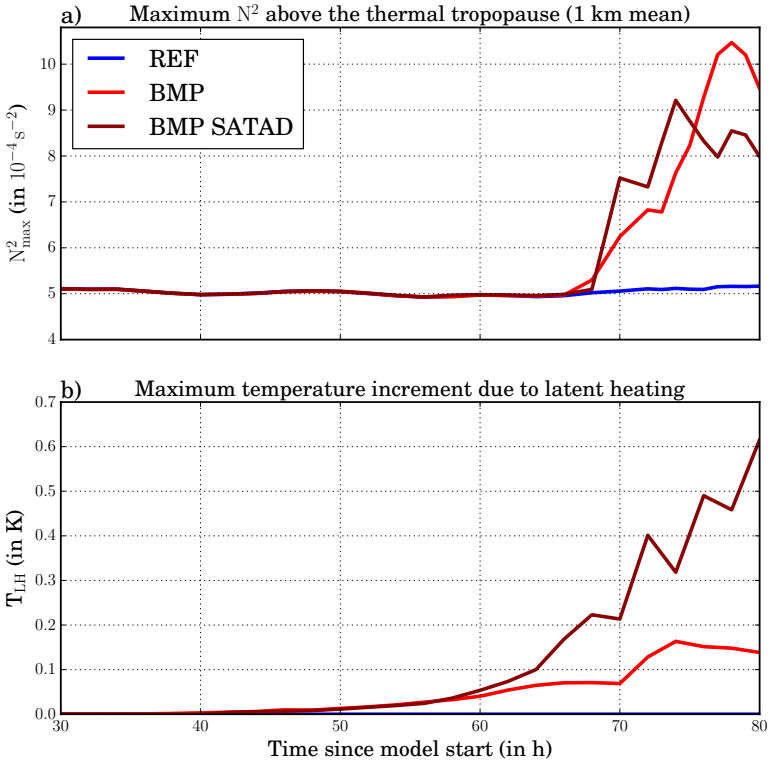

Figure 5. Temporal evolution between 30 h and 80 h after simulation start of **(a)** the maximum static stability N^2_{max} (in $10^{-4}\,\text{s}^{-2}$) above the thermal tropopause and **(b)** the maximum temperature increment due to latent heating T_{LH} (in K) in the model domain for REF (blue lines), BMP (red lines), and BMP SATAD (dark red lines).

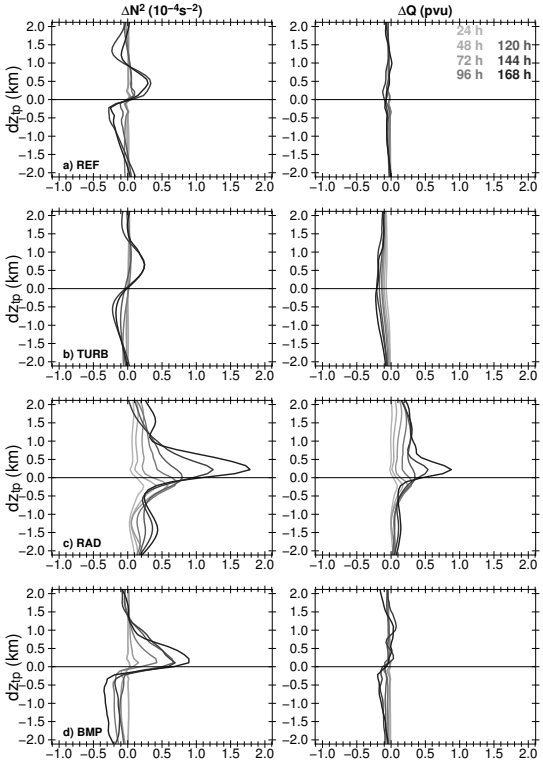

Figure 6. Instantaneous thermal tropopause based domain mean values of ΔN^2 (in $10^{-4}\,\mathrm{s}^{-2}$) in the left panels and ΔQ (in pvu) in the right panels for **(a)** REF, **(b)** TURB, **(c)** RAD, and **(d)** BMP. The domain mean is calculated within 25–65° latitude and the entire zonal domain. The intensity of the gray colors indicates the time since model start in 24 h intervals. ΔN^2 is the difference between the current static stability N^2 and the advected initial static stability N_0^2, ΔQ is the difference between the current potential vorticity Q and the advected initial potential vorticity Q_0. dz_{tp} is the distance to the height of the thermal tropopause.

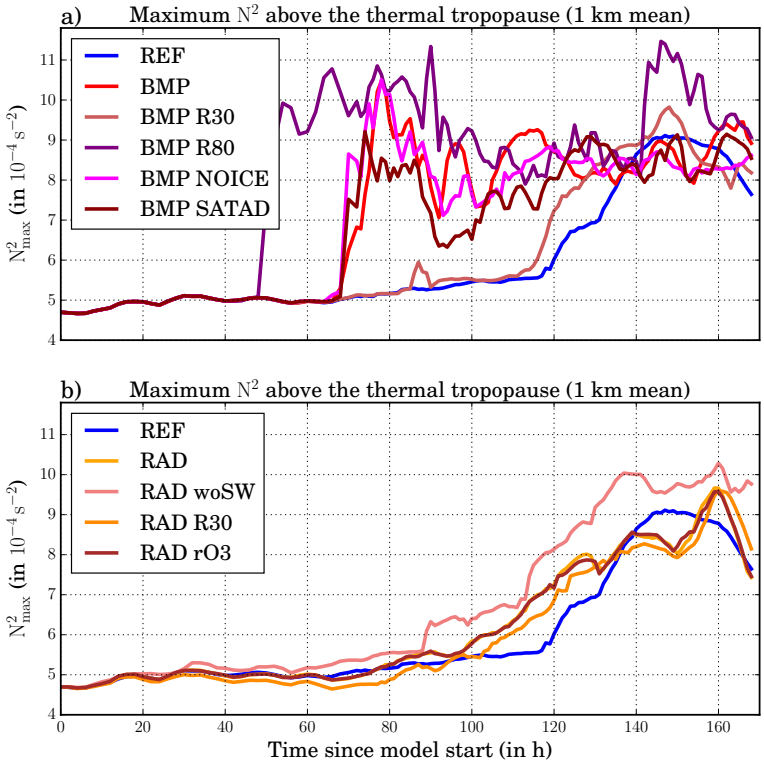

Figure 7. Temporal evolution of the maximum static stability N^2_{max} (in $10^{-4}\,\mathrm{s}^{-2}$) above the thermal tropopause for sensitivity simulations of **(a)** BMP and **(b)** RAD. In **(a)** N^2_{max} is shown for REF (blue), BMP (red), BMP R30 (light red), BMP R80 (purple), BMP NOICE (magenta), and BMP SATAD (dark red). In **(b)** N^2_{max} is shown for REF (blue), RAD (orange), RAD woSW (coral), RAD R30 (dark orange), and RAD rO3 (brown).

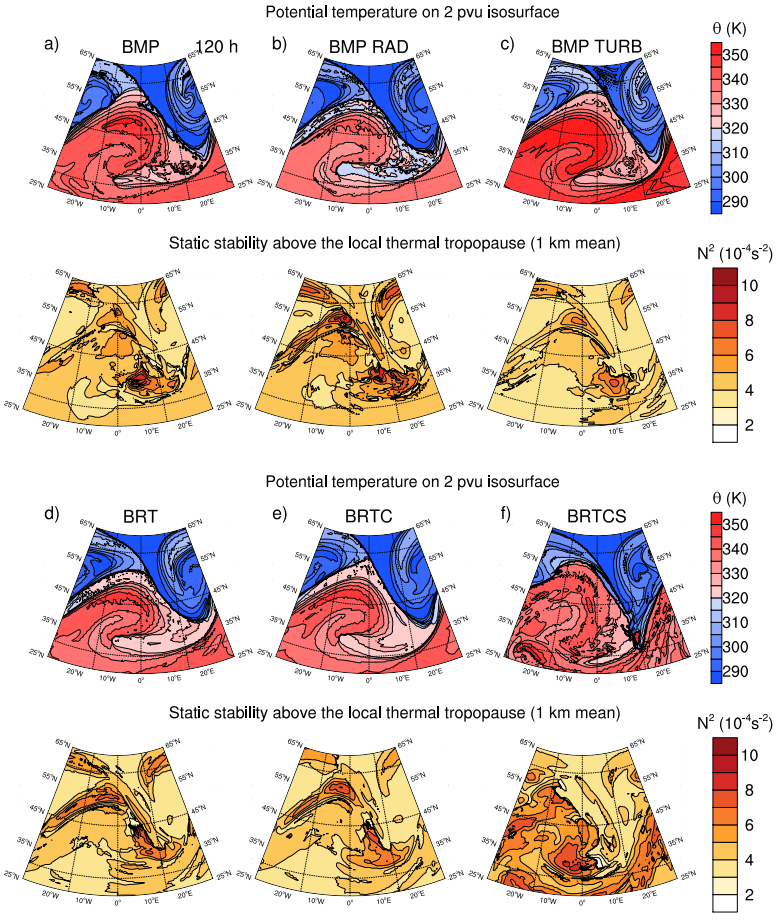

Figure 8. Dynamical and thermodynamical state of baroclinic life cycles after 120 h of model integration. In the upper rows of the six panels the distribution of potential temperature Θ (in K) on the dynamical tropopause is depicted, while the lower rows show the distribution of static stability N^2 (in $10^{-4}\,\mathrm{s}^{-2}$) averaged over the first kilometer above the thermal tropopause for **(a)** BMP, **(b)** BMP RAD, **(c)** BMP TURB, **(d)** BRT, **(e)** BRTC, and **(f)** BRTCS.

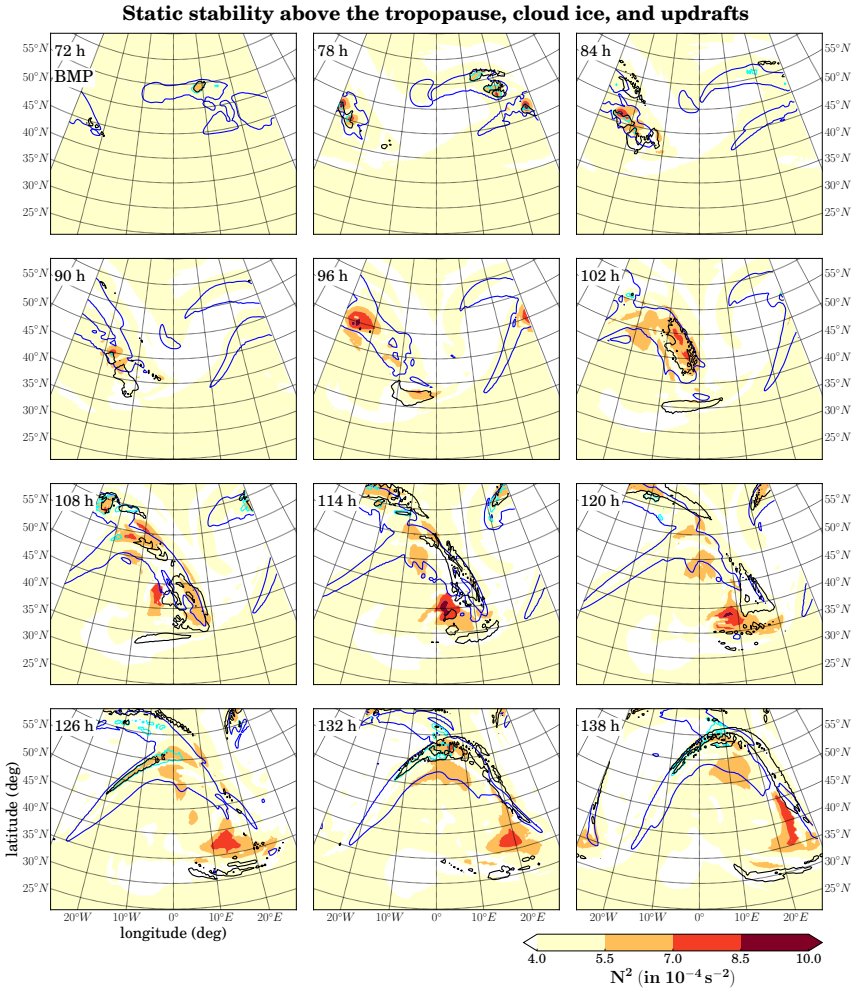

Figure 9. Static stability N^2 (color-coded, in $10^{-4}\,\mathrm{s}^{-2}$) above the thermal tropopause, Δz (black lines, in $2.5\,\mathrm{km}$), column integrated cloud ice content tq_i (blue lines, in $0.01\,\mathrm{kg\,m}^{-2}$), and tropopause close column integrated cloud ice content $tq_\mathrm{i,tp}$ (cyan lines, in $0.001\,\mathrm{kg\,m}^{-2}$). Tropopause close means the region between the thermal tropopause and $500\,\mathrm{m}$ below. The distribution is shown for BMP between $78\,\mathrm{h}$ and $138\,\mathrm{h}$ after simulation start in a six hourly interval.

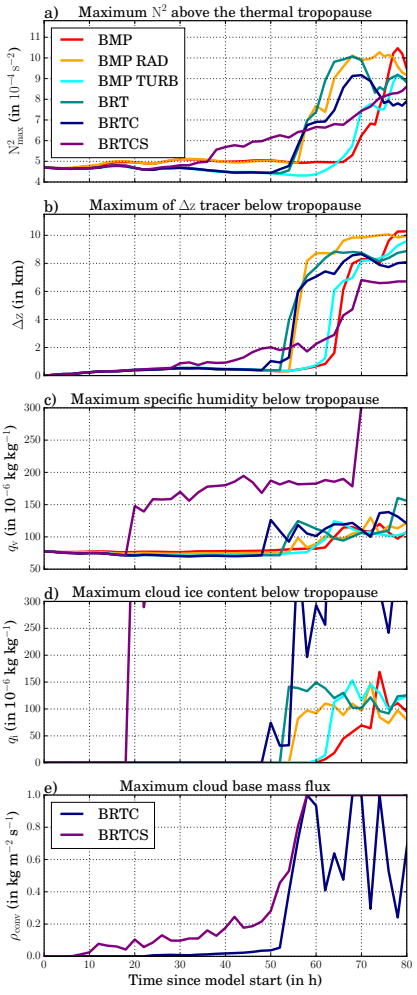

Figure 10. Temporal evolution over the first 80 h of the life cycles of **(a)** $N^2_{\max}$ (in $10^{-4}\,\mathrm{s}^{-2}$) above the thermal tropopause, **(b)** the maximum of the Δz tracer (in km) in a 500 m thick layer below the thermal tropopause, **(c)** the maximum specific humidity q_v in a 500 m thick layer below the thermal tropopause (in $10^{-6}\,\mathrm{kg\,kg}^{-1}$), **(d)** the maximum specific cloud ice content q_i in a 500 m thick layer below the thermal tropopause (in $10^{-6}\,\mathrm{kg\,kg}^{-1}$), and **(e)** the maximum cloud base mass-flux ρ_CONV (in $\mathrm{kg\,m}^{-2}\mathrm{s}^{-1}$). The time of TIL occurrence is split into three time sectors. Without radiation and convection, the TIL appears after 65 h, with radiation between 50 h-65 h, and with strong convection before 50 h (more information is given in the text). The colored lines indicate the following simulations: BMP (red), BMP RAD (orange), BMP TURB (cyan), BRT (dark cyan), BRTC (dark blue), and BRTCS (purple).

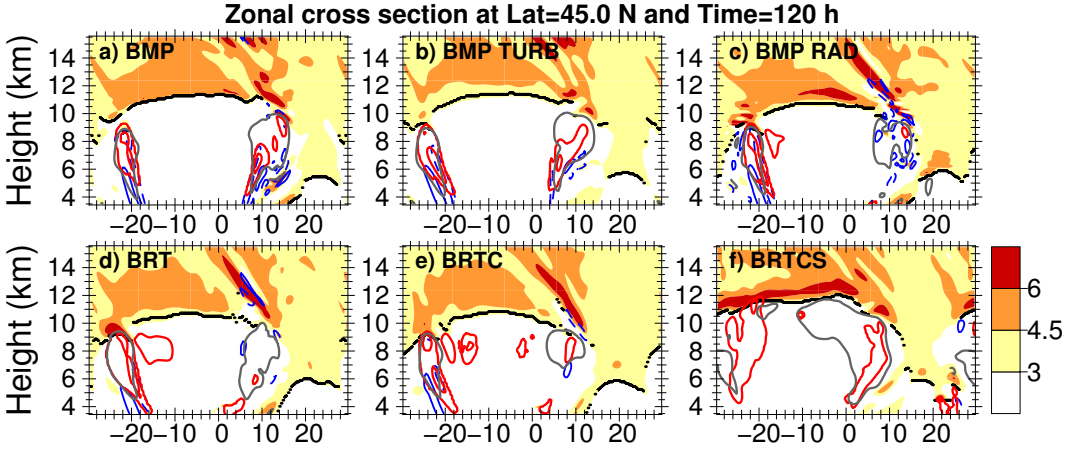

Figure 11. Zonal cross sections along 45° N of static stability N^2 (in $10^{-4}\,\mathrm{s}^{-2}$) after 120 h of model integration. Red lines show specific cloud ice content q_i (for $5.0\times10^{-6}\,\mathrm{kg\,kg}^{-1}$), solid blue lines show regions with positive values of $\partial w/\partial z$ (for $10.0\times10^{-5}\,\mathrm{s}^{-1}$), dashed blue lines show negative values (for $-10.0\times10^{-5}\,\mathrm{s}^{-1}$), and solid gray lines show regions with Δz tracer larger than $2.5\,\mathrm{km}$. The thick black line is the thermal tropopause. The six panels show **(a)** BMP, **(b)** BMP RAD, **(c)** BMP TURB, **(d)** BRT, **(e)** BRTC, and **(f)** BRTCS.

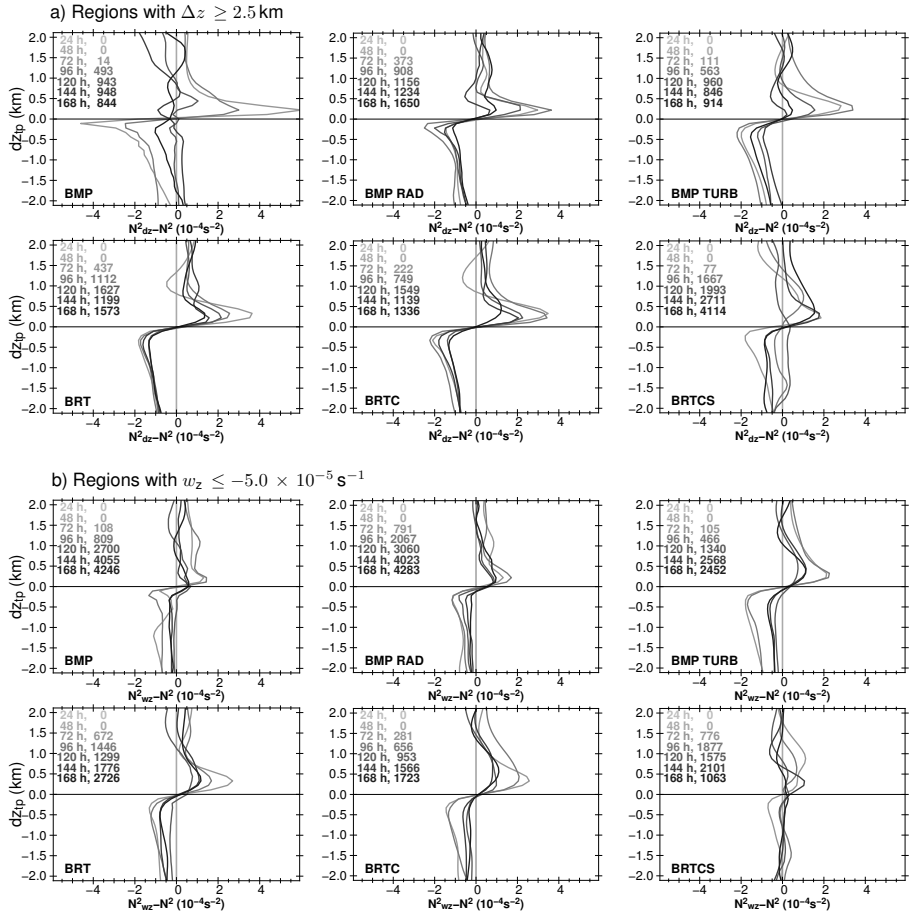

Figure 12. (a) Instantaneous thermal tropopause based vertical profiles of difference between the mean of static stability in regions with $\Delta z > 2.5\,\mathrm{km}$ N^2_{dz} and the domain mean N^2 (in $10^{-4}\,\mathrm{s}^{-2}$) for each 24 h of the model integration. **(b)** Differences for regions with $\partial w/\partial z \leq -5.0 \times 10^{-5}\,\mathrm{s}^{-1}$. The values in the top left corner of each panel show the number of individual profiles used for calculating the respective mean profile of N^2_{dz} and N^2_{wz}. dz_{tp} is the distance to the height of the thermal tropopause.

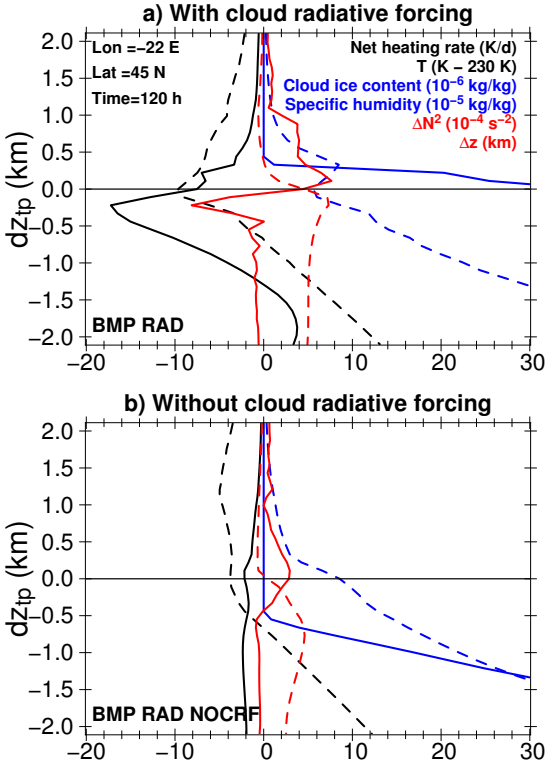

Figure 13. Tropopause based vertical profiles through an ice cloud along the central latitude at 120 h for **(a)** a simulation with cloud radiative forcing (BMP RAD) and **(b)** a simulation without cloud radiative forcing (BMP RAD NOCRF). Solid lines show net radiative heating (in $\mathrm{K\,d^{-1}}$, scaled for better comparability, black), cloud ice content (in $10^{-6}\,\mathrm{kg\,kg^{-1}}$, blue), and ΔN^2 (in $10^{-4}\,\mathrm{s^{-2}}$, red). Dashed lines show temperature (in $\mathrm{K} - 230\,\mathrm{K}$, black), specific humidity (in $10^{-5}\,\mathrm{kg\,kg^{-1}}$, blue), and Δz (in km, red). dz_{tp} is the distance to the height of the thermal tropopause.

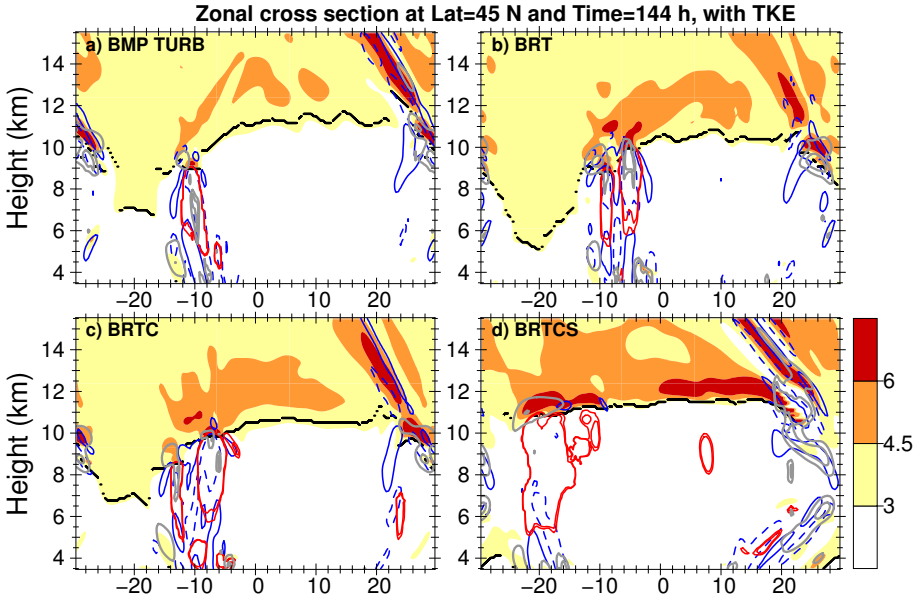

Figure 14. Zonal cross sections along 45° N of static stability N^2 (in $10^{-4}\,\mathrm{s}^{-2}$) after 144 h of model integration. Solid blue lines show regions with positive values of the vertical divergence $\partial w/\partial z$ (for $5.0,\ 50.0 \times 10^{-5}\,\mathrm{s}^{-1}$), dashed blue lines show negative values (for $-5.0,\ -50.0 \times 10^{-5}\,\mathrm{s}^{-1}$). Red lines show specific cloud ice content q_i (for $5.0,\ 10.0,\ \times 10^{-6}\,\mathrm{kg\,kg}^{-1}$). Gray lines show turbulent kinetic energy (TKE) (in $0.5, 1.0, 5.0\,\mathrm{m}^2\mathrm{s}^{-2}$). The four panels show **(a)** BMP TURB, **(b)** BRT, **(c)** BRTC, and **(d)** BRTCS.

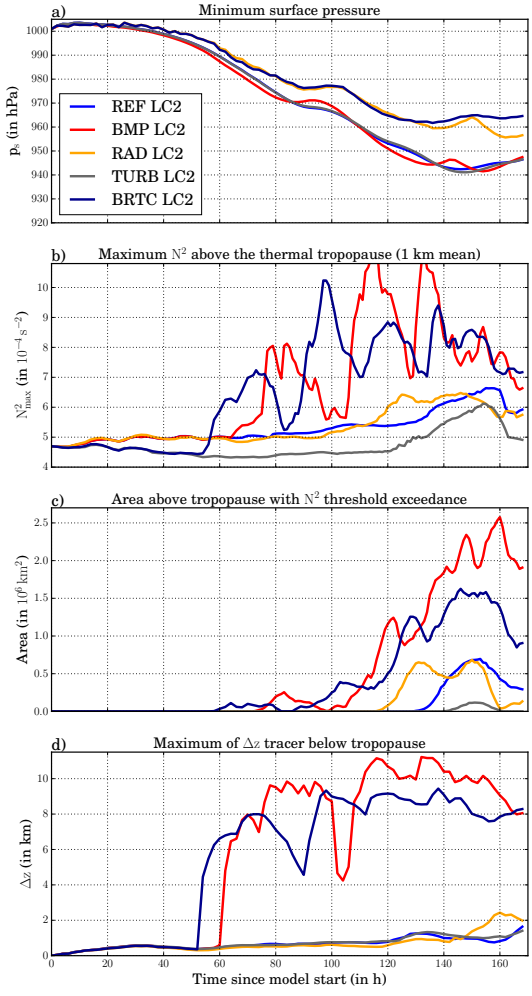

Figure 15. Temporal evolution over the entire simulated life cycles of **(a)** the minimum surface pressure p_s (in hPa), **(b)** the maximum static stability N^2_max (in $10^{-4}\,\mathrm{s}^{-2}$) above the thermal tropopause, **(c)** the area $A_{5.5}$ (in $10^6\,\mathrm{km}^2$) of N^2 threshold exceedance above the thermal tropopause (with a threshold of $N^2 = 5.5 \times 10^{-4}\,\mathrm{s}^{-2}$), and **(d)** the maximum of the Δz tracer (in km) in a 500 m thick layer below the thermal tropopause. The colored lines indicate the following simulations: REF LC2 (blue), BMP LC2 (red), RAD LC2 (orange), TURB LC2 (gray), and BRTC LC2 (dark blue).

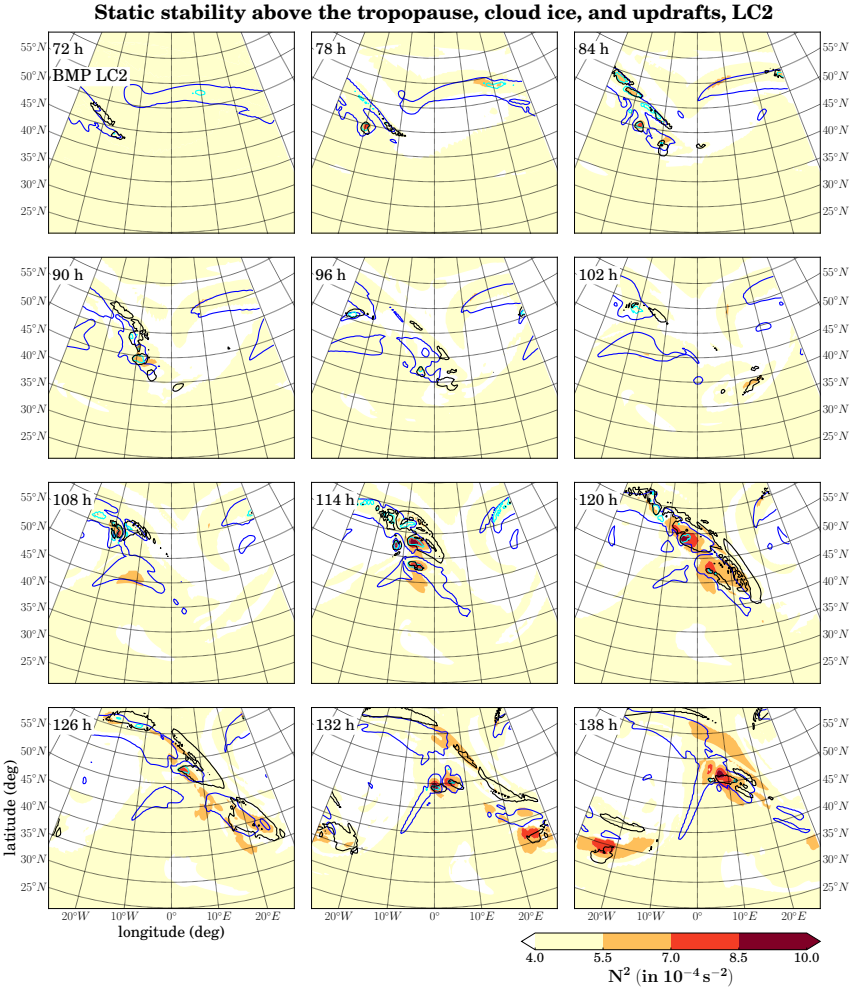

Figure 16. As Figure 9, but for BMP LC2.

Manuscript prepared for Atmos. Chem. Phys.
with version 2015/04/24 7.83 Copernicus papers of the LaTeX class copernicus.cls.
Date: 24 November 2015

The tropopause inversion layer in baroclinic life ~~cycles~~ cycle experiments: the role of diabatic ~~and mixing~~ processes

Daniel Kunkel[1], Peter Hoor[1], and Volkmar Wirth[1]

[1]Institute for Atmospheric Physics, Johannes-Gutenberg University Mainz, Germany

Correspondence to: Daniel Kunkel (dkunkel@uni-mainz.de)

Abstract. Recent studies on the formation of a quasi-permanent layer of enhanced static stability above the thermal tropopause revealed the contributions of dynamical and radiative processes. Dry dynamics lead to the evolution of a tropopause inversion layer (TIL) which is, however, too weak compared to observations and thus diabatic contributions are required. In this study we aim to assess the importance of diabatic ~~as well as mixing~~ processes in the understanding of TIL formation at midlatitudes. The non-hydrostatic model COSMO is applied in an idealized mid-latitude channel configuration to simulate baroclinic life cycles. The effect of individual diabatic ~~, i.e.~~ processes related to humidity~~and~~ , radiation, and ~~turbulent processes~~ turbulence is studied first to estimate the ~~additional contribution of~~ contribution of each of these processes to the TIL formation in addition to dry dynamics. In a second step these processes are stepwise included in the model to increase the complexity and finally estimate the relative importance of each process. The results suggest that including turbulence leads to a weaker TIL than in a dry reference simulation. In contrast, the TIL evolves stronger when radiation is included but the temporal ~~occurrence~~ evolution is still comparable to the reference. Using various cloud schemes in the model shows that latent heat release and consecutive increased vertical motions foster an earlier and stronger appearance of the TIL than in all other life cycles. Furthermore, updrafts moisten the upper troposphere and as such increase the radiative effect from water vapor. Particularly, this process becomes more relevant for maintaining the TIL during later stages of the life cycles. Increased convergence of the vertical wind induced by updrafts and by propagating ~~and potentially dissipating~~ inertia-gravity waves, which potentially dissipate, further contributes to the enhanced stability of the lower stratosphere. Furthermore, radiative feedback of ice clouds reaching up to the tropopause is identified to potentially further affect the strength of the TIL in the region of the ~~cloud.~~ clouds.

1 Introduction

The sharpness of the tropopause in the extratropics has gained increased attention in recent years (e.g., Gettelman and Wang, 2015). Local maxima of static stability, usually measured by the squared

Brunt–Vaisala frequency $N^2 = g/\Theta \cdot \partial\Theta/\partial z$ with g, the gravitational acceleration, Θ, the potential temperature, and z, the geometric altitude, inferred from radiosonde measurements (e.g., Birner et al., 2002; Birner, 2006) and Global Positioning System (GPS) radio occultation measurements (Randel et al., 2007), revealed the existence of a quasi-permanent inversion layer above the thermal tropopause. This tropopause inversion layer (TIL) is a distinct feature of the region of the upper troposphere and lower stratosphere (UTLS), from tropical to polar regions (e.g., Grise et al., 2010) and is also evident in general circulation models and climate analysis data sets (e.g., Birner et al., 2006).

Global studies of GPS temperature profiles and reanalysis data sets showed that the TIL is present at all latitudes (Grise et al., 2010; Gettelman and Wang, 2015). In the tropical lower stratosphere two maxima of enhanced static stability are found at about 17 and 19 km altitude. The upper peak shows a seasonal cycle with a winter maximum, while the lower peak has relatively large values all year round (Grise et al., 2010). In polar regions a distinct summer maximum occurs (Randel and Wu, 2010), while the TIL is evident in midlatitudes throughout the entire year with a slightly deeper appearance during winter (Bell and Geller, 2008). Generally, the smallest values of static stability above the thermal tropopause are evident in the region of the subtropical jet (Grise et al., 2010).

In several studies it was shown that a TIL can form from balanced, adiabatic and frictionless dynamics without explicit contributions from radiation in the extratropics. These idealized model simulations span the range from local to global scales, with studies of the dynamics of upper-level anomalies of potential vorticity (further abbreviated with PV) (Wirth, 2003, 2004), of baroclinic life cycles (Erler and Wirth, 2011), and of the dynamical response to a forcing of a Held–Suarez test (Held and Suarez, 1994) in a dry general circulation model (Son and Polvani, 2007). In the latter case, the TIL forms spontaneously under a wide variety of model parameters, such as horizontal and vertical model resolution. From the analysis of positive and negative PV-anomalies it was found that the sharpening of the tropopause was linked to the convergence of the vertical wind. Particularly, this was related to a cross-frontal circulation (Wirth, 2004). Furthermore, the TIL evolved stronger above ~~anticyclonic~~ anti-cyclonic than over cyclonic flow (Wirth, 2003). This result was confirmed in studies of adiabatic baroclinic life cycles, in which the TIL became evident after breaking of baroclinic waves (Erler and Wirth, 2011). Recently, the impact of dissipating inertia-gravity waves was suggested to persistently contribute to the formation and maintenance of the TIL. These waves result from imbalances along the jet and the dissipation may alter the thermal structure through energy dissipation, local heating, and turbulent motions (Kunkel et al., 2014). Moreover, Birner (2010) showed that the vertical structure of the residual circulation in the stratosphere contributes to the sharpening of the tropopause by inducing a dipole forcing of static stability around the tropopause. This process was identified to significantly add to the tropopause sharpening during winter in the midlatitudes.

Balanced dynamics alone, however, can not explain all features related to the TIL (Son and Polvani, 2007) and as has been shown by Randel et al. (2007) radiative processes contribute sig-

nificantly to the TIL. From fixed dynamical radiative transfer calculations it was concluded that water vapor cooling around the tropopause and heating by ozone in the lower and middle stratosphere contribute to a layer of enhanced static stability above the thermal tropopause. Particularly, the water vapor cooling has been identified to be a major process for the summer TIL in polar regions (Randel and Wu, 2010).

Thus, several mechanisms have been identified so far to explain the strength and occurrence of the TIL at all latitudes. Since dry dynamics are not sufficient to fully explain all features of the TIL, processes beyond adiabatic and frictionless dynamics are required to close this gap. Especially in the midlatitude tropopause region, all processes, synoptic-scale and stratospheric dynamics as well as the radiative forcings, need to be considered. With this knowledge we can ask the question which of the before mentioned processes is most important to form and maintain the TIL. In this study we aim to address this question in the framework of idealized baroclinic life cycles with a limited area, non-hydrostatic model. We extend the work of Erler and Wirth (2011) and include diabatic ~~and mixing~~ processes, i.e., related to humidity, radiation, or turbulence. These processes can violate material conservation of potential vorticity Q and are further referred to as non-conservative processes in this study. Since we focus on a rather short time scale, we assume that the effect of the stratospheric circulation is rather small and exclude this effect in the interpretation of our results. Thus, we focus mainly on the following questions: (1) How do non-conservative processes, i.e., diabatic ~~and mixing~~ processes, alter the TIL evolution in baroclinic life cycles compared to the well-known evolution in the adiabatic and frictionless case? (2) What is the relative importance of individual processes that contribute to the formation the TIL during different stages of the life cycles?

To answer these questions we structured our analysis as follows. In Sect. 2 we introduce the model setup along with the physical parameterizations and a summary of the conducted simulations. We then present results from two sets of simulations of so-called anti-cyclonic life cycles. In Sect. 3 we show results from baroclinic life cycles in which only one individual non-conservative process is turned on separately to address question (1). In a second set of simulations we show results of simulations with a successively increasing number of physical processes to address question (2) (Sect. 4). ~~We~~ Before we summarize our results and give further conclusions in Sect. 6~~.~~, we discuss the evolution of the tropopause inversion layer in experiments of the cyclonic life cycle in Sect. 5.

2 Model formulation and baroclinic life cycle experiments

2.1 Adiabatic model configuration and initial state

We conducted baroclinic life cycle experiments in an idealized, spherical, midlatitude channel configuration of the non-hydrostatic regional model COSMO (COnsortium for Small-scale MOdelling, Steppeler et al., 2003). For the adiabatic model we only ~~used~~ use the dynamical core of the model which solves the hydro-thermodynamical equations. Only a fourth order horizontal hyper-diffusion

had has to be applied to guarantee numerical stability. Physical processes such as microphysics, convection, turbulence, radiation are introduced in more detail further below (see Sect. 2.2). Time integration was is performed with a third order, two-time-level Runge–Kutta scheme, in which fast terms, i.e., sound and gravity waves, are stepped forward in time with a smaller time step. We use a fifth order centered finite difference approximation in the horizontal and a third order scheme in the vertical. Passive tracer advection was is done with a fourth order Bott Scheme with Strang splitting (Doms, 2011).

We studied study baroclinic waves with wavenumber six with a model setup similar to Erler and Wirth (2011) and Kunkel et al. (2014). Our model domain spans over $60°$ longitude and $70°$ latitude, from the surface up to a height of $25.0\,\mathrm{km}$ and with a grid spacing of $0.4°$ ($\sim 44\,\mathrm{km}$) in the horizontal and $110\,\mathrm{m}$ in the vertical in the region of the tropopause. Consequently, we obtain an aspect ratio ($\Delta z/\Delta x$) of about $1/400$ which is considered favorable to study the TIL (Birner et al., 2006; Erler and Wirth, 2011). In the uppermost seven kilometer of the model domain Rayleigh damping is applied to avoid reflection of upward propagating signals and there is no orography at the bottom. In meridional direction the boundary conditions are relaxed towards the initial values to avoid reflection of outgoing signals, while periodic boundary conditions are specified in the zonal direction.

For the initial conditions we follow Olson and Colle (2007) and Schemm et al. (2013) with slight adaptations to account for the spherical geometry of our approach. A background state is obtained for three dimensional fields of temperature, T, and pressure, p, from which a thermally balanced wind is calculated as in Erler and Wirth (2011). The initial vertical wind, w, is zero and the background state is baroclinically unstable by construction. However, to allow a fast evolution of the baroclinic wave, this state is superimposed by perturbation fields for p, T, u, and v which result from an inversion of a specified PV anomaly. This circular anomaly is introduced in the middle of the domain at the altitude of the tropopause. Slight changes in the initial state allow us to study various types of baroclinic life cycles (for details we refer to Olson and Colle, 2007). However, our focus To obtain a solution of our experiments that is known as LC2 (Thorncroft et al., 1993) , an additional cyclonic barotropic shear is added to the background state described above. However, the main focus of this study is on the classical LC1 wave type (Thorncroft et al., 1993), since it produces a stronger TIL in the adiabatic case (Erler and Wirth, 2011). This In Section 5 we will present differences in the evolution of the TIL in LC2 experiments. The LC1 type is characterized by a thinning trough which then forms a streamer and later a cut-off cyclone, while the baroclinic wave breaks anti-cyclonically. Thus, the LC1 is also known as the anti-cyclonic case. In contrast, in the LC2 a large cyclonic trough dominates the evolution of the wave with no streamer and no cut-off cyclone being evident. This case is known as the cyclonic case, since the wave breaks cyclonically. More details on the development of this wave these waves and the corresponding sharpening evolution of the tropopause type inversion layer are generally given in Erler and Wirth (2011) and for this setup especially the

LC1 setup specifically in Kunkel et al. (2014), where the authors used a higher resolution version of this model. It is noted here that the lower resolution model well reproduces the results of Kunkel et al. (2014). For this reason and because of the vast number of conducted model simulations (see Table 1), we decided to use a coarser grid spacing in our simulations.

Figure 1 shows the initial state in the center of our model domain. The zonal wind u has its maximum velocity between the thermal and dynamical tropopause (here defined as the $Q = 2.0\,\mathrm{pvu}$ contour line, with pvu = potential vorticity units, and $1.0\,\mathrm{pvu} = 1.0 \times 10^{-6}\,\mathrm{K\,m^2\,kg^{-1}\,s^{-1}}$). For the thermal tropopause we follow the definition given in *WMO* (1957) , where the tropopause is defined as the lowest level where the temperature lapse rate falls below $2.0\,\mathrm{K/km}$ and its average between this level and all higher levels within two km above this level remains below this value. The thermal tropopause further separates tropospheric ($N^2 < 1.5 \times 10^{-4}\,\mathrm{s^{-2}}$) from the stratospheric ($N^2 > 4.0 \times 10^{-4}\,\mathrm{s^{-2}}$) background values of static stability. The initial zonally symmetric specific humidity field, depicted with the blue lines, has been constructed such that it is comparable in magnitude and distribution to moisture profiles from re-analysis data. For this it is constructed as follows: a constant surface relative humidity ($\mathrm{RH_s}$) is given which decreases linearly with height everywhere. If not specified otherwise, $\mathrm{RH_s}$ is $60\,\%$ and decreases with a gradient of $10\,\%/2\,\mathrm{km}$. Thus, above $12\,\mathrm{km}$ altitude the relative humidity (RH) is zero. The model, however, requires specific humidity q_v as input variable. This quantity is obtained by multiplication of the relative humidity with the saturation specific humidity ($q_\mathrm{vs} : q_\mathrm{v} = \mathrm{RH}/100 \cdot q_\mathrm{vs}$). The latter quantity is computed from the saturation water vapor, which is computed with the parameterization of Magnus (Murray, 1967). A final constraint is given for the initial distribution of q_v, i.e., that $\min(q_\mathrm{v}) = 2.0 \times 10^{-6}\,\mathrm{kg\,kg^{-1}}$. Note that this leads to a constant initial value of $q_\mathrm{v} = 2.0 \times 10^{-6}\,\mathrm{kg\,kg^{-1}}$ in the stratosphere in our simulations.

We further use passive tracers to diagnose particular features of our baroclinic life cycles. These tracers are purely advected and not explicitly mixed vertically or horizontally by a parameterization scheme. However, mixing due to numerical reasons does still affect the tracer distribution. In particular, we use three tracers which carry information of the initial state of the baroclinic life cycles: (1) the initial height of each grid box z_0, (2) the initial static stability N_0^2, and (3) the initial potential vorticity Q_0. With these tracers it is possible to calculate the differences between the current and the initial distribution of these quantities and as such obtain information about whether an air parcel has gained or lost (1) altitude, measured by $\Delta z = z - z_0$, (2) static stability, measured by $\Delta N^2 = N^2 - N_0^2$, and (3) changed their potential vorticity because of non-conservative processes, measured by $\Delta Q = Q - Q_0$, with $Q = \varrho^{-1}\boldsymbol{\eta} \cdot \nabla\Theta$ and ϱ air density, $\boldsymbol{\eta}$ absolute vorticity, and Θ potential temperature.

2.2 Formulation of non-conservative processes in COSMO

2.2.1 Turbulence

Turbulence is calculated for the three dimensional wind (u, v, and w), the liquid water potential temperature (Θ_l), and the total water (q_w) which is the sum of specific water vapor q_v and specific cloud water q_c. Budget equations for the second order moments are reduced under application of a closure of level 2.5 (in the notation of Mellor and Yamada, 1982), i.e., local equilibrium is assumed for all moments except for turbulent kinetic energy (TKE), for which advection and turbulent transport is retained. Three dimensional turbulent effects are neglected which is a valid approximation for simulations on the mesoscale, which means that horizontal homogeneity is assumed. Hence, only vertical turbulent fluxes are parameterized under consideration of the Boussinesq approximation. Moreover, the TKE budget equation depends significantly on the vertical shear of the horizontal wind components and the vertical change in Θ_l and q_w. More details are given in Doms (2011).

2.2.2 Cloud microphysics

Cloud microphysics follow a bulk approach using a single moment scheme with five types of water categories being treated prognostically: specific humidity q_v for the gas phase, two non-precipitating cloud types, i.e., cloud water q_c and cloud ice q_i, as well as two precipitating types, i.e., rain q_r and snow q_s. These five water types can interact within various processes such as cloud condensation and evaporation, depositional growth and sublimation of snow, evaporation of snow and rain, melting of snow and cloud ice, homogeneous and heterogeneous nucleation of cloud ice, autoconversion, collection and freezing. More details are given in Doms (2011) and Joos and Wernli (2012).

2.2.3 Radiation

Radiation is parameterized by the δ-2 stream approximation, i.e., separate treatment of solar and terrestrial wavelengths. In total, eight spectral bands are considered, five in the solar range and three infrared bands. Absorbing and scattering gases are water vapor ($\mathrm{H_2O}$) with a variable content as well as $\mathrm{CO_2}$, $\mathrm{O_3}$, $\mathrm{CH_4}$, $\mathrm{N_2O}$, and $\mathrm{O_2}$ with fixed amounts. Aerosols have been totally neglected whereas a cloud radiative feedback can be calculated in all spectral bands. Further details about the general scheme are given in Ritter and Geleyn (1992) and about the implementation in Doms (2011).

2.2.4 Convection

The scheme of Tiedtke (1989) is used to parameterize sub-grid scale convective clouds and their effects on the large scale environment. This approach uses moisture convergence in the boundary layer to estimate the cloud base mass-flux. The convection scheme then affects the large-scale budgets of the environmental dry static energy, the specific humidity, and the potential energy.

2.2.5 Surface fluxes

Instead of using a bottom free-slip boundary condition surface fluxes of momentum and heat are calculated explicitly in one experiment. This results in non-zero turbulent transfer coefficients of momentum and heat and thus affects the roughness length and the fluxes of latent and sensible heat. As we will show later, this has some significant effects on the initiation of convection.

2.3 Simulations of baroclinic life cycles

In total we present the results of 17 different simulations of ~~baroclinic life cycles~~ the anti-cyclonic and of five different simulations of the cyclonic baroclinic life cycle (see Table 1). Variations between the individual simulations are introduced by either the kind or the number of non-conservative processes. Moreover, additional variability is created by changing the initial humidity as well as by the complexity of treating cloud related processes.

In a first set of simulations, we conducted four different baroclinic life cycles. Using the adiabatic and frictionless life cycle as conservative reference simulation (REF), we obtain further results from life cycles additionally including either turbulence, further denoted as TURB, or radiation, RAD, or bulk microphysics, BMP. For these simulations we apply the standard physical parameterizations of COSMO, which were briefly described in the previous section.

We performed further sensitivity simulations for BMP and RAD to test for the impact of initial conditions as well as the model formulation of a diabatic process. For microphysics we conducted in total four additional life cycle experiments. We first tested for the initial specific humidity q_v. In one case we reduced the initial q_v by setting the surface relative humidity to $30\,\%$ and the gradient to $5.0\,\%/2\,\mathrm{km}$ (BMP R30), while we increased the initial q_v by using $\mathrm{RH_s} = 80\,\%$ and a gradient of $13.33\,\%/2\,\mathrm{km}$ in another case (BMP R80). Furthermore, we conducted simulations in which we used different schemes to represent cloud processes. In one simulation only warm phase clouds are considered, excluding cloud ice (BMP NOICE). In another simulation condensation and evaporation between water vapor and cloud water is realized by a saturation adjustment process (BMP SATAD). Since this simulation includes only large scale diabatic effects from latent heating, it has the least additional effects compared to the dry reference (Schemm et al., 2013). ~~Thus, we refer to this case as quasi-adiabatic case (QADI).~~

In case of radiation we performed sensitivity simulations with respect to the initial distribution of specific humidity and ozone. These two trace gases are thought to have the largest impact on the thermal structure around the tropopause (e.g., Randel et al., 2007; Riese et al., 2012). We conducted one simulation with reduced initial specific humidity (RAD R30), similar to BMP R30, while we explicitly set the specific humidity to zero above the tropopause in another simulation (RAD woSW). In another case we reduced the amount of ozone (RAD rO3). However, we explicitly note here that ozone is poorly represented in the model. Instead of a three dimensional distribution, only a simple

vertical distribution is assumed which has a maximum concentration at altitudes which are close to our model top at a pressure of $42\,\mathrm{hPa}$ and a total vertically integrated ozone partial pressure of $0.06\,\mathrm{Pa}$. These two parameters are used in the radiation code to calculate the feedback of the solar and thermal extinction by ozone. We reduced the total amount of ozone by one third to estimate whether this has an impact on the strength of the TIL.

In a next step we use a set of simulations with combinations of non-conservative processes to study potential additive effects as well as to assess the relative contribution of individual processes on the TIL formation and maintenance during different stages of the life cycles. For this we compare results from BMP (here as a reference) to results from simulations where we first add radiation (BMP RAD) and turbulence (BMP TURB) individually and then together (abbreviated with BRT for BMP RAD TURB). In further simulations we include convective clouds (~~BMP RAD TURB CONV~~BRTC) and surface fluxes (~~BMP RAD TURB CONV SURF~~BRTCS). The convective activity is much stronger in the simulation with surface fluxes than in the simulation with the free-slip boundary condition. Hence, ~~BMP RAD TURB CONV SURF~~BRTCS can be regarded as simulation with strong convection, while ~~BMP RAD TURB CONV~~BRTC can rather be seen as life cycle with weak to moderate convective activity. A final sensitivity study was conducted in which the cloud radiative forcing has been neglected to study the effect of this feedback in the region of the tropopause (BMP RAD NOCRF).

3 Non-conservative processes and the formation of a TIL in baroclinic life cycles

In a first step we aim to answer the question which non-conservative process, i.e., related to clouds, radiation, or turbulent mixing has the largest impact on the formation of the TIL in baroclinic life cycles. For this we compare first the results of four ~~life cycles,~~ anti-cyclonic life cycles (REF, ~~BMP~~TURB, RAD~~), vertical turbulence TURB, and~~ , and ~~REF~~BMP), before we discuss the effects of initial conditions and process formulations on the model results.

3.1 Impact of non-conservative processes on the TIL evolution

The baroclinic life cycle 1, also known as LC1, has been discussed under various aspects (e.g., Thorncroft et al., 1993) and also in light of the evolution of the tropopause inversion layer (Erler and Wirth, 2011). Our REF simulation features the same general characteristics of this life cycle and is described in more detail in Kunkel et al. (2014). One dominant feature of the LC1 is the thinning trough, the so-called stratospheric streamer (often also referred to as Θ- or PV-streamer, e.g., Sprenger et al., 2003). In the mature stage of the baroclinic wave this feature is evident for instance in the distribution of potential temperature Θ on an isosurface of potential vorticity, e.g., $Q = 2.0\,\mathrm{pvu}$. The distribution of potential temperature for our four cases is shown in the upper row

of Fig. 2. After 120 h of model integration we see similar structures for REF, TURB, and RAD with minor differences in the exact location of the streamer and the absolute values of Θ in the warm sector (red colors). The most complex distribution occurs in BMP with ~~higher~~ warmer temperatures than in the other three simulations at the southern tip of the streamer. These warmer temperatures are associated with cloud processes and the release of latent heat during rapid ascent. Moreover, the entire Θ-field shows a more in-homogeneous appearance compared to the other three simulations.

Our main focus is, however, on the static stability N^2 in the lowermost stratosphere. In particular, we are interested in the regions where the stability increases significantly during the life cycle. This is typically the case within the first kilometer above the thermal tropopause. However, the spatial appearance is not homogeneous, as is evident from the lower panels in Fig. 2. These panels depict the vertical mean of N^2 over the first kilometer above the thermal tropopause. In all four cases large values of N^2 appear in the warm sector west of the streamer, which is in the region of anti-cyclonic flow. This region has been shown to exhibit a stronger TIL in models (Erler and Wirth, 2011; Wirth, 2003) and in observations (Randel et al., 2007). The life cycle with turbulence shows the lowest values of N^2, while the static stability has generally larger values in the case of radiation than in the reference simulation. In the life cycle with cloud processes we additionally see enhanced values of N^2 on smaller scales than in the other cases. As we will show later these enhancements are related to moist dynamics and vertical motions.

The moist life cycle shows the strongest development in terms of minimum surface pressure, p_s, evolution, in contrast to the life cycle with radiation (Fig. 3a). While all other life cycles show still a deepening of p_s, the absolute minimum pressure has already been reached in BMP after 140 h of model integration. Moreover, by considering two metrics to trace the evolution of the TIL in our life cycles, we infer that the TIL formation differs most significantly from the dry reference case in the moist life cycle. The maximum static stability N^2_max increases rather ~~spontaneously~~ suddenly in BMP instead of more gradually as in the other three simulations (Fig. 3b). After reaching its absolute maximum value, N^2_max keeps values above $7.0 \times 10^{-4}\,\mathrm{s}^{-2}$ at consecutive times. Only after about 130 h after model start N^2_max in RAD~~than~~, and a little bit later in REF and TURB, has reached the same magnitude as in the moist simulation. Furthermore, an earlier increase of N^2_max is evident in RAD than in REF and TURB, while in the latter case N^2_max is smaller than in the reference case at all times. A similar picture is obtained from the metric that is used as a proxy for the spatial extent of the TIL in the life cycles, i.e., the area in which $N^2 > 5.5 \times 10^{-4}\,\mathrm{s}^{-2}$, denoted as $A_{5.5}$ (Fig. 3c). The earliest appearance is evident in BMP, the latest in TURB. Moreover, the temporal evolution of $A_{5.5}$ clearly shows that the TIL covers a larger area when ~~diabatic~~ moist or radiative processes are included in the life cycles. We also tested other thresholds for N^2 for this metric with no significant changes with respect to the qualitative interpretation of our results.

So far, we provided a rather descriptive view on the TIL evolution in our life cycles without giving details about the underlying processes. For the case with turbulence the TIL appears weaker due to

the tendency of turbulence to reduce strong vertical gradients. Turbulence acts against the effects of dry dynamics which enhance the lower stratospheric stability during the life cycle. Consequently, only a weak TIL forms in this case.

Including radiation results in a stronger TIL than in the reference case. This is related to the radiative feedback of water vapor, which increases over time in the region of the tropopause (Fig. 4a). Since no microphysics is included in RAD, water vapor is transported as a passive tracer in this simulation. Upward motions in the troposphere and tropopause dynamics lead to more water vapor at the altitude of the tropopause, finally changing the water vapor gradient significantly (Fig. 4b). This causes differential cooling by water vapor in the UTLS, which then results in a non-uniform change of the thermal structure (e.g., Zierl and Wirth, 1997). Additionally, recently lifted, moist air is then partly located also in the lower stratosphere, where its residence time is longer and thus can potentially affect the thermal structure over longer time scales. This process further enhances the static stability directly above the tropopause and thus strengthens the TIL which also forms by the dynamics of the baroclinic wave. Thus, a process directly changing the thermal structure alters the appearance of the TIL in the case with radiation.

In the moist case we present evidence that a process at lower tropospheric levels is responsible for the different appearance of the TIL. The spontaneous increase in N^2_{max} is well correlated with the earliest release of latent heat in the model (Fig. 5a and b). Since the same effect is evident from the simulation with the saturation adjustment scheme (~~QADI~~BMP SATAD), we can conclude that it is the release of latent heat rather than a microphysical process being responsible for the observed effect. Latent heat release is, however, not only a sign of condensation but also fosters vertical motions in the model. These vertical motions reach in many cases the tropopause and often lift this vertical transport barrier. Consequently, also the air above is slightly lifted~~which increases the convergence of isentropic surfaces and thus enhances the~~ , thereby increasing the vertical gradient of potential temperature, resulting in enhanced static stability above the tropopause. This process differs, however, fundamentally from the process related to dry dynamics on spatial and temporal scales. While the latter is rather slow and occurs predominantly in an anti-cyclonic flow region with on average descending air motion, this lifting process is fast, occurs on small scales, and is related to upward motions. Thus taken together, the incorporation of water in the model fosters a stronger TIL development as consequence of enhanced upward motions within the life cycle due to the release of latent heat.~~The relation between moisture and vertical motions in~~ Our results agree with those obtained by Gutowski et al. (1992) . They compared dry and moist baroclinic life cycles ~~has also been discussed by Gutowski et al. (1992)~~ and showed that including moisture leads to stronger updrafts as well as to a faster evolution of the life cycle.

Although the temporal and spatial appearance of the TIL is rather heterogeneous in all four simulations, the TIL becomes also evident in the domain mean vertical profiles of N^2. These averages are obtained between 25°–65° N in the meridional direction and in the entire zonal direction. ΔN^2

represents the difference between the current N^2 and the passively advected tracer N_0^2 (Fig. 6~~a~~, left panels) and ΔQ the difference between the current potential vorticity Q and the passively advected initial potential vorticity Q_0 (Fig. 6~~b~~, right panels), respectively. The vertical profiles of ΔN^2 and ΔQ are given in a tropopause based coordinate system for every 24 h of the model integration and the thin solid line shows the location of the tropopause. In all four simulations an increase in static stability forms sooner or later during the life cycles just above the tropopause. While the domain mean TIL appears only during the late stages in REF and TURB, it is much earlier obvious in RAD and BMP. However, PV at the tropopause shows significant positive changes only in the simulation with radiation. The location of the maximum diabatic change in PV correlates temporally and spatially (relative to the thermal tropopause) well with the changing gradient of water vapor (see Fig. 4). Moreover, this change in PV occurs over large areas in the model domain (not explicitly shown) and is thus clearly evident in the mean vertical profile of ΔQ. In simulations of real extratropical cyclones over the North Atlantic, the evolution of a dipole structure with a positive PV anomaly above the tropopause and a negative anomaly below have been reported by Chagnon et al. (2013) . They could also show that these anomalies are largely related the radiation scheme in their model. In contrast, only minor changes of PV are found in the simulations with turbulence and cloud processes. In the latter case the largest changes of PV occur rather at low- and mid-tropospheric altitudes where the major release of latent heat occurs. These changes occur, however, on smaller spatial areas, and more specifically not always at the same altitude relative to the tropopause. Thus, compared to RAD ΔQ has no pronounced tendency in the domain mean in case of BMP. In the reference case the minor changes of potential vorticity are solely related to the numerics, especially to the tracer advection scheme (Kunkel et al., 2014). Thus, in case of radiation the formation of the TIL is directly related to a diabatic process in the tropopause region, while the diabatic processes related to clouds have an indirect impact on the TIL, i.e., the diabatic processes and the response of the static stability above the tropopause occur at a different places. Mixing, like radiation, also directly affects the TIL but to a much lesser extent.

3.2 Sensitivity of individual diabatic processes

In the next paragraphs we briefly discuss the impact of initial conditions on the model results, focusing especially on experiments with cloud microphysics and radiation.

For microphysics we tested for the amount of initial specific humidity, comparing BMP to BMP R30, and BMP R80, as well as for the representation of the cloud processes, comparing BMP to BMP NOICE, and ~~QADI~~BMP SATAD. From the temporal evolution of $N^2_{\max}$ (Fig. 7a) we infer that the amount of specific humidity is more important than the model formulation of cloud processes. If more water is initially present, then the TIL appears earlier. In contrast, with less initial water the TIL appears later and the entire appearance approximates towards the adiabatic case. Moreover, the occurrence of the

TIL is relatively insensitive to the representation of the cloud processes as long as the initial amount of specific humidity is the same as it is the case in BMP, BMP NOICE, and ~~QADI~~BMP SATAD.

In case of radiation we tested for the initial amount and distribution of water, comparing RAD to RAD R30, and RAD woSW, as well as for the amount of ozone, comparing RAD to RAD rO3. We find only minor differences in the evolution of $N^2_{\max}$ for the various sensitivity simulations (Fig. 7b). Reducing the amount of water leads to a reduced radiative feedback and thus to a less strong TIL. Changing the amount of ozone has, in our case, no significant effect at all, however, with the caveat of the simple representation of ozone in our model. The largest difference is found if we completely remove the water in the stratosphere. This results in an artificially ~~high~~ large water vapor gradient between the troposphere and the stratosphere. As we have seen before (Fig. 4), a strong water vapor gradient results in a sharp tropopause. A similar result has been discussed by Fusina and Spichtinger (2010) who studied amongst many other features the response of the static stability to the sharpness of a gradient between saturated and unsaturated air.

4 Relative importance of dynamical and diabatic processes on the TIL formation

Until here we provided new insights of the isolated effect of individual physical processes on the formation of the tropopause inversion layer in baroclinic life cycles. Now we turn our discussion to the relative importance of these processes, and especially whether the dynamical or the radiative forcing is more important for the TIL formation and maintenance. For this purpose we use our second set of baroclinic life cycle experiments where we successively increase the number of processes and as such increase complexity. The simulation with cloud processes (BMP) serves as reference while we first add radiation (BMP RAD) and turbulence (BMP TURB) separately and then combine all three processes (~~BMP RAD TURB~~BRT). We further add convection (~~BMP RAD TURB CONV~~BRTC) and then also surface fluxes of momentum and heat (~~BMP RAD TURB CONV SURF~~BRTCS).

The six life cycles evolve similar, all forming a Θ-streamer and anti-cyclonic wave breaking. Again the temperature distribution at the southern tip of the streamer varies most between the individual life cycles (Fig. 8). Moreover, in some cases a smooth Θ-distribution is evident, e.g., BMP TURB, ~~BMP TURB RAD~~BRT, or ~~BMP TURB RAD CONV~~BRTC, while the distribution is more variable and shows more small scale features in other life cycles, especially in ~~BMP RAD TURB CONV SURF~~BRTCS. ~~The~~ In all six cases the static stability above the tropopause ~~has its largest values~~ is larger in the anti-cyclonic part of the wave ~~where often two maxima~~ than in the cyclonic part (not explicitly shown). After 120 h at least two regions with enhanced values of N^2 are evident. ~~The first maximum occurs~~ One is further to the north along the cold front ahead of the cyclonic center~~where the~~. The other is more located at the south-western edge of the streamer. As evident from the time series in Figure 9 both maxima are related to the outflow of the warm conveyor belt (WCB)~~lifts moist~~. This airstream

lifts moist, low-tropospheric air masses into the tropopause region. ~~Such a~~ The existence of a relation between WCB and TIL has been proposed by ~~Peevey et al. (2014)~~ Peevey et al. (2014) who used HIRDLS satellite and ECMWF model data to obtain their results. ~~The other maximum is located more at the western side of the streamer where~~ Moreover, Figure 9 shows that enhanced values of static stability above the tropopause are closely related to the location of strong updrafts and cirrus clouds at the time of the first TIL appearance. The cirrus clouds are identified by the cloud ice content below the tropopause. We refer to strong updrafts here, when an air mass has been lifted by at least 2.5 km since model start. This change in altitude of an air parcel is calculated from the difference of the current altitude z of this air parcel and its initial altitude z_0, which is carried by a passive tracer. We further denote this difference as Δz which is positive if an air parcel raised and negative if an air parcel descended since model start. The static stability is enhanced almost at all times in the center of the WCB outflow, where the ice cloud branches towards the north-west and south-east. From 102 h onward a second maximum is evident in the south-eastern branch of the ice cloud which moves further to the south in subsequent hours. This maximum is located more in the region where inertia-gravity waves are generated and influence the thermal structure of the tropopause (Kunkel et al., 2014). This influence is such that the static stability maximum keeps its large values almost entirely constant at subsequent hours of the simulation. In case of ~~BMP RAD TURB CONV SURF~~BRTCS a larger area exhibits enhanced static stability values above the tropopause which is the result of convective activity as we will see later in more detail.

In the following we aim to answer the question why the TIL appears earlier in some life cycles and how the TIL is maintained after it has been generated. We first compare the time of first appearance of the TIL between the six life cycles. Figure ~~9~~10a–e shows the first 80 h of model integration for various variables. The initial increase of N^2_{max} can be divided into three sections which are related to the physical processes considered in the respective life cycle (Fig. ~~9~~10a). The latest TIL appearance after about 65 h is found when considering only cloud processes and turbulence. Including radiation to the model simulations shifts the time of appearance ten hours ahead, while the earliest TIL formation starts already after about 35 h in case of considering convection and surface fluxes. This division into three time sectors correlates well with ~~a~~ the proxy for strong updrafts ~~, for which we use the tracer which carries the initial height information of an air parcel. With this information we can calculate the difference~~ Δz ~~which is positive if an air parcel raised and is negative if air parcel descended since model start~~. Figure ~~9~~10b depicts the maximum Δz in the layer between the thermal tropopause and 500 m below this level, from which we infer that there is strong temporal coincidence between the first appearance of N^2_{max} and updrafts originating at low levels. The earlier appearance of updrafts in case with radiation and convection is related to the these processes, since they foster an earlier emerging of ~~conditional instability.~~ updrafts in the model. This finding supports our results from the previous section that moist dynamics including ~~strong updrafts~~ stronger updrafts than in the dry case has a strong impact on the first appearance of the TIL. These up-

drafts further enhance the local convergence of the vertical wind just above the tropopause as we will see later. Moreover, we find good agreement between the temporal increase of $N^2_{\max}$ and two tracers for moisture, specific humidity q_v (Fig. ~~9~~10c) and specific cloud ice content q_i (Fig. ~~9~~10d). Thus, the updrafts moisten the upper troposphere below the tropopause which, as shown before, supports the TIL formation by differential radiative cooling. The gradual increase of $N^2_{\max}$ in case of ~~BMP RAD TURB CONV SURF~~BRTCS can further be related to another tracer for updrafts, which is the cloud base mass flux which is available for the two simulations in which the convective cloud parameterization is switched on (Fig. ~~9~~10e). This quantity serves as proxy for convective activity and starts to increase gradually in the case with surface fluxes early during the simulation. Thus, these findings further support our suggestion from Sect. 3 that vertical motions are the essential key parameter for the initial TIL appearance in baroclinic life cycles with ~~diabatic and mixing~~ moist diabatic processes.

We further provide evidence that there is not only a temporal but also a spatial coincidence between updrafts and TIL occurrence. Figure ~~10~~ 11 shows zonal cross-sections of N^2 for the six simulations along 45° N after ~~144 h~~ 120 h of model integration. Indications of increased static stability are found in all cases above the updrafts which reach the tropopause. Clouds often form in the regions of the updrafts and in the lowermost stratosphere we find regions of convergence of the vertical wind. This convergence results from emerging gravity waves from the updrafts, but is also present in regions of propagating inertia-gravity in the eastern most region of the cross-sections. Gravity waves can alter the TIL temporarily during propagation (Otsuka et al., 2014) and possibly permanently by breaking or wave capture (Kunkel et al., 2014). In addition to the effects of dry dynamics, i.e., distribution of cyclonic and anti-cyclonic flow and breaking of the baroclinic wave (see Erler and Wirth, 2011), the effects from updrafts, small-scale convergence, and radiation, contribute most strongly to the TIL formation. Furthermore, note that low-, and mid-tropospheric diabatic heating causes a negative change in PV above the region of maximum heating, thus enhancing the anti-cyclonic flow in the tropopause region above ~~(e.g., Joos and Wernli, 2012)~~ (e.g., Joos and Wernli, 2012; Wernli and Davies, 1997) , which further has a positive feedback on the TIL evolution.

To this point we ~~showed that updrafts~~ demonstrated that updrafts reaching the tropopause level are initially important to form the TIL. However, this ~~contribution seems to~~ could be a transient effect on the static stability in the stratosphere and as such its contribution could decrease over time ~~. To support this hypothesis we calculated the difference between the mean~~ with other effects becoming more important. One other potential process might be related to the convergence of the vertical wind $\partial w/\partial z$. If this term becomes negative at or just above the tropopause, the static stability is increased in this region (Wirth, 2004) . Convergence can occur on small scales when gravity waves are present or on large scales in anti-cyclonic flow. We introduce here another metric to measure the impact of updrafts and convergent regions on enhanced static stability. For this we calculate the domain mean vertical profile of static stability N^2 as well as the mean vertical profile of static stability in

regions ~~of~~ with strong updrafts N^2_{dz}, i.e., ~~where $\Delta z \geq 2.5$, and the domain mean N^2, denoted as~~ $\Delta z \geq 2.5\,\mathrm{km}$ below the tropopause, and in regions with strong convergence of the vertical wind N^2_{wz}, i.e., $\partial w/\partial z \leq -5.0 \times 10^{-5}\,\mathrm{s}^{-1}$. We subtract the domain mean from these values to obtain quantitative measures how strong the TIL is enhanced in the respective regions compared to the TIL in the entire domain. Figure 12 shows the tropopause-based vertical profiles of $N^2_{\mathrm{dz}} - N^2$ (~~see Fig. 11) . We did this~~ upper panel a) and $N^2_{\mathrm{wz}} - N^2$ (lower panel b) for every 24 h~~of model integration and use a tropopausebased coordinate system. From this we conclude that the difference $N^2_{\mathrm{dz}} - N^2$ becomes generally smaller over time~~. In $N^2_{\mathrm{dz}} - N^2$ a TIL like vertical profile (i.e., with maximum values just above the tropopause) is evident in all six cases, especially in the first days of the simulations. However, the difference becomes smaller with time, which is partly ~~attributable to the domain mean TIL which becomes stronger but also to the fact that~~ related to the fact that the TIL becomes more evident in the domain mean N^2. Moreover, the number of ~~model grid cells in which $\Delta z \geq 2.5$does not significantly grow during the last days (see~~ grid cells contributing to N^2_{dz} stagnates at later times, indicating the decreasing number of new updrafts over time, which reach the tropopause (compare the numbers in the top left corners ~~). We did the same analysis for convergent regions, with a threshold of $\partial w/\partial z \leq 5.0 \times 10^{-5}\,\mathrm{s}^{-1}$ and calculated the mean profile N^2_{wz}. The difference~~ in each panel of Fig. 12). The differences $N^2_{\mathrm{wz}} - N^2$ ~~becomes smaller with integration timebut also the region which contributes to~~ also become smaller above the tropopause with time, i.e., the TIL like shape is less evident. However, compared to the relative decreases of the differences $N^2_{\mathrm{dz}} - N^2$, the decreases of $N^2_{\mathrm{wz}} - N^2$ over time are relatively smaller. Moreover, the number of grid cells contributing to N^2_{wz} ~~increases, especially at times when vertical motions rather tend to have a smaller impact.Only in the case with surface fluxes the convective updrafts dominate over the entire life cycle. Nevertheless, we can conclude that convergence of the vertical wind is important in forming and maintaining the TIL. However, the process leading to the convergence may differ with time during the life cycle. While updrafts are~~ becomes significantly larger over time and is in most cases also larger than the number for N^2_{dz}. From this we follow that updrafts might be potentially more important during the ~~period of first TILoccurrence, propagating (inertia-) gravity waves become more important at later times .~~ initial formation of the TIL. In contrast, the convergence of the vertical wind might become relatively more important in maintaining the TIL during later times of the life cycles.

We already saw that moistening the upper troposphere fosters the evolution of the TIL. Since ice clouds also reach the level of the tropopause, we briefly discuss their potential impact on the thermal structure above the tropopause. We only use cloud processes and radiation in this analysis here and exclude the effects of mixing and convection. We conducted a further simulation in which we turned off the cloud radiative feedback ~~feedback~~ (BMP RAD NOCRF) and compare the results to those from a simulation with feedback (BMP RAD) to assess the impact of ice clouds on TIL in the model. From instantaneous vertical profiles of meteorological and tracer quantities within ~~regions which~~

~~exhibit~~ a region which exhibits a TIL and ice clouds up to the tropopause we infer the following points (Fig. ~~12~~13): (1) the net heating rate is much more negative in the upper troposphere when the forcing is turned on, with the cooling being strongest just below the thermal tropopause (black solid lines); (2) the temperature profile in the UTLS differs significantly between both cases – while there is a clear minimum in the case with cloud radiative forcing, an almost neutral temperature profile is evident in the first two kilometers above the tropopause in BMP RAD NOCRF (black dashed lines); (3) the upper edge of the ice cloud is located slightly above the tropopause in BMP RAD and slightly below in the other case (blue solid lines); (4) the specific humidity has a local maximum at the top of the ice cloud which is stronger in the case with feedback (blue dashed lines); (5) the static stability is increased in both cases with a slightly higher located and stronger maximum in case with feedback (red solid lines); (6) the height tracer indicates lifted air mass in the troposphere below the maximum of static stability, however, with stronger updrafts in the case with feedback (red dashed lines). From points (1), (2), and (5) we conclude that the tropopause can be sharper due to strong differential cooling in the UTLS, if ice clouds are present. Moreover, from (3), (4), and (6) it follows that the potential to moisten the lower stratosphere is also increased which might in turn enhance the radiative formation process of the TIL. Thus, the results from this sensitivity suggest that there is a larger potential to obtain a stronger TIL when clouds reach up to the level of the tropopause. Moreover, this might be of further interest, since ice clouds, or ice super-saturated regions, have been shown to occur frequently in the lower stratosphere (e.g., Spichtinger et al., 2003; Spang et al., 2015).

So far we mainly focused on ~~diabatic~~ radiative and moist effects. In the last paragraph we turn to the effect of mixing and analyze where turbulent mixing occurs at the tropopause and whether this spatially and temporally coincides with the appearance of the TIL. Turbulent mixing contributes to the process of small scale stratosphere-troposphere exchange (STE). It has been speculated in several studies that TIL and STE are causally related beyond a pure spatial coincidence (e.g., Gettelman and Wang, 2015). Kunz et al. (2009) used airborne measurements and ECMWF analysis data from which they concluded that mixing at the tropopause is a synoptic scale process on rather short time scales which, however, enhances the concentration of radiatively active trace gases in the mixing layer. This then leads to an increase in static stability further downwind of the region of the STE event. Thus, they focused on the long term relation between mixing and N^2. On the other hand we see that values of turbulent kinetic energy (TKE) are often increased in regions where a TIL is present (Fig. ~~13~~14). These values are smaller than in the boundary layer, but nevertheless increased compared to the background values in the tropopause region at other locations and times in our model simulations. Such exchange events may have only spatial extension of a few ~~tenth~~ tenths of kilometers or even less. Müller et al. (2015) recently reported a comparable event based on airborne in-situ measurements of nitrous oxide, ozone, and ice cloud particles. However, since our model is

not capable of resolving this process with sufficient accuracy to conduct a quantitative estimate of STE, we will leave a more detailed analysis open to further studies.

5 The TIL in cyclonic life cycle experiments

So far, the discussion of the results focused on the anti-cyclonic life cycle (LC1, Thorncroft et al., 1993) . We will now extend the analysis and show results for five selected cyclonic life cycles (LC2). We obtain this life cycle by adding a cyclonic shear to the background state of the LC1 (see Section 2.1). We briefly compare the results of the LC1 and LC2 and discuss the main difference in the following paragraphs. For this we analyze the results from a dry reference experiment (REF LC2), from three simulations with one additional diabatic process, i.e., with clouds (BMP LC2), with radiation (RAD LC2), and with turbulence (TURB LC2), and from one simulation with a more complex setup including clouds and convection, radiation, and turbulence (BRTC LC2).

Generally, LC2 experiments show a less strong deepening of the minimum surface pressure compared to their LC1 counterparts (Fig. 15a). Similarly to the LC1 waves, the deepening of the surface cyclone is less strong, when radiation is included in the simulations (RAD LC2, BRTC LC2). N^2_{max} above the thermal tropopause shows several differences between LC1 and LC2. In the cases without moisture (REF LC2, RAD LC2, and TURB LC2) the maximum values are always below $7.0 \times 10^{-4}\,\text{s}^{-2}$. Moreover, in contrast to the sudden increase of N^2_{max} in all moist LC1 cases, N^2_{max} increases rather stepwise, in particular in the BMP LC2 case. The absolute maximum is reached only after 110 h after simulation start and thus much later than in the LC1 BMP case (compare Fig. 3b). Furthermore, at the end of the simulated period N^2_{max} is almost equal in all LC1 cases, which is, however, not the case in the LC2 cases. The TIL area ($A_{5.5}$, see Figure 15c) is largest for BMP LC2 and shows even comparable numbers to its LC1 counterpart. However, in the other cases the $A_{5.5}$ is much smaller in the LC2 cases than in the LC1 cases. Thus, the TIL evolves less strong in amplitude and spatial extent in the LC2 compared to the LC1. Generally, this is in agreement with the results from Erler and Wirth (2011) for dry adiabatic life cycles.

The processes relevant for the TIL formation are rather similar between LC1 and LC2. In the moist cases BMP LC2 and BRTC LC2 N^2_{max} shows a strong correlation to Δz (see Figure 15d) and thus updrafts may be as important in the LC2 as they are in the LC1 to initially form the TIL in the life cycles. This relation is further obvious when the spatial co-occurrence between updrafts and enhanced static stability is studied (Figure 16). The first enhancement of N^2 in the lower stratosphere are again present just above regions which exhibit strong updrafts and also ice clouds just below the tropopause. Thus, except for the difference in the timing of the first vertical ascent patterns, there is no major difference to the LC1 baroclinic life cycle. However, the temporal variability of N^2_{max} in BMP LC2 and BRTC LC2 is slightly larger than in their LC1 counterparts. This might be related to the less strong evolving gravity waves in the LC2 simulations. In particular, gravity waves

from the jet-front system are much more evident in LC1 than in LC2 which has been discussed in Kunkel et al. (2014) . Thus, the effect of gravity waves on the TIL maintenance might be less strong in case of LC2. Taken together the LC2 cases generally show a less strong developed TIL compared with their LC1 counterparts. Nevertheless, the physical processes leading the TIL formation seem to be similar in LC1 and LC2.

6 Conclusions and summary

By conducting various simulations of baroclinic life cycles we aimed to improve the understanding whether dynamical or diabatic processes are more relevant to form a tropopause inversion layer (TIL). For this we used the non-hydrostatic, limited area model COSMO in a midlatitude channel configuration along with a varying number of physical parameterizations. We first analyzed the effect of individual diabatic processes, i.e., related to clouds~~and~~ , radiation, and mixing processes before we estimated the relative importance of each process.

In a first set of simulations the evolution of the TIL has been compared in baroclinic life cycles. A life cycle experiment with only dry dynamics served as reference ~~, while in three more life cycles one additional~~ case, while three additional life cycle experiments have been performed with individual non-conservative ~~processes~~process added. We further assessed the impact of initial conditions and process formulation in the diabatic cases. In a second step we successively increased the number of processes to assess the relative importance of the various dynamical and diabatic processes to the TIL evolution. We further conducted sensitivity experiments to study differences between life cycles of type 1 (LC1) and 2 (LC2).

Most importantly, our experiments highlighted the role of different moisture related processes for the formation and evolution of the TIL with varying relevance and strength in different phases of the baroclinic life cycles. In detail, we derived the following results:

1. A TIL forms in baroclinic life cycles with only dry dynamics as well as in life cycles with additionally either vertical turbulence, cloud processes, or radiation. Compared to the dry reference case the TIL appears weaker with respect to its maximum value as well as to the spatial appearance in the case with turbulence. The opposite is evident in the case with radiation with a larger maximum static stability and larger spatial appearance. The temporal evolution is, however, still similar to the reference case. This is different with cloud processes. The TIL emerges much earlier and shows generally the largest maximum values and spatial extension.

2. The processes forming the TIL in the cases with diabatic ~~and mixing~~ processes are as follows. Turbulence acts against the forming process from dynamics, ~~i.e., sharpening the lower stratosphere,~~ and as such a weaker TIL is the final result. With only radiative processes, the (passive) transport of moisture from low to high levels leads to an increase in the moisture burden in the UTLS and to a change in the moisture gradient in this region. The UTLS is then

cooled non-uniformly which finally further enhances the static stability above the tropopause. The important process with clouds is the release of latent heat during condensation. This increases the frequency and strength of vertical motions which locally increase the static stability above the regions of the updrafts. Especially, the TIL forms in the region of the warm conveyor belt. In contrast to the direct diabatic forcing (occurring in the region of the tropopause) in the case with radiation, the enhancement of static stability results from a diabatic forcing at lower levels in the case with clouds.

3. Analysis of initial conditions and process formulations showed that the TIL formation in the model is ~~relative~~ relatively insensitive to the formulation of the cloud forming process itself and more dependent on the initial amount of specific humidity. For radiation no significant dependency on the initial water or ozone amount is evident. Here, the change of the gradient of specific humidity is the more important process.

4. Further simulations of baroclinic life cycles with varying complexity with respect to the number of incorporated physical processes showed that there is a correlation between the first appearance of the TIL and of updrafts reaching the tropopause. However, the exact timing of this first occurrence further depends on the included physical processes. The TIL emerges latest when only cloud processes and turbulence are considered while it appears earlier when radiation is incorporated and even more with convection. From this result it is concluded that updrafts are the key process in the initial formation of the TIL in moist baroclinic life cycles, however, noting that their effect is probably fading with time.

5. The updrafts that reach the tropopause lead to the emission of gravity wave in the lower stratosphere. Such small scale waves have a further source in the jet-front system (inertia-gravity waves). ~~It~~ In recent studies (e.g., Kunkel et al., 2014; Otsuka et al., 2014) it has been shown that these small-scale disturbances can alter the thermal structure above the tropopause temporarily as well as permanently and as such affect the TIL during the entire life cycle after their first appearance.

   At least in parts, the appearance and strength of such gravity waves might explain the weaker appearance of the TIL in the cyclonic life cycles compared to their anti-cyclonic counterparts.

6. Finally, updrafts enhance the moisture content of the upper troposphere, not only by transporting water vapor to this altitude. Clouds also form within the updrafts ~~. These clouds locally influence~~ and locally alter the thermal structure of the upper troposphere~~such that there is a larger potential to obtain a stronger TIL. Generally, the~~ . Especially, at the top of the clouds a strong cooling can occur which further contributes to the formation and maintenance of a strong TIL. In general, radiative impacts become more relevant during later stages of the life cycle.

Thus, the various dynamical and diabatic processes lead to a highly variable temporal and spatial appearance of the TIL on the time-scale of a week. While updrafts are important for the first appearance of the TIL when moisture is included in the baroclinic life cycles, the radiative effects as well as the convergence of the vertical wind are more important in maintaining the TIL during later phases of the life cycles. In reality the TIL in the midlatitudes may be restrengthened by each passing baroclinic wave and the lifted water vapor serves as a cooling agent in the upper troposphere and even in the lower stratosphere over a longer time-scale than a week. ~~Including the frequency of occurrence of baroclinic waves~~ Taking into account that baroclinic waves occur relatively frequent at midlatitudes, especially from autumn to spring, might further help to explain the quasi-permanent appearance of a layer of enhanced static stability.

Acknowledgements. D. Kunkel acknowledges funding from the German Science Foundation under grant HO 4225/2-1. The authors thank A. Roches, U. Blahak, and S. Schemm for model support and the HPC team of the university of Mainz for computing time. We further thank P. Spichtinger for valuable comments on an earlier version of the manuscript. The comments on the discussion paper from S. Schemm, G. Craig, and an anonymous referee helped to significantly improve the final manuscript. Further information on data (model code and output) relevant to this paper can be obtained upon request via email to the authors (dkunkel@uni-mainz.de).

References

Bell, S. W. and Geller, M. A.: Tropopause inversion layer: ~~aeasonal~~ seasonal and latitudinal variations and representation in standard radiosonde data and global models, J. Geophys. Res.-Atmos., 113, D05109, doi:10.1029/2007JD009022, 2008.

Birner, T.: Fine-scale structure of the extratropical tropopause region, J. Geophys. Res., 111, D04104, doi:10.1029/2005JD006301, 2006.

Birner, T.: Residual Circulation and Tropopause Structure, J. Atmos. Sci., 67, 2582–2600, doi:10.1175/2010JAS3287.1, 2010.

Birner, T., Dörnbrack, A., and Schumann, U.: How sharp is the tropopause at midlatitudes?, Geophys. Res. Lett., 29, 1700, doi:10.1029/2002GL015142, 2002.

Birner, T., Sankey, D., and Shepherd, T. G.: The tropopause inversion layer in models and analyses, Geophys. Res. Lett., 33, L14804, doi:10.1029/2006GL026549, 2006.

Chagnon, J. M. Gray, S. L., and Methven, J.: Diabatic processes modifying potential vorticity in a North Atlantic cyclone, Q. J. Roy. Meteor. Soc., 139, 1270–1282, doi:10.1002/qj.2037, 2013.

Doms, G.: A Description of the Nonhydrostatic Regional COSMO-Model, Part I: Dynamics and Numerics, Tech. rep., Deutscher Wetterdienst, Offenbach, Germany, 2011.

Erler, A. R. and Wirth, V.: The static stability of the tropopause region in adiabatic baroclinic life cycle experiments, J. Atmos. Sci., 68, 1178–1193, doi:10.1175/2010JAS3694.1, 2011.

Fusina, F. and Spichtinger, P.: Cirrus clouds triggered by radiation, a multiscale phenomenon, Atmos. Chem. Phys., 10, 5179–5190, doi:10.5194/acp-10-5179-2010, 2010.

Gettelman, A. and Wang, T.: Structural diagnostics of the tropopause inversion layer and its evolution, J. Geophys. Res.-Atmos., 120, 46–62, doi:10.1002/2014JD021846, 2015.

Grise, K. M., Thompson, D. W. J., and Birner, T.: A global survey of static stability in the stratosphere and upper troposphere, J. Climate, 23, 2275–2292, doi:10.1175/2009JCLI3369.1, 2010.

Gutowski, W. J., Branscome, L. E., and Stewart, D. A.: Life cycles of moist baroclinic eddies, J. Atmos. Sci., 49, 306–319, doi:10.1175/1520-0469(1992)049<0306:LCOMBE>2.0.CO;2, 1992.

Held, I. M. and Suarez, M. J.: A proposal for the intercomparison of the dynamical cores of atmospheric general circulation models, B. Am. Meteorol. Soc., 75, 1825–1830, doi:10.1175/1520-0477(1994)075<1825:APFTIO>2.0.CO;2, 1994.

Joos, H. and Wernli, H.: Influence of microphysical processes on the potential vorticity development in a warm conveyor belt: a case-study with the limited-area model COSMO, Q. J. Roy. Meteor. Soc., 138, 407–418, doi:10.1002/qj.934, 2012.

Kunkel, D., Hoor, P., and Wirth, V.: Can inertia-gravity waves persistently alter the tropopause inversion layer?, Geophys. Res. Lett., 41, 7822–7829, doi:10.1002/2014GL061970, 2014.

Kunz, A., Konopka, P., Müller, R., Pan, L. L., Schiller, C., and Rohrer, F.: High static stability in the mixing layer above the extratropical tropopause, J. Geophys. Res., 114, D16305, doi:10.1029/2009JD011840, 2009.

Mellor, G. L. and Yamada, T.: Development of a turbulence closure model for geophysical fluid problems, Rev. Geophys., 20, 851, doi:10.1029/RG020i004p00851, 1982.

Müller, S., Hoor, P., Berkes, F., Bozem, H., Klingebiel, M., Reutter, P., Smit, H. G. J., Wendisch, M., Spichtinger, P., and Borrmann, S.: In situ detection of stratosphere-troposphere exchange of cirrus particles in the midlatitudes, Geophys. Res. Lett., 42, 949–955, doi:10.1002/2014GL062556, 2015.

Murray, F. W.: On the computation of saturation vapor pressure, J. Appl. Meteorol., 6, 203–204, doi:10.1175/1520-0450(1967)006<0203:OTCOSV>2.0.CO;2, 1967.

Olson, J. B. and Colle, B.: A modified approach to initialize an idealized extratropical cyclone within a mesoscale model, Mon. Weather Rev., 135, 1614–1624, doi:10.1175/MWR3364.1, 2007.

Otsuka, S., Takeshita, M., and Yoden, S.: A numerical experiment on the formation of the tropopause inversion layer associated with an explosive cyclogenesis: possible role of gravity waves, Progress in Earth and Planetary Science, 1, 19, doi:10.1186/s40645-014-0019-0, 2014.

Peevey, T. R., Gille, J. C., Homeyer, C. R., and Manney, G. L.: The double tropopause and its dynamical relationship to the tropopause inversion layer in storm track regions, J. Geophys. Res.-Atmos., 119, 10194–10212, doi:10.1002/2014JD021808, 2014.

Randel, W. J. and Wu, F.: The Polar summer tropopause inversion layer, J. Atmos. Sci., 67, 2572–2581, doi:10.1175/2010JAS3430.1, 2010.

Randel, W. J., Wu, F., and Forster, P.: The extratropical tropopause inversion layer: global observations with GPS data, and a radiative forcing mechanism, J. Atmos. Sci., 64, 4489–4496, doi:10.1175/2007JAS2412.1, 2007.

Riese, M., Ploeger, F., Rap, A., Vogel, B., Konopka, P., Dameris, M., and Forster, P.: Impact of uncertainties in atmospheric mixing on simulated UTLS composition and related radiative effects, J. Geophys. Res., 117, D16305, doi:10.1029/2012JD017751, 2012.

Ritter, B. and Geleyn, J.-F.: A comprehensive radiation scheme for numerical weather prediction models with potential applications in climate simulations, Mon. Weather Rev., 120, 303–325, doi:10.1175/1520-0493(1992)120<0303:ACRSFN>2.0.CO;2, 1992.

Schemm, S., Wernli, H., and Papritz, L.: Warm conveyor belts in idealized moist baroclinic wave simulations, J. Atmos. Sci., 70, 627–652, doi:10.1175/JAS-D-12-0147.1, 2013.

Son, S.-W. and Polvani, L. M.: Dynamical formation of an extra-tropical tropopause inversion layer in a relatively simple general circulation model, Geophys. Res. Lett., 34, L17806, doi:10.1029/2007GL030564, 2007.

Spang, R., Günther, G., Riese, M., Hoffmann, L., Müller, R., and Griessbach, S.: Satellite observations of cirrus clouds in the Northern Hemisphere lowermost stratosphere, Atmos. Chem. Phys., 15, 927–950, doi:10.5194/acp-15-927-2015, 2015.

Spichtinger, P., Gierens, K., Leiterer, U., and Dier, H.: Ice supersaturation in the tropopause region over Lindenberg, Germany, Meteorol. Z., 12, 143–156, doi:10.1127/0941-2948/2003/0012-0143, 2003.

Sprenger, M., Croci Maspoli, M., and Wernli, H.: Tropopause folds and cross-tropopause exchange: a global investigation based upon ECMWF analyses for the time period March 2000 to February 2001, J. Geophys. Res.-Atmos., 108, 8518, doi:10.1029/2002JD002587, 2003.

Steppeler, J., Doms, G., Schättler, U., Bitzer, H. W., Gassmann, A., Damrath, U., and Gregoric, G.: Meso-gamma scale forecasts using the nonhydrostatic model LM, Meteorol. Atmos. Phys., 82, 75–96, doi:10.1007/s00703-001-0592-9, 2003.

Table 1. Summary of experiment acronyms, description, and water treatment

Experiment	Short description	Water species
REF	adiabatic reference simulation	no water species
BMP	standard cloud microphysics	interactive water
RAD	standard radiation scheme	passive water vapor
TURB	standard turbulence scheme	no water species
BMP R30	BMP sensitivity, reduced specific water vapor	interactive water
BMP R80	BMP sensitivity, increased specific water	interactive water
BMP NOICE	BMP sensitivity, only warm clouds	interactive water, no ice phase
~~QADI~~ BMP SATAD	BMP sensitivity, saturation adjustment	water vapor and cloud water
RAD woSW	RAD sensitivity, no stratospheric water	passive water vapor
RAD R30	RAD sensitivity, reduced specific water vapor	passive water vapor
RAD rO3	RAD sensitivity, reduced ozone concentration	passive water vapor
BMP RAD	cloud microphysics and radiation	interactive water
BMP RAD	cloud microphysics and radiation	interactive water
NOCRF	no cloud radiative feedback	
BMP TURB	cloud microphysics and turbulence	interactive water
~~BMP RAD~~ BRT	cloud microphysics, radiation, and turbulence	interactive water
~~TURB~~ BRTC	~~and turbulence~~cloud microphysics, radiation, turbulence, and convection	interactive water
~~BMP RAD~~ BRTCS	cloud microphysics, radiation, turbulence,	interactive water
~~TURB CONV~~	~~turbulence, and convection~~ convection, and surface fluxes for momentum and heat	
REF LC2	adiabatic reference simulation for LC2	no water species
BMP ~~RAD~~ LC2	~~cloud microphysics, radiation,~~ standard cloud microphysics for LC2	interactive water
~~TURB CONV~~ RAD LC2	~~turbulence, convection, and surface~~ standard radiation scheme for LC2	passive water vapor
~~SURF~~ TURB LC2	~~fluxes for momentum and heat~~ standard turbulence scheme for LC2	no water species
BRTC LC2	cloud microphysics, radiation, turbulence, and convection for LC2	interactive water

Thorncroft, C. D., Hoskins, B. J., and McIntyre, M. E.: Two paradigms of baroclinic-wave life-cycle behaviour, Q. J. Roy. Meteor. Soc., 119, 17–55, doi:10.1002/qj.49711950903, 1993.

Tiedtke, M.: A comprehensive mass flux scheme for cumulus parameterization in large-scale models, Mon. Weather Rev., 117, 1779–1800, doi:10.1175/1520-0493(1989)117<1779:ACMFSF>2.0.CO;2, 1989.

Wernli, H. and Davies, H. C.: A lagrangian-based analysis of extratropical cyclones. I: The method and some applications, Q. J. Roy. Meteor. Soc., 123, 467–489, doi:10.1002/qj.49712353811, 1997.

Wirth, V.: Static stability in the extratropical tropopause region, J. Atmos. Sci., 60, 1395–1409, doi:10.1175/1520-0469(2003)060<1395:SSITET>2.0.CO;2, 2003.

Wirth, V.: A dynamical mechanism for tropopause sharpening, Meteorol. Z., 13, 477–484, 2004.

WMO (1957), Meteorology - a three dimensional science, *WMO Bulletin*, pp. 134–138.

Zierl, B. and Wirth, V.: The influence of radiation on tropopause behavior and stratosphere-troposphere exchange in an upper tropospheric anticyclone, J. Geophys. Res., 102, 23883, doi:10.1029/97JD01667, 1997.

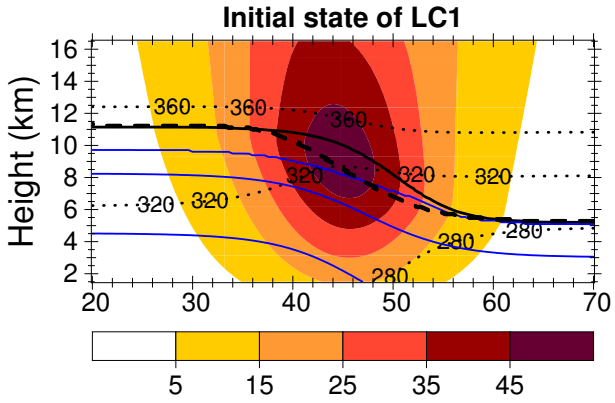

Figure 1. Meridional cross section of the initial state at the center of the model domain: the zonal wind U is color-coded for values of ~~10~~5, ~~20~~15, ~~30~~25, ~~40~~35, and ~~50~~ 45 ms^{-1}; the potential temperature Θ is shown by the black dotted lines for 280, 320, and 360 K (from bottom to top); the water vapor mixing ratio is shown by the blue lines for values of ~~2.0, 0.2, and 0.002 gkg^{-1}~~ 2.0, 0.2, and 0.02 gkg^{-1} (from bottom to top); the location of thermal tropopause is indicated by the solid thick black line and separates also the region of tropospheric values ($N^2 < 1.5 \times 10^{-4}\,\mathrm{s}^{-2}$) from stratospheric values ($N^2 \sim 4.0 \times 10^{-4}\,\mathrm{s}^{-2}$) of static stability; the location of the dynamical tropopause, defined as the isosurface of potential vorticity $Q = 2.0\,\mathrm{pvu}$, is shown by the dashed thick line.

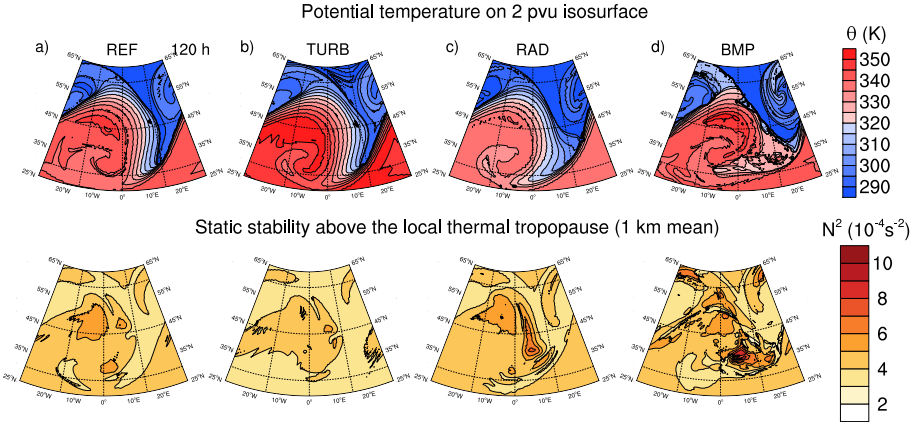

Figure 2. Dynamical and thermodynamical state of the baroclinic life cycles after 120 h of model integration. In the upper row the distribution of potential temperature Θ (in K) on the dynamical tropopause is depicted, while the lower row shows the distribution of static stability N^2 (in $10^{-4}\,\mathrm{s}^{-2}$) averaged over the first kilometer above the thermal tropopause. The four columns show from left to right the following simulations: **(a)** REF, **(b)** TURB, **(c)** RAD, and **(d)** BMP.

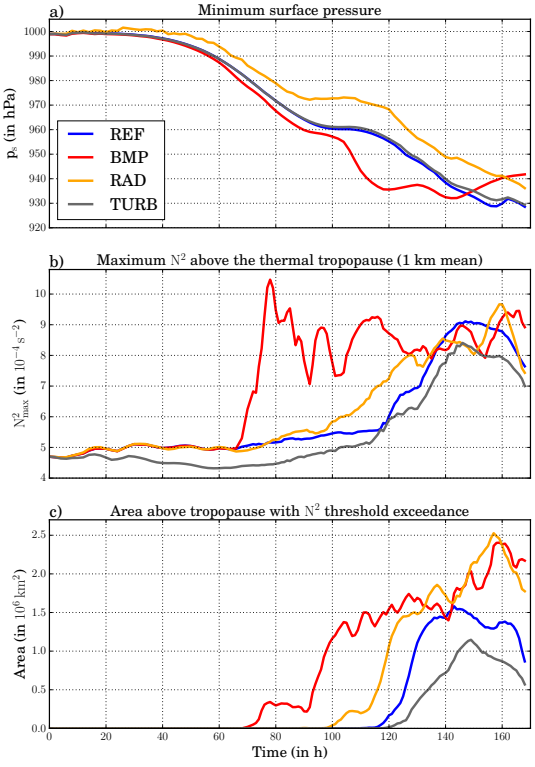

Figure 3. Temporal evolution over the entire simulated life cycles of **(a)** the minimum surface pressure p_s (in hPa), **(b)** the maximum static stability N^2_{max} (in $10^{-4}\,s^{-2}$) above the thermal tropopause, and **(c)** the area $A_{5.5}$ (in $10^6\,km^2$) of N^2 threshold exceedance above the thermal tropopause (with a threshold of $N^2 = 5.5 \times 10^{-4}\,s^{-2}$). ~~Dark blue~~ The colored lines ~~show N^2_{max} of~~ indicate the following simulations: REF ~~, light~~ (blue~~of~~), BMP (red), ~~yellow of~~ RAD (orange), and ~~dark red of~~ TURB (gray).

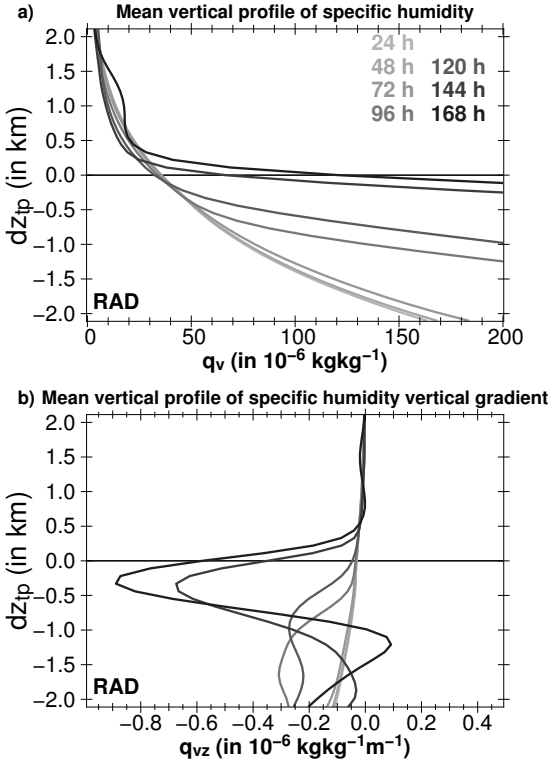

Figure 4. Instantaneous thermal tropopause based domain mean values of **(a)** specific humidity q_v (in $10^{-6}\,\mathrm{kg\,kg^{-1}}$) and **(b)** the vertical gradient of specific humidity $\partial q_\mathrm{v}/\partial z$ (in $10^{-6}\,\mathrm{kg\,kg^{-1}\,m^{-1}}$) for RAD. The domain mean is calculated within 25–65° latitude and the entire zonal domain. dz_tp is the distance to the height of the thermal tropopause. The intensity of the gray colors indicates the time since model start in 24 h intervals.

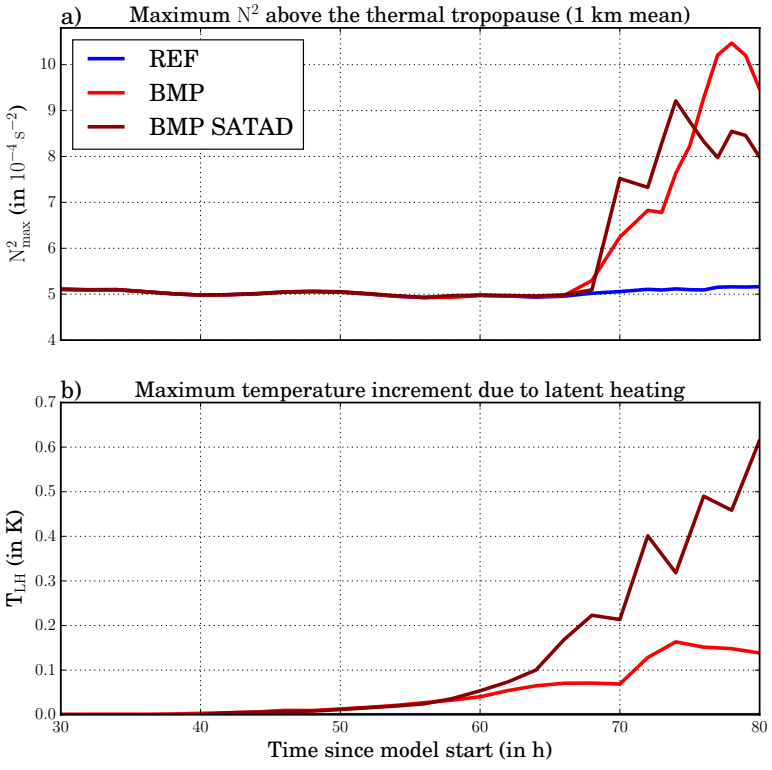

Figure 5. Temporal evolution ~~over the entire simulated life cycles~~ between 30 h and 80 h after simulation start of **(a)** the maximum static stability $N^2_{\max}$ (in $10^{-4}\,\mathrm{s}^{-2}$) above the thermal tropopause and **(b)** the maximum temperature increment due to latent heating T_{LH} (in K) in the model domain for REF (blue lines), BMP (red lines), and ~~QADI~~ BMP SATAD (~~cyan~~ dark red lines).

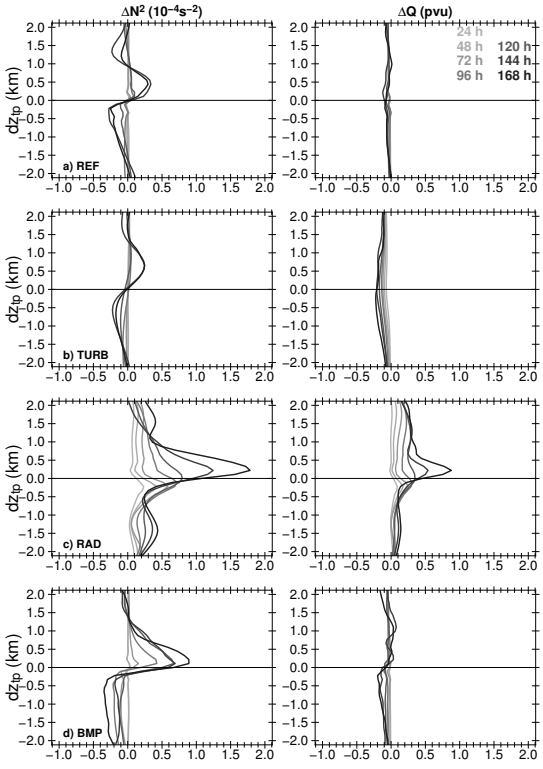

Figure 6. Instantaneous thermal tropopause based domain mean values of ΔN^2 (in $10^{-4}\,\mathrm{s}^{-2}$) in the ~~upper row~~ left panels and ΔQ (in pvu) in the ~~lower row~~ right panels for **(a)** REF, **(b)** TURB, **(c)** RAD, and **(d)** BMP. The domain mean is calculated within 25–65° latitude and the entire zonal domain. The intensity of the gray colors indicates the time since model start in 24 h intervals. ΔN^2 is the difference between the current static stability N^2 and the advected initial static stability ~~ADV(N_0^2)~~N_0^2, ΔQ is the difference between the current potential vorticity Q and the advected initial potential vorticity ~~ADV(Q_0)~~Q_0. dz_{tp} is the distance to the height of the thermal tropopause.

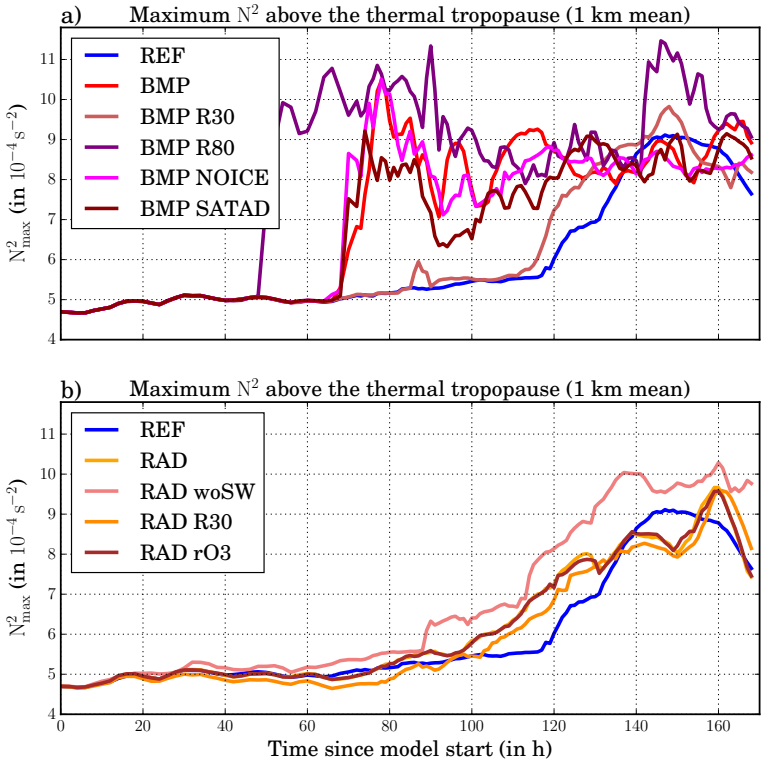

Figure 7. Temporal evolution of the maximum static stability $N^2_{\max}$ (in $10^{-4}\,\mathrm{s}^{-2}$) above the thermal tropopause for sensitivity simulations of **(a)** BMP and **(b)** RAD. In **(a)** $N^2_{\max}$ is shown for REF (~~dark~~ blue), BMP (~~blue~~red), BMP R30 (light ~~blue~~red), BMP R80 (~~green~~purple), BMP NOICE (~~orange~~magenta), and ~~QADI~~ BMP SATAD (dark red). In **(b)** $N^2_{\max}$ is shown for REF (~~dark~~ blue), RAD (~~blue~~orange), RAD woSW (~~green~~coral), RAD R30 (dark orange), and RAD rO3 (~~dark red~~brown).

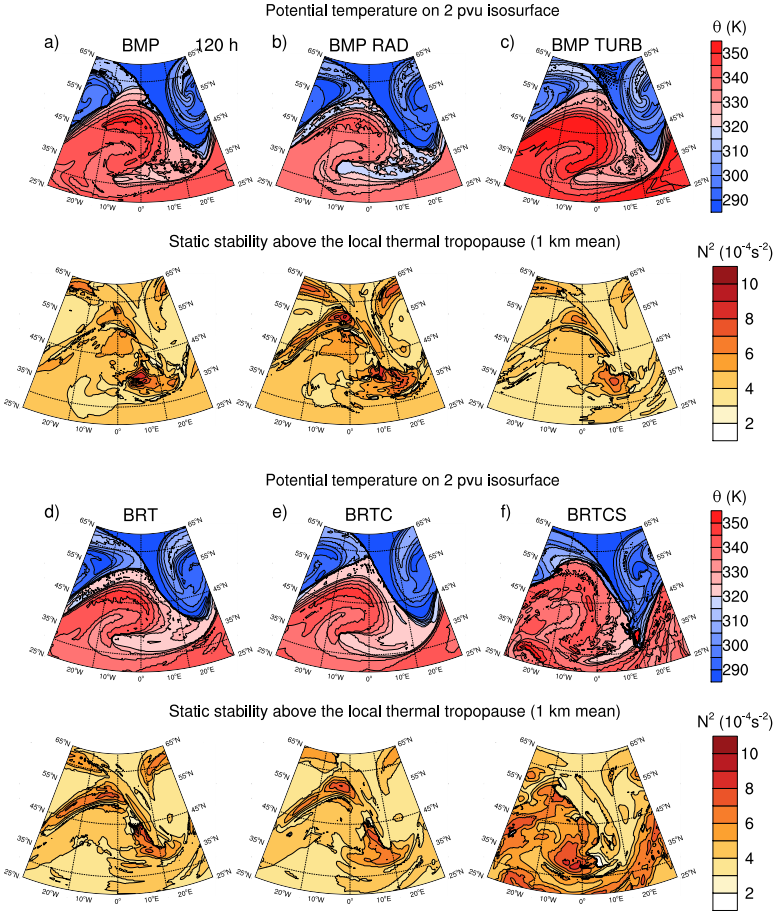

Figure 8. Dynamical and thermodynamical state of baroclinic life cycles after 120 h of model integration. In the upper rows of the six panels the distribution of potential temperature Θ (in K) on the dynamical tropopause is depicted, while the lower rows show the distribution of static stability N^2 (in $10^{-4}\,\mathrm{s}^{-2}$) averaged over the first kilometer above the thermal tropopause for **(a)** BMP, **(b)** BMP RAD, **(c)** BMP TURB, **(d)** ~~BMP RAD TURB~~BRT, **(e)** ~~BMP RAD TURB CONV~~BRTC, and **(f)** ~~BMP RAD TURB CONV SURF~~BRTCS.

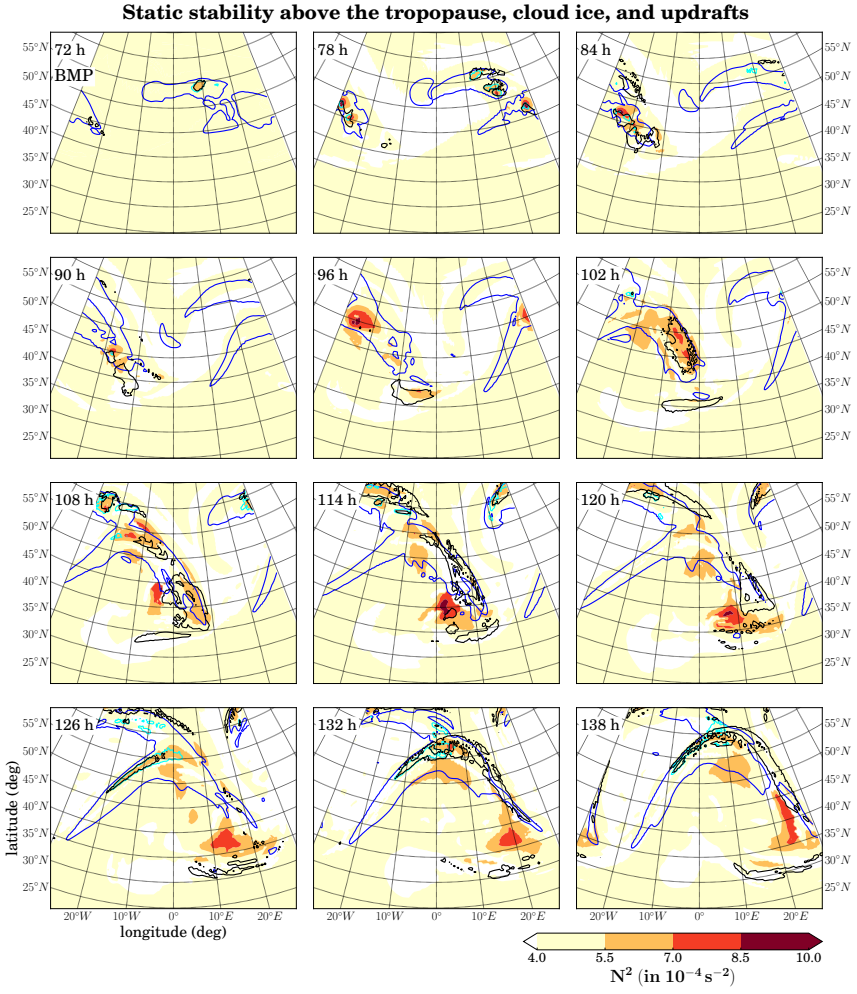

Figure 9. Static stability N^2 (color-coded, in $10^{-4}\,\mathrm{s}^{-2}$) above the thermal tropopause, Δz (black lines, in 2.5 km), column integrated cloud ice content tq_i (blue lines, in $0.01\,\mathrm{kg\,m}^{-2}$), and tropopause close column integrated cloud ice content $tq_\mathrm{i,tp}$ (cyan lines, in $0.001\,\mathrm{kg\,m}^{-2}$). Tropopause close means the region between the thermal tropopause and 500 m below. The distribution is shown for BMP between 78 h and 138 h after simulation start in a six hourly interval.

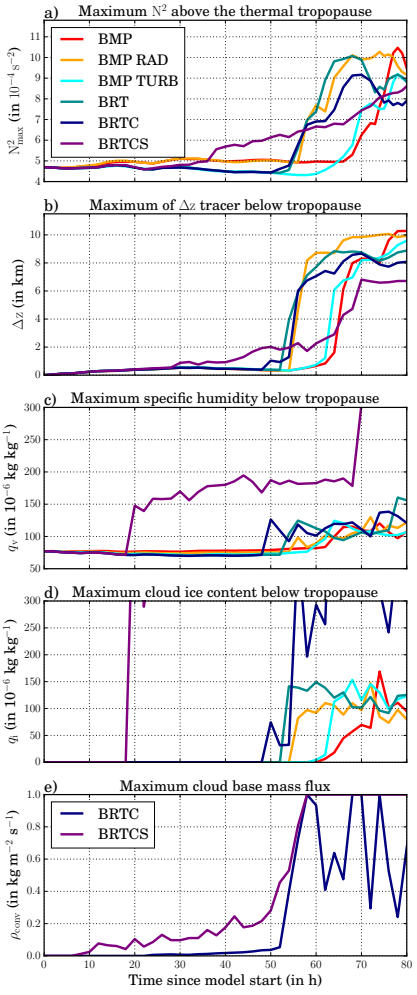

Figure 10. Temporal evolution over the first 80 h of the life cycles of **(a)** $N^2_{\max}$ (in $10^{-4}\,\mathrm{s}^{-2}$) above the thermal tropopause, **(b)** the maximum of the Δz tracer (in km) in a 500 m thick layer below the thermal tropopause, **(c)** the maximum specific humidity q_v in a 500 m thick layer below the thermal tropopause (in $10^{-6}\,\mathrm{kg\,kg}^{-1}$), **(d)** the maximum specific cloud ice content q_i in a 500 m thick layer below the thermal tropopause (in $10^{-6}\,\mathrm{kg\,kg}^{-1}$), and **(e)** the maximum cloud base mass-flux ρ_CONV (in $\mathrm{kg\,m}^{-2}\mathrm{s}^{-1}$). ~~For (a–c)~~ The time of TIL occurrence is split into three time sectors. Without radiation and convection, the TIL appears after 65 h, with radiation between 50 h-65 h, and with strong convection before 50 h (more information is given in the text). The colored lines indicate the following simulations: ~~REF (dark blue),~~ BMP (~~blue~~red), BMP RAD (~~light blue~~orange), BMP TURB (~~green~~cyan), ~~BMP RAD TURB~~ BRT (~~yellow~~dark cyan), ~~BMP RAD TURB CONV~~ BRTC (~~orange), and BMP RAD TURB CONV SURF (~~dark ~~red). For (f) only the simulations with convection are considered: BMP RAD TURB CONV (dark~~ blue), and ~~BMP RAD TURB CONV SURF~~ BRTCS (~~dark red~~purple).

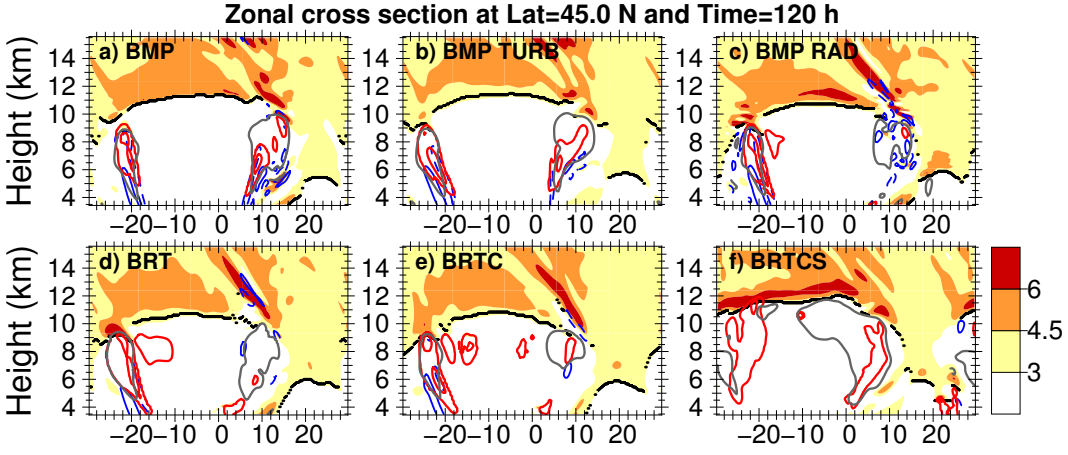

Figure 11. Zonal cross sections along 45° N of static stability N^2 (in $10^{-4}\,\mathrm{s}^{-2}$) after ~~144~~120 h of model integration. Red lines show specific cloud ice content q_i (for $5.0 \times 10^{-6}\,\mathrm{kg\,kg}^{-1}$), solid blue lines show regions with positive values of $\partial w/\partial z$ (for $10.0 \times 10^{-5}\,\mathrm{s}^{-1}$), dashed blue lines show negative values (for $-10.0 \times 10^{-5}\,\mathrm{s}^{-1}$), and solid gray lines show regions with Δz tracer larger than 2.5 km. The thick black line is the thermal tropopause. The six panels show **(a)** BMP, **(b)** BMP RAD, **(c)** BMP TURB, **(d)** ~~BMP RAD TURB~~BRT, **(e)** ~~BMP RAD TURB CONV~~BRTC, and **(f)** ~~BMP RAD TURB CONV SURF~~BRTCS.

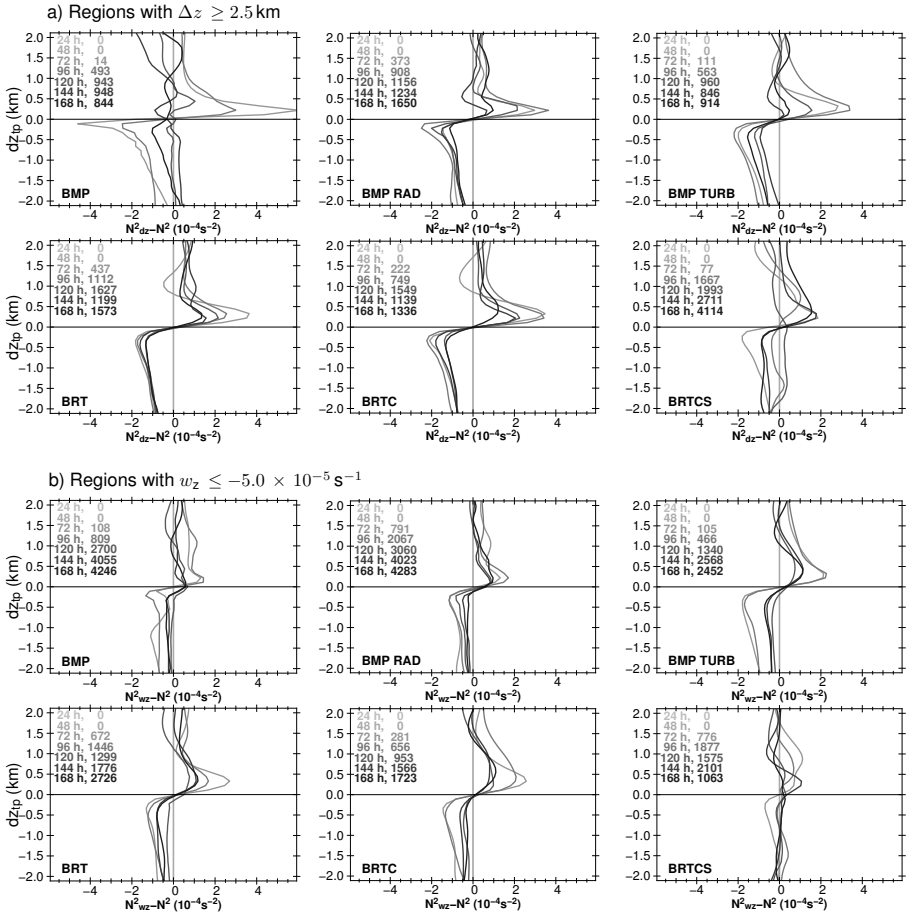

Figure 12. (a) Instantaneous thermal tropopause based vertical profiles of difference between the mean of static stability in regions with $\Delta z > 2.5\,\mathrm{km}$ N^2_{dz} and the domain mean N^2 (in $10^{-4}\,\mathrm{s}^{-2}$) for each 24 h of the model integration. **(b)** Differences for regions with $\partial w/\partial z \leq -5.0 \times 10^{-5}\,\mathrm{s}^{-1}$. The values in the top left corner of each panel show the number of individual profiles used for calculating the respective mean profile of N^2_{dz} and N^2_{wz}. dz_{tp} is the distance to the height of the thermal tropopause.

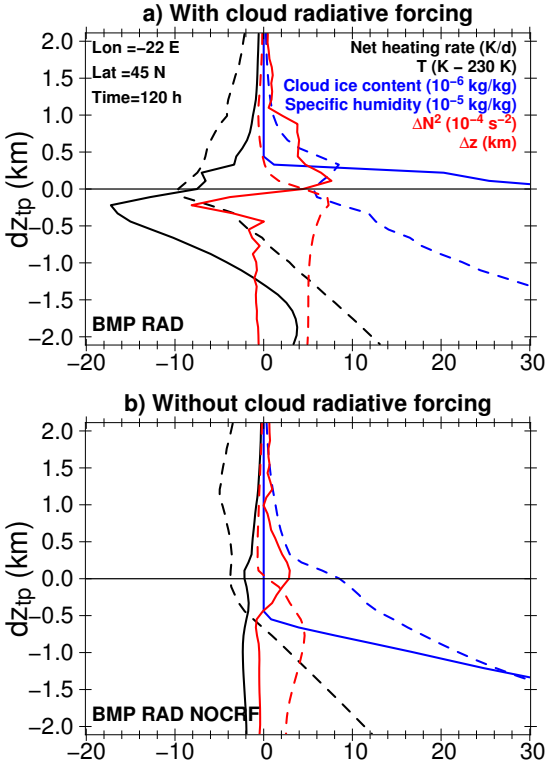

Figure 13. Tropopause based vertical profiles through an ice cloud along the central latitude at 120 h for **(a)** a simulation with cloud radiative forcing (BMP RAD) and **(b)** a simulation without cloud radiative forcing (BMP RAD NOCRF). Solid lines show net radiative heating (in $\mathrm{K\,d^{-1}}$, scaled for better comparability, black), cloud ice content (in $10^{-6}\,\mathrm{kg\,kg^{-1}}$, blue), and ΔN^2 (in $10^{-4}\,\mathrm{s^{-2}}$, red). Dashed lines show temperature (in $\mathrm{K} - 230\,\mathrm{K}$, black), specific humidity (in $10^{-5}\,\mathrm{kg\,kg^{-1}}$, blue), and Δz (in km, red). dz_{tp} is the distance to the height of the thermal tropopause.

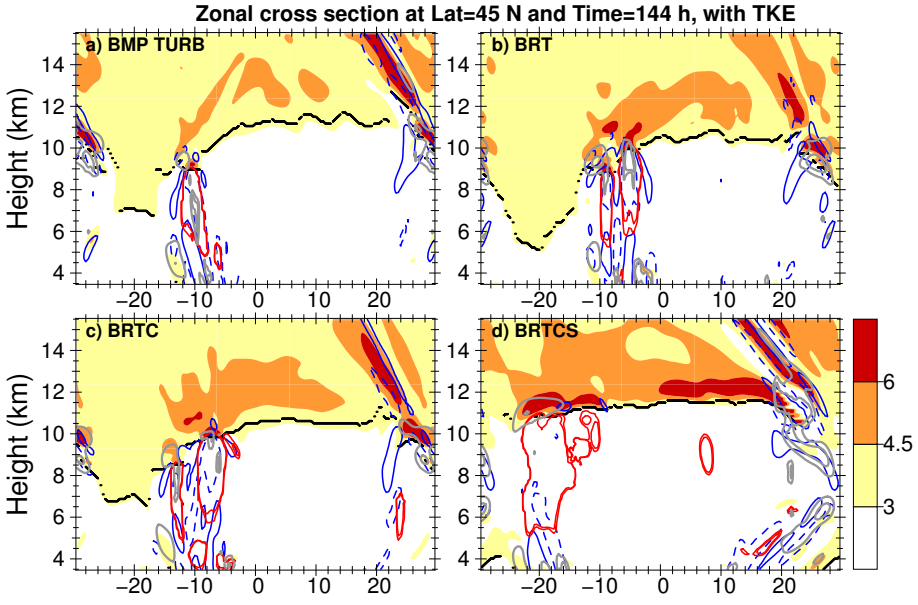

Figure 14. Zonal cross sections along 45° N of static stability N^2 (in $10^{-4}\,\mathrm{s}^{-2}$) after 144 h of model integration. Solid blue lines show regions with positive values of the vertical divergence $\partial w/\partial z$ (for $5.0, 50.0 \times 10^{-5}\,\mathrm{s}^{-1}$), dashed blue lines show negative values (for $-5.0, -50.0 \times 10^{-5}\,\mathrm{s}^{-1}$). Red lines show specific cloud ice content q_i (for $5.0, 10.0, \times 10^{-6}\,\mathrm{kg\,kg}^{-1}$). Gray lines show turbulent kinetic energy (TKE) (in $0.5, 1.0, 5.0\,\mathrm{m}^2\mathrm{s}^{-2}$). The four panels show **(a)** BMP TURB, **(b)** BRT, **(c)** BRTC, and **(d)** BRTCS.

~~Zonal cross sections along 45°N of static stability N^2 (in $10^{-4}\,\mathrm{s}^{-2}$) after 144of model integration. Solid blue lines show regions with positive values of the vertical divergence $\partial w/\partial z$ (for $5.0, 50.0 \times 10^{-5}\,\mathrm{s}^{-1}$), dashed blue lines show negative values (for $-5.0, -50.0 \times 10^{-5}\,\mathrm{s}^{-1}$). Red lines show specific cloud ice content q_i (for $5.0, 10.0, \times 10^{-6}\,\mathrm{kg\,kg}^{-1}$). Gray lines show turbulent kinetic energy (TKE) (in $0.5, 1.0, 5.0\,\mathrm{m}^2\mathrm{s}^{-2}$). The four panels show **(a)** BMP TURB, **(b)** BMP RAD TURB, **(c)** BMP RAD TURB CONV, and **(d)** BMP RAD TURB CONV SURF.~~

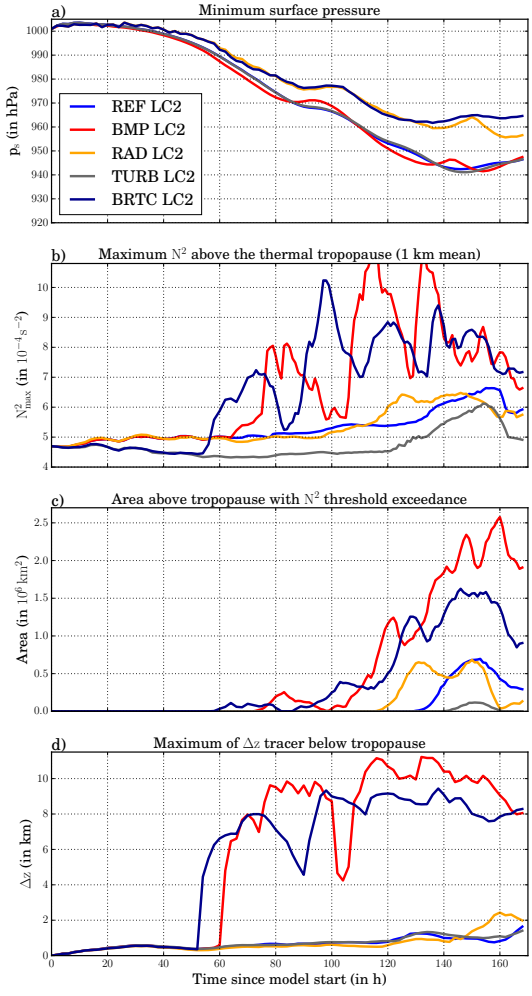

Figure 15. Temporal evolution over the entire simulated life cycles of **(a)** the minimum surface pressure p_s (in hPa), **(b)** the maximum static stability N^2_{max} (in $10^{-4}\,s^{-2}$) above the thermal tropopause, **(c)** the area $A_{5.5}$ (in $10^6\,km^2$) of N^2 threshold exceedance above the thermal tropopause (with a threshold of $N^2 = 5.5 \times 10^{-4}\,s^{-2}$), and **(d)** the maximum of the Δz tracer (in km) in a 500 m thick layer below the thermal tropopause. The colored lines indicate the following simulations: REF LC2 (blue), BMP LC2 (red), RAD LC2 (orange), TURB LC2 (gray), and BRTC LC2 (dark blue).

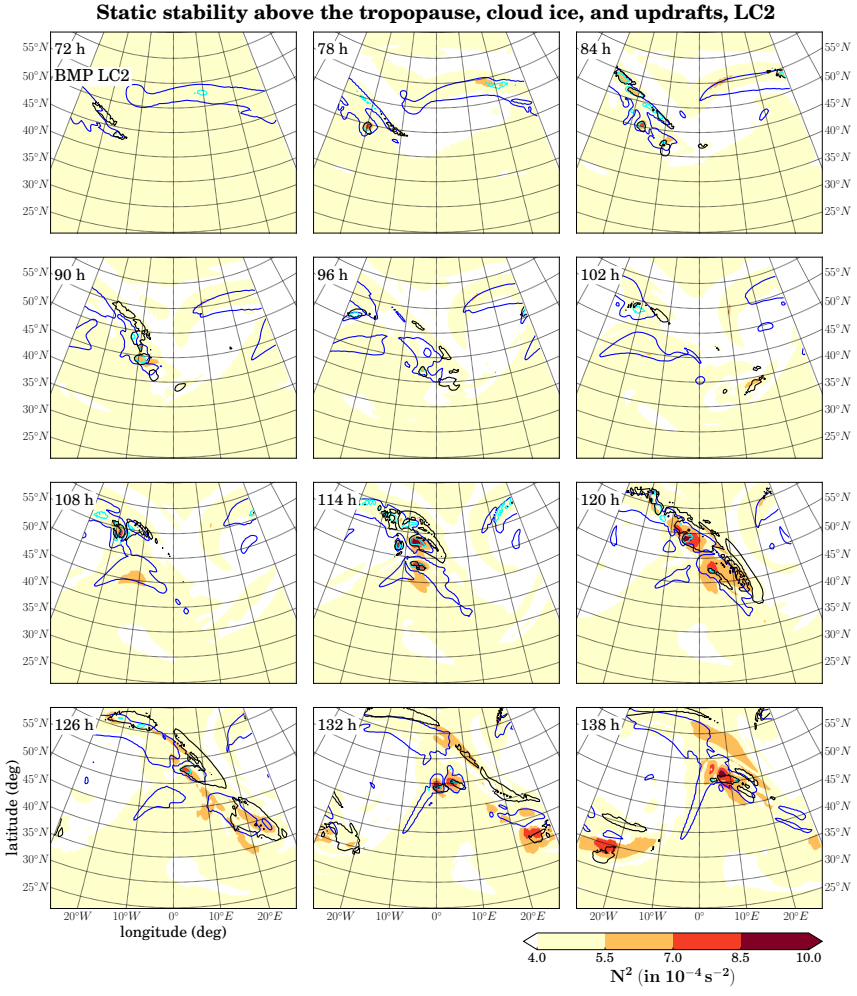

Figure 16. As Figure 9, but for BMP LC2.

Reply to Sebastian Schemm

The authors appreciate the valuable comments on the manuscript which led to a significant improvement. Referee comments are given in bold, the answers in standard font. Changes to the text are in italics.

Generally, we note that we revised most of the figures based on suggestions from the three referees. We also changed some of the acronyms of our experiments. Moreover, we included three more figures (new Figures 9, 15, and 16 in the revised manuscript) and based on questions and comments from Sebastian Schemm and George Craig we included a new section (Section 5 in the revised manuscript) in which results from LC2 experiments are discussed.

General comments
I am confused by the title which suggests that mixing is a process distinct from diabatic processes? If you refer to turbulence I would argue that turbulence is a diabatic process because it is not conserving enthalpy. Do you refer to moist diabatic processes to distinguish it from friction and turbulent mixing?

We agree that turbulence is a diabatic process, since entropy is not conserved, just as with moist or radiative processes. In the initial manuscript we decided to list turbulence separately, since the term diabatic is sometimes used as synonym for moist and/or radiative processes and we wanted to make sure that it is recognized that we also study mixing. However, for the final manuscript we decided to avoid to list turbulence separately when speaking of diabatic processes and changed the text in the revised manuscript accordingly.

The study addresses only life cycles of type LC1. I do recognize that the authors already present numerous simulations and additional simulations might exceed the reasonable amount of presentable material. Nevertheless I argue that any comparisons of the presented findings with measured inversion layers or inversion layers obtain from global climate simulations are hampered, because in reality various types of life cycles may occur (LC2, LC3). In particular the relative importance of dry dynamics and turbulence may vary significantly in a cyclonic life cycle that develops in a cyclonic sheared environment. I therefore highly recommend that the authors include a discussion on this issue and indicate if they think that their findings might significantly differ in a LC2. Such a discussion may build upon the findings presented in Wirth (2003) where different flow regimes (cyclonic/anticyclonic) are discussed. I leave it open for the authors, to perform for example one LC2 of their choice that shows that the findings to not differ significantly and present this as an appendix.

Since a similar request/suggestion is given by G. Craig, we decided to include an entire new section on LC2 (new section 5). The appearance of the TIL is slightly different, in particular it is weaker in LC2 than in LC1 experiments. The processes

that generally lead to the formation of the TIL are the same. Thus, the overall conclusions do not change significantly. Rather the conclusions from studies of dry adiabatic simulations of baroclinic waves (Erler and Wirth, 2011) are confirmed that the TIL appears to be stronger in LC1 cases than in LC2 cases (compare Figure 3 and new Figure 15 in the revised manuscript).

The authors clearly state the overall aim is to rank and identify the processes underlying the formation of the TIL. Given the large number of simulations at hand, I suggest that the author could use this opportunity to broaden the scope of the study. Although I don't want to force my view too strongly on this, I would appreciate to see a discussion relating the presented findings to more general concepts of baroclinic life cycles. The authors could show at which stage of the Shapiro Keyser life cycle the TIL forms, e.g., during frontal fracture? During the T-bone stage? Before or after the wave breaking? This might also include an outlook discussion of potential feedbacks of a strong TIL on the life cycle.
I suppose that enhanced stability above the surface low can alter its circulation (if PV is conserved, vorticity decreases around the TIL because stability gradients increase?). Such a discussion has the potential to broaden the scope of the study and making it of interest to a wider part of the community. At the moment it appears very specific. Such a section can also have a speculative character in which the authors relate their findings more clearly to synoptic-scale or mesoscale characteristics of a cyclone: for example, the conveyor belts, wave breaking or the jet stream. For example, one major finding is the strong relation between the TIL and vertical motion. Is the TIL forming preferentially in the right entrance of the jet streak, which is forming at the tip of the stratospheric trough, or is it the warm conveyor belt outflow or both (From Fig. 8 I think both are true)? Because both are promoting vertical motion. I would appreciate such a discussion at the end of the study, which classifies the findings a little bit more into a conceptual broader framework of cyclonic life cycles.

We generally agree that the simulations conducted for this study do have the potential to discuss more features of baroclinic life cycles and to possibly further relate the TIL to other aspects of the baroclinic waves. The main topic that we wanted to address in this manuscript is the contribution of diabatic processes on the formation of the tropopause inversion layer in baroclinic life cycles. We further link the occurrence of the TIL to specific features of the life cycles. In the dry case we state that the TIL forms after wave breaking (see introduction, page 21498, line 7ff of the discussion paper) as it was also reported by Erler and Wirth (2011). In case with radiation and turbulence this is to a large extent also the case (discussion of Figure 3, page 21507, line 20ff of the discussion paper). Only with moisture we can expect a significant earlier appearance of the TIL, i.e., before wave breaking. We link the TIL evolution to the appearance of the first vertical ascent that reaches up to the tropopause. Along with the discussion around the new Figure 9 this is further related to the warm conveyor belt. Moreover, at the jet exit we also find enhanced values of static stability, which are related to gravity

waves from the jet-front system, at least in our simulations.
The effect of an initially present tropopause inversion layer on the evolution of baroclinic life cycles is topic of another analysis that we are working on. However, the discussion of this topic is sufficient for another manuscript and thus will be addressed in a follow up study in which we will compare the evolution of life cycles with and without an initially present TIL.

The study carefully examines a number of individual processes and their role in the initial formation of the TIL. However I am missing a discussion on the role of advection in all of this. I assume that after the initial formation of the TIL, the air that constituted initially the TIL is advected downstream and weakly stratified air is advected into the area where the TIL initially formed. Advection may explain the observed weakening of the TIL during the life cycle which in the presented version of the manuscript is only partly explained. Differential advection during the life cycle may for example affect the temporal evolution of the vertical profiles of N (Fig.11). In the current version of the manuscript the discussion suggests that the observed differences in the vertical profiles can be attributed to the added process in the numerical simulation. A discussion of the role of differential advection might be important, because the study has not a Lagrangian focus. Advection may play a minor role (see equation in my next comment) in the initial formation of the TIL but may add an important contribution to its temporal evolution and the variations between the model runs because it cannot be assumed to be equally strong in all of the runs.

Following on my comment above regarding the discussion on the role of advection, I would like to propose the authors an additional way of quantifying the role of different physical mechanisms leading to the formation of the TIL. The local tendency of forming a zone of enhanced/reduced static stability (N ~ ∂Θ/∂z), like the TIL, may be understood in terms of the vertical component of the frontogenesis equation. For convenience I write it down below:

$$\frac{\partial}{\partial t}\frac{\partial \Theta}{\partial z} = -\mathbf{u}\cdot\nabla\frac{\partial \Theta}{\partial z} + \frac{\partial}{\partial z}\dot{\Theta} - \left(\frac{\partial u}{\partial z}\frac{\partial \Theta}{\partial x} + \frac{\partial v}{\partial z}\frac{\partial \Theta}{\partial y} + \frac{\partial w}{\partial z}\frac{\partial \Theta}{\partial z}\right)$$

The notation is mostly standard. The first term on the right hand side is the advection, the second term the vertical gradient of diabatic heating and the last term in brackets a collection of some deformation terms and one tilting term (typically the last term is referred to as tilting).
The calculation of all three terms in the TIL region might be straightforward and if you can obtain the diabatic tendency from the different physical parameterization of the model you can even estimate the importance of them individually. If this is not possible you can still estimate a total diabatic tendency to obtain an estimate for the second term on the r.h.s of the equation. I leave it open to the authors to use this equation, but it appears to me an excellent way to quantify the

underlying physical mechanisms forming the TIL.

Since from our point of the view the last two comments are related to one topic, we will address them together in one answer. The role of advection has been studied before in Wirth (2003, 2004), Wirth and Szabo (2007), and in Erler and Wirth (2011). We started our analysis based on the results presented in Erler and Wirth (2011) with the goal to extend their analysis by including diabatic processes in the framework of baroclinic life cycle experiments.
In the current study the focus is on the additional effects from diabatic tendencies. Of course, the advective tendencies also affect our results, which we noted in the manuscript (e.g., in the abstract: *"The effect of individual diabatic processes related to humidity, radiation, and turbulence is studied first to estimate the contribution of each of these processes to the TIL formation in addition to dry dynamics."*). Thus, the role of advection is not neglected, we rather want to focus on the additional effects from the diabatic processes.
In section 3 we explicitly discuss the differences from the diabatic tendencies to the results from the adiabatic life cycle, especially in the discussions around Figures 3-6. We admit that we do not extensively quantify the differences between advection and diabatic processes. However, we think that we included sufficient information in our discussion to show how strong diabatic contributions change the appearance and shape of the TIL in the life cycles. Especially, in Figure 6 some quantitative aspects are shown and are also discussed in the text. Obtaining further quantitative estimates of the individual terms is, however, beyond the scope of the present study.

I am not sure if the timing of the TIL formation is at least partly different between the model runs because the time when the TIL is forming is measured with respect to the start of the model simulation. Since the stage of the life cycles will likely differ between your runs (i.e., frontal fracture occurs after 24 hours of integration in one simulation but after 28 in another simulation), the TIL might form earlier in one case simply because the life cycle is accelerated as a whole. I recommend introducing a relative measure instead of the start of the simulation. For example you additionally show the minimum SLP of your cyclones in Fig3. You could compare the time when the TIL forms relative to the time when the minimum SLP occurs in your runs or when eddy kinetic energy has a maximum in the channel or relative to the strongest deepening rate within a reasonable time window or the occurrence of the first stronger vertical motion. I would argue that we gain a more general view on the formation of the TIL within a baroclinic life cycle if its formation can be related to such a relative measure. It will also allow researchers to compare the formation of the TIL in real case studies to your findings and thereby add an important information to the existing literature.

Since minimum sea level pressure or eddy kinetic energy are commonly used in the analysis of baroclinic life cycles, we started our analysis by comparing these quantities to the evolution of the maximum N^2. However, the link between minimum surface pressure or maximum eddy kinetic energy to the maximum TIL

or first appearance of the TIL were not so significant. As mentioned in the answer to the third comment we related the appearance of the TIL to features of the life cycles (e.g., before/after wave breaking, WCB occurrence). Furthermore, one of the major results is that the Δz-tracer and N^2max correlate well, temporally and spatially (see Figure 9, 10, and 11 in the revised manuscript). If we had used a normalized time axis, with t0 equal the time of first strong increase in Δz, there would have been almost no difference in the timing of first TIL occurrence between the moist life cycles. In the manuscript we wanted to show how the TIL appearance varies when more and more processes are included in the experiments are for this decided to show the temporal evolution relative to the model start.

Comments which the authors may choose to address:

I recommend summarizing your findings in a diagram, which may help readers to further appreciate your work. For example a diagram with two y axes and one x axis, where x shows the type of simulation (or process), y1 shows the onset of the TIL and y2 shows the strength of the TIL. Such a multi-axes figure may also help to simplify some of the current figures.

Generally, we think that summarizing the major findings in one figure is a valuable addition to a manuscript. However, since we already have a large number of figures included in the manuscript (13 in the discussion paper and 16 in the revised manuscript), we omit to include another one. We point out that we already highlighted the major findings in the item section in the conclusion. We also added one more sentence in the final paragraph of the conclusion that summarizes the main results of this study:
"While updrafts are important for the first appearance of the TIL when moisture is included in the baroclinic life cycles, the radiative effects as well as the convergence of the vertical wind are more important in maintaining the TIL during later phases of the life cycles."

Previous studies suggest differences in the character of the TIL during winter and summer seasons. To allow for a simpler comparison with earlier findings the authors may introduce a short discussion whether their TIL relates more to a summer of winter time TIL.

The TIL with the strongest annual cycle is found in polar regions (see Randel et al., 2010). At midlatitudes several processes contribute to the sharpness of the tropopause, i.e., stratospheric dynamics (Birner, 2010), radiative forcing by water vapor (Randel et al., 2007), and also synoptic-scale dynamics (Erler and Wirth, 2011). We study the additional contribution from the synoptic-scale dynamics that could be attributed to diabatic processes, focusing on tropospheric forcings in contrast to diabatic processes in the stratosphere (see Birner, 2010). Including these diabatic processes leads to a stronger TIL than in dry experiments of baroclinic life cycles. Moreover, we conduct simulations over a time period of 168 hours and thus discuss how the static stability changes rather on a synoptic time scale and not on a seasonal time scale. Also we start from a background state

with no TIL. Thus, a fair comparison between the TIL from our experiments and the observed (seasonal) TIL is beyond the scope of this study.

If the TIL forms in an outflow area of the warm conveyor belt, is the TIL destroyed in the area of the dry air intrusion behind the warm sector? Consider speculating on this based on the experience you gained during the analyses. If so this might open new research question left open for an outlook section.

This is correct, the static stability is reduced in this area. This is somehow the opposite from what happens in the region of the warm conveyor belt or any other updraft. Stratospheric air descends into the troposphere and thus the vertical gradient of potential temperature becomes smaller. This then leads to a slightly reduced static stability in this region.

General comments on the formation of the TIL

I am wondering whether the formation of the TIL can be understood in terms of two fluids with different stratifications lying above each other (troposphere and stratosphere).
If vertical motion occurs in the weakly stratified fluid, vertical motion of an individual fluid parcel is damped at the boundary to the strongly stratified fluid and momentum is transferred across the boundary and deformation occurs. Typically we would expect the growth of a deformation zone characterized by enhanced stratification comparable to a collision zone (inelastic collision; the isentropes in the stratosphere are squeezed/pushed together by vertical motion from below; like in a car crash). Is this explaining the correlation between vertical motion and the formation of the TIL (at least for the dry case)? If so I would appreciate if the authors can include such a simplified explanation for the formation of a TIL and have a quick look at deformation.

To illustrate the deformation at the tropopause, we included another version of the new Figure 9 in the revised manuscript here. Instead of drawing an isoline of Δz, we included an isoline for the deformation at the thermal tropopause (Figure A). On a brief glance, Figure A and new Figure 9 do not differ significantly. However, we interpret the deformation, just like the change in static stability, rather as a consequence of the tropospheric forcing, i.e., the updrafts, and not as the initial physical process that leads to the increased stability in the lowermost stratosphere.

Figure A: Static stability (color-coded) above the thermal tropopause, column integrated cloud ice content (blue lines, in 0.01 kg m^{-2}), deformation (black lines, in 15x10^{-5} s^{-1}), and tropopause close column integrated cloud ice content tqi (cyan lines, in 0.001 kg m^{-2}). Tropopause close means the region between the thermal tropopause and 500 m below. The distribution is shown for BMP between 78 h and 138h after simulation start in a six hourly interval.

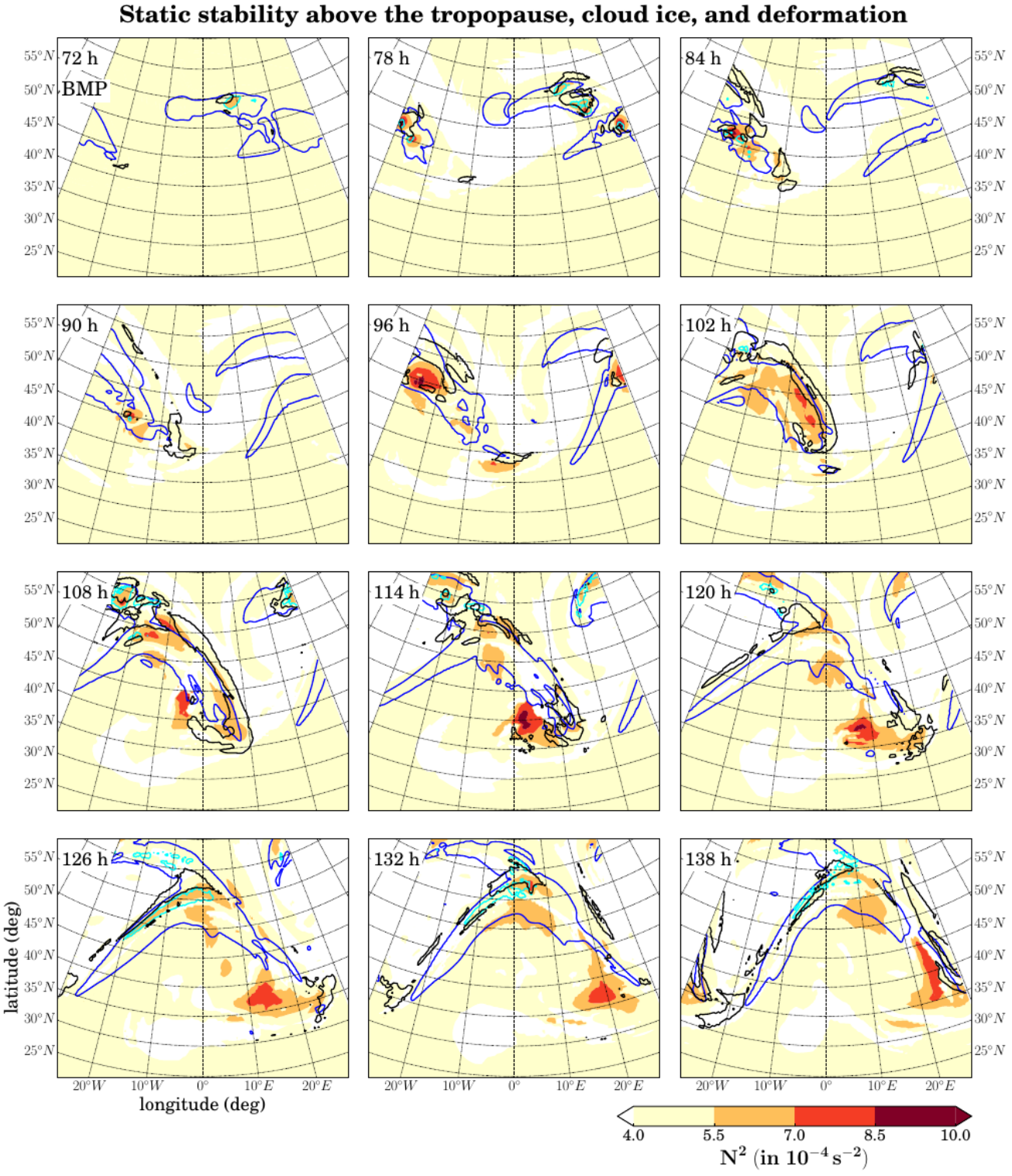

How is the TIL and the presented findings related to the PV dipole that has been described in earlier studies as a consequence of longwave radiation. If the author can relate their findings to this literature they will broaden their study significantly and link it better with the existing literature on diabatic modification of baroclinic life cycles. … Is the TIL distinct from the PV dipoles described in these studies or is it the same phenomena.

As we show in Figure 6c in the manuscript, radiation causes a significant increase in potential vorticity just around the thermal tropopause. The PV dipole discussed for instance in Chagnon et al. (2013) is also caused by radiative processes (longwave cooling). Thus, TIL and PV dipole are most probably related to each other. We included the reference of Chagnon et al. (2013) in our manuscript in the discussion of Figure 6:

"In simulations of real extratropical cyclones over the North Atlantic, the evolution of a dipole structure with a positive PV anomaly above the tropopause and a negative anomaly below have been reported by Chagnon et al. (2013). They could also show that these anomalies are largely related the radiation scheme in their model."

Further comments

Consider increasing the size of figure labels in Fig.8, I even recommend to split it into two different panels. You may also use only one color table and put it vertically to the left/right of the figures, this might help to increase the size of the individual figures.

We did as suggested.

The discussion of Fig.8 is rather limited. There is almost no comment on Fig.8a-e. Consider including a minor discussion on the main differences.

Figure 8 was included in the manuscript to show that the main features of the baroclinic wave (e.g., evolution of a stratospheric streamer, relative position of the trough after 120 h) are rather similar in all simulations. We revised the discussion partly and have now a combined discussion of Figure 8 and the new Figure 9 in the revised manuscript.

Would it be more insightful to show the differences between the individual runs compared to the reference run, instead of absolute fields? For example some interesting differences between the runs in Fig.8 might be masked. Similar for Fig.2.

We decided to show absolute numbers and not differences because there are differences in the simulations and their temporal evolution, thus corresponding stages of the life cycle evolution occur not exactly at the same time. One example is that the trough position is slightly different in all simulations. Showing a

difference plot would result in a strong dipole pattern at the edges of the trough that might mask smaller scale features.

Consider inserting one or two (green) contours of vertical motion in Fig.2 and Fig8. These contours would allow the reader to compare the areas where a TIL forms to the area of strongest vertical motion., which is one of your key findings.

We included the new Figure 9 which shows N^2 at the tropopause as well as contour lines for column integrated cloud ice water content as well as contour lines of the Δz tracer. Furthermore, we show and discuss the spatial link between updrafts and TIL in Figures 10, 12, and 13 (in the revised manuscript Figures 11, 13, and 14).

Consider increasing the size of Fig.11, I had a hard time to visually inspect the figures. For example by splitting it into two figures instead of one panel with a and b. Maybe you can even show all axis labels only in one figure and not in all figures of the panel, this would allow you to move the single figures closer together and to increase the panel as a whole. Consider summarizing the key finding in one sentence in the figure caption.

We changed the figure and hope that it is now easier to read. We will also be in touch with the production office to ensure that the final version of this figure is large enough.

Page 21512, L 11: In the discussion on Fig.9a I recommend to include a statement on the spatial differences. How different is the position of the first occurrence of the TIL and relate it to the difference in the timing of its formation. This might be helpful at this stage (a comment related to my more general comment above).

We hope that Figure 9 gives sufficient proof that there is a strong spatial correlation between the TIL and the first updrafts that reach the tropopause.

Page 21512, L 14: The latest appearance is “when considering cloud processes and turbulence only”, from Fig.9 I would argue that the latest appearance is in BMP (dark blue) and not BMW TURB (light blue).

This statement was thought to distinguish the last time sector from the other two time sectors. The last time sector includes only two simulations, i.e., the one with only cloud processes (BMP) and the one with cloud processes and turbulence (BMP TURB).

Page 21512, L18: “This division into three time sectors...”. How are they defined? t<35h, 35h<t<65h,t>65h? Consider inserting a thick vertical line at these time steps in Fig.9 to highlight the three time periods.

Yes, these are the time sectors which also are mentioned in the two sentences before. For this we do not see the necessity to include more information at this point, also not directly in the figure by additional lines. Nevertheless, we added the following sentences to the Figure caption (Fig.10 in the revised manuscript):
“The time of TIL occurrence is split into three time sectors. Without radiation and convection, the TIL appears after 65 h, with radiation between 50 h-65 h, and with strong convection before 50 h (more information is given in the text).”

Page 21512, L27: "since they foster an earlier emerging of conditional instability”. How do you know that conditional instability is emerging earlier in your life cycle? I am not sure if this statement has been sufficiently shown by the presented analyses. Conditional instability may occur in any of the presented simulations but only with parameterization of moist convection the model is able to release the instability. Without it, the instability needs to grow until resolvable by the large-scale motion.

It is correct, we do not explicitly show the presence of conditional instability. However, we show the consequences, i.e., an increase in the Δz tracer just below the tropopause. Moreover, since we added processes individually, we can link effects from specific processes, e.g., from radiation or convection, to our results. Using this information we came to the conclusion that radiation and convection lead to earlier appearance of vertically ascending air masses and that this is related to their impact on the temperature in the troposphere (e.g., radiation) and/or to the smaller scale on which the scheme operates (e.g., convection). However, since we do not explicitly address conditional instability in our analysis, we rephrased the sentence to:
“since they foster an earlier emerging of updrafts in the model.”

Page 21512, L 27: “This finding supports our results from the previous section that moist dynamics including strong updrafts has a strong impact on the first appearance of the TIL”. Please clarify this statement. Because dry dynamics can also include strong updrafts, I suggest to say: “moist dynamics has a strong impact. . ..because of stronger/increased updrafts compared to a dry run” (or comparable).

We do not show it explicitly for the dry case, but the updrafts are stronger in the moist cases. We rephrase this sentence to:
“This finding supports our results from the previous section that moist dynamics including stronger updrafts than in the dry case has a strong impact on the first appearance of the TIL.”

Page 21513, L15: “Indications of increased static stability are found in all cases above the updrafts which reach the tropopause.” Because we are looking at dry static stability, is this also supporting my deformation-collision argument from above? Would it be possible, and I think this might be novel in the discussion of the TIL, to include a contour of deformation in the discussed figure (Fig.10)?

We refer here to the answer given above on the deformation at the tropopause.

Page 2153, L 28: Consider Wernli and Davies (1997), as main reference if you decide to show only one reference.

We also added Wernli and Davies, 1997.

Page 21514, L 8: “. . .to the domain mean TIL which becomes stronger but also to the fact that the number of model grid cells in...” Why don't you show a more straightforward number such as “(area > 2.5km)/total channel area”? I find the analysis between the two types of N a bit odd. Comparable to the area you discuss on page 21508.

From our point of view the number of grid cells contributing to the average is more straight forward than an area of threshold exceedance. So we directly quantify how many grid boxes contribute to the mean vertical profile which is a valuable information in this case.

First paragraph on page 21514: Although I tend to agree with your discussion, I am wondering to what extend the first contribution of vertical motion to the formation of the TIL is later during the life cycle superseded by advection? Because your are showing vertical profiles which are averaged over the domain, the role of advection of air with high N values in the stratosphere is not clear. Is the region of initial TIL formation unaffected by advection of the strongly stratified air downstream away from its source region and weakly stratified air into the region above the convective cloud?

As stated in the manuscript, the contribution of the vertical motion is reduced later in the life cycle (see discussion about Figure 11 in the discussion paper, page 21514, lines 1-19). At later stages of the life cycle, radiative processes become more important in maintaining the TIL. Moreover, the contributions from large scale convergence discussed in Wirth and Szabo (2007) and Erler and Wirth (2011) as well as potentially small scale features such as gravity waves become more important.

Page 21515, last paragraph: I am wondering why the author do not treat turbulence as a diabatic process. The formulation suggests that it is a distinct process. I think it is a diabatic process because it is not conserving entropy (see below); maybe you refer to moist diabatic process if you refer to condensation/evaporation/ice formation instead?

As stated in the answer to the first comment, we treat turbulence as a diabatic process, however, initially decided to list it separately.

Following on the discussion on turbulence, I am wondering how turbulence is altering the stratification. Is the interpretation of

turbulence as heat flux by Shaprio (1976) a possible explanation? If so, the author may choose to include a short discussion on this into the paragraph.

This is an interesting reference. However, it is not supported by our conclusions. We see rather a decrease in potential vorticity as well as a decrease in stability. This might be a topic that is worth looking into it more in detail in the future.

Comments concerning the conclusion

"showed that there is a correlation between the first appearance of the TIL and of updrafts reaching the tropopause". Is this correlation surprising of given my simplified view on the TIL (presented above) to a little extend an expected result?

It might sound simple and one could have anticipated that this result might be relevant but to the authors' knowledge it has not been shown before explicitly.

Conclusion 5. Strictly speaking this is not shown in the current but in the foregoing study. Consider moving this out of the item environment.

This conclusion is an extension of and link to the results given in Kunkel et al., 2014. Moreover, in the revised manuscript the comparison between LC1 and LC2 showed that gravity waves might be of importance to explain some of the difference of the TIL appearance between these two baroclinic wave types. Thus, we decided to keep this item in the list.

Conclusion 6. I am not sure how to understand this sentence. Consider rewriting it. For example start the second sentence with "Because, clouds ."

We rephrased conclusion 6:
"Finally, updrafts enhance the moisture content of the upper troposphere, not only by transporting water vapor to this altitude. Clouds also form within the updrafts and locally alter the thermal structure of the upper troposphere. Especially, at the top of the clouds a strong cooling can occur which further contributes to the formation and maintenance of a strong TIL. In general, radiative impacts become more relevant during later stages of the life cycle."

Last sentence: "Including the frequency of occurrence of baroclinic waves might further help to . . ." I don not understand what is meant with frequency of occurrence here? Where should it be included? Please clarify this statement.

This sentence refers to the sentence before and simply states that baroclinic waves are found frequently at midlatitudes. We rewrote the sentence:
"Taking into account that baroclinic waves occur relatively frequent at midlatitudes, especially from autumn to spring, might further help to

explain the quasi-permanent appearance of a layer of enhanced static stability."

It would be worthwhile to include a final statement which simulation produces a TIL comparable to the one which is observed.

Since we start from a state without a TIL, such a comparison is difficult to realize. The observed TIL is also affect by other large-scale forcing such as the stratospheric circulation and also by disturbances below the resolved scales of our model. We have shown that by including diabatic processes we at least minimized the discrepancy that has been reported between the TIL from dry baroclinic life cycle experiments and the observed TIL significantly.

Comments related to language/notation

At various places the formulations used in this study suggest that diabatic effects are a mechanism distinct from turbulence. I would argue that turbulence is a diabatic mechanism (process which is not conserving entropy). Consider rewriting throughout.
In addition to the answer to the first comment, we changed the text throughout the manuscript.

P 21500: Consider adding one sentence to explain why the aspect ration of 1/400 is favourable for studies of the TIL.
From simulations of baroclinic life cycles (Erler and Wirth, 2011) and from GCM studies (Birner et al., 2006) it was inferred that this aspect ratio resulted in the most pronounced TIL.

P 21497, L 4: Consider writing N in pressure coordinates, because you speak about the measurement in the following sentence (these are likely taken in pressure coordinates).
We think that the equation for static stability in height based coordinates is sufficient to show here.

P 21496, L 9: "The effect of individual diabatic, i.e. related to humidity and radiation, and turbulent processes is studied first to estimate the additional contribution of these processes to dry dynamics". Consider rewriting for clarity. For example: Firstly, the effect of individual diabatic processes, e.g., radiation, condensation and turbulence, are examined to assess their individual contributions to the formation of the TIL in addition to dry dynamics.

We rephrased the sentence:
"The effect of individual diabatic processes related to humidity, radiation, and turbulence is studied first to estimate the contribution of these processes to the TIL formation in addition to dry dynamics."

Section 2 is written in past tense: "we studied", consider using present

tense throughout.
Thanks for pointing this out. We replaced the few occurrences of past tense in section 2 where it was inappropriate.

References:
Birner, T., Sankey, D., and Shepherd, T. G.: The tropopause inversion layer in models and analyses, Geophys. Res. Lett., 33, L14804, doi:10.1029/2006GL026549, 2006.

Birner, T.: Residual Circulation and Tropopause Structure, J. Atmos. Sci., 67, 2582–2600, doi:10.1175/2010JAS3287.1, 2010.

Chagnon, J. M. Gray, S. L., and Methven, J.: Diabatic processes modifying potential vorticity in a North Atlantic cyclone, Q. J. Roy. Meteor. Soc., 139, 1270–1282, doi:10.1002/qj.2037, 2013.

Erler, A. R. and Wirth, V.: The static stability of the tropopause region in adiabatic baroclinic life cycle experiments, J. Atmos. Sci., 68, 1178–1193, doi:10.1175/2010JAS3694.1, 2011.

Randel, W. J. and Wu, F.: The Polar summer tropopause inversion layer, J. Atmos. Sci., 67, 2572–2581, doi:10.1175/2010JAS3430.1, 2010.

Randel, W. J., Wu, F., and Forster, P.: The extratropical tropopause inversion layer: global observations with GPS data, and a radiative forcing mechanism, J. Atmos. Sci., 64, 4489–4496, doi:10.1175/2007JAS2412.1, 2007.

Wernli, H. and Davies, H. C.: A lagrangian-based analysis of extratropical cyclones. I: The method and some applications, Q. J. Roy. Meteor. Soc., 123, 467–489, doi:10.1002/qj.49712353811, 1997.

Wirth, V.: Static stability in the extratropical tropopause region, J. Atmos. Sci., 60, 1395–1409, doi:10.1175/1520-0469(2003)060<1395:SSITET>2.0.CO;2, 2003.

Wirth, V.: A dynamical mechanism for tropopause sharpening, Meteorol. Z., 13, 477–484, 2004.

Wirth, V. and Szabo, T.: Sharpness of the extratropical tropopause in baroclinic life cycle experiments, Geo. Phys. Res. Let., 34, L02809, doi: 10.1029/2006GL028369, 2007.

Reply to referee George Craig

The authors appreciate the valuable comments on the manuscript which led to a significant improvement. Referee comments are given in bold, the answers in standard font. Changes to the text are in italics.

Generally, we note that we revised most of the figures based on suggestions from the three referees. We also changed some of the acronyms of our experiments. Moreover, we included three more figures (new Figures 9, 15, and 16 in the revised manuscript) and based on questions and comments from Sebastian Schemm and George Craig we included a new section (Section 5 in the revised manuscript) in which results from LC2 experiments are discussed.

Answers to specific comments

In particular whether different vertical ascent patterns in an LC2 case would give different sensitivities, and what would happen in complex developments involving multiple and secondary cyclones which contribute to the global TIL.

Following this comment and a comment by S. Schemm we added a new section on the TIL in LC2 experiments (new Section 5). However, the overall conclusion stay the same, since the results from the LC2 experiments further support those results already presented in the manuscript for LC1. However, the role of gravity waves is discussed a bit more in detail in this context.
The evolution of the TIL in complex situation, especially regarding the maintenance of enhanced static stability as a product of multiple processes is for sure a question of interest and will be addressed in a consecutive study. However, since such analyses require a new design of the experiments, they are beyond the scope of the current study.

l.277. Could you give a definition or reference to the definition of "thermal tropopause". There are so many versions around that I would like to be sure I have the right one.
We follow the definition given in WMO, 1957. The thermal tropopause is defined as the lowest level where the temperature lapse rate falls below 2 K/km and its average between this level and all higher levels within two km above this level remains below this value. We added the description and the reference to the manuscript in Section 2.

l.299-300. The metric for spatial extent of the TIL involves arbitrary thresholds. Has this been used in previous work, and is there a reference that looks at sensitivity to the choices of parameters?
To our knowledge this metric has not been used in other studies. We wanted to have a further metric for the spatial extent of the TIL and not only one for the maximum values. We have chosen the threshold such that it is significantly larger

than the initial maximum value of N^2 in the lower stratosphere. We also tested other (larger) threshold values which showed qualitatively the same results. We added this information to the manuscript.

l.332#. I found this discussion confusing. Comparing Fig. 2 (a) and (d), it looks like the main difference is located at the southern end of the trough, rather than in the WCB outflow as in some of the later experiments, which one would guess would be more related to convection (resolved vertical ascent since the parameterization is not used) than slantwise ascent. The Gutowski reference would be more useful if there was a brief mention of what he said about the two processes.

Figure 2 shows the distributions of N^2 after 120 h. The new Figure 9 in the revised manuscript shows the distribution of static stability N^2 as well as contour lines of the column integrated cloud ice content for the times between 78h and 138h in 6 hourly intervals for BMP. After its first appearance large values of static stability do not only stay directly above the center of the WCB but are also evident in a region south east of the WCB outflow that moves away from the WCB center. In this region the static stability values stay large, although the forcing from below is not evident anymore. As far as we can analyze it is related to an interaction with gravity waves that are present in this region (see also Kunkel et al., 2014). We hope that this new Figure helps to reduce the confusion resulting from Figure 2.

Gutowski et al. (1992) conducted dry and moist baroclinic life cycle experiments. Their analysis showed that the largest effects of condensation are associated with increased vertical transport and that the moist life cycle evolves faster than the dry one due to an increased energy conversion due to stronger vertical motions. We rephrased the according sentence to:
“Our results agree with those obtained by Gutowski et al. (1992). They compared dry and moist baroclinic life cycles and showed that including moisture leads to stronger updrafts as well as to a faster evolution of the life cycle.

Fig.10,13. Why are these not plotted at 120 hrs? I would have liked to compare with Fig.8 (and maybe 12).

Both figures could be plotted at 120 hours and 144 hours, since there is no big difference with respect to the physical interpretation that we wanted to make at this point. Nevertheless, to obtain a better comparability with Figure 8 and 12 we change Fig. 10 and show the same cross sections at 120 hours (new Figure 11 in the revised manuscript). To reduce the redundancy we keep showing Fig. 13 at 144 hrs. For completeness we show Fig. 13 also at 120 hours here (Figure A).

l.565ff. Is it possible to summarize in a couple of sentences what the effect of gravity waves is, or is it sufficiently complex or random that one must read the entire paper?

Gravity waves, in particular inertia-gravity waves (IGWs) with a relatively slow speed of propagation and quasi-horizontal direction of propagation, can potentially break in the region above the tropopause. This is the case, if they modify the background such that Kelvin Helmholtz instability develops which is a sufficient criterion for IGWs to break. Breaking gravity waves can lead to energy transfer to smaller scales as well as to the generation of turbulence. Both the energy transfer and turbulence have impacts on the stratification but are not yet fully quantified. This has been discussed in Kunkel et al. (2014) using model simulations and linear instability theory. Otsuka et al. (2014) and Zhang et al. (2015) also presented analyses that link gravity waves with the tropopause inversion layer.

Typos:
title: ...life cycle experiments...
Corrected.
l.293. spontaneously -> suddenly
Corrected.
l.296 than -> then
Changed to: *“Only after about 130 h after model start N2max in RAD, and a little bit later in REF and TURB, has reached the same magnitude as in the moist simulation.”*
l.511. tenth -> tenths
Changed as suggested.
l.523-525. Sentence fragment
Changed to: *“A life cycle experiment with only dry dynamics served as reference case, while three additional life cycle experiments have been performed with individual non-conservative process added. “*

References:
Gutowski, W. J., Branscome, L. E., and Stewart, D. A.: Life cycles of moist baroclinic eddies, J. Atmos. Sci., 49, 306–319, doi:10.1175/1520-0469(1992)049 <0306:LCOMBE>2.0.CO;2, 1992.

Kunkel, D., Hoor, P., and Wirth, V.: Can inertia-gravity waves persistently alter the tropopause inversion layer?, Geophys. Res. Lett., 41, 7822–7829, doi:10.1002/2014GL061970, 2014.

Otsuka, S., Takeshita, M., and Yoden, S.: A numerical experiment on the formation of the tropopause inversion layer associated with an explosive cyclogenesis: possible role of gravity waves, Progress in Earth and Planetary Science, 1, 19, doi:10.1186/s40645-014-0019-0, 2014.

WMO, Meteorology-a three dimensional science, WMO Bulletin, pp. 134-138, 1957

Zhang, Y. et al.: The Interaction between the Tropopause Inversion Layer and the Inertial Gravity Wave activities revealed by radiosonde observations at a

midlatitude station, J. Geophys. Res. , doi: 10.1002/2015JD023115, 2015.

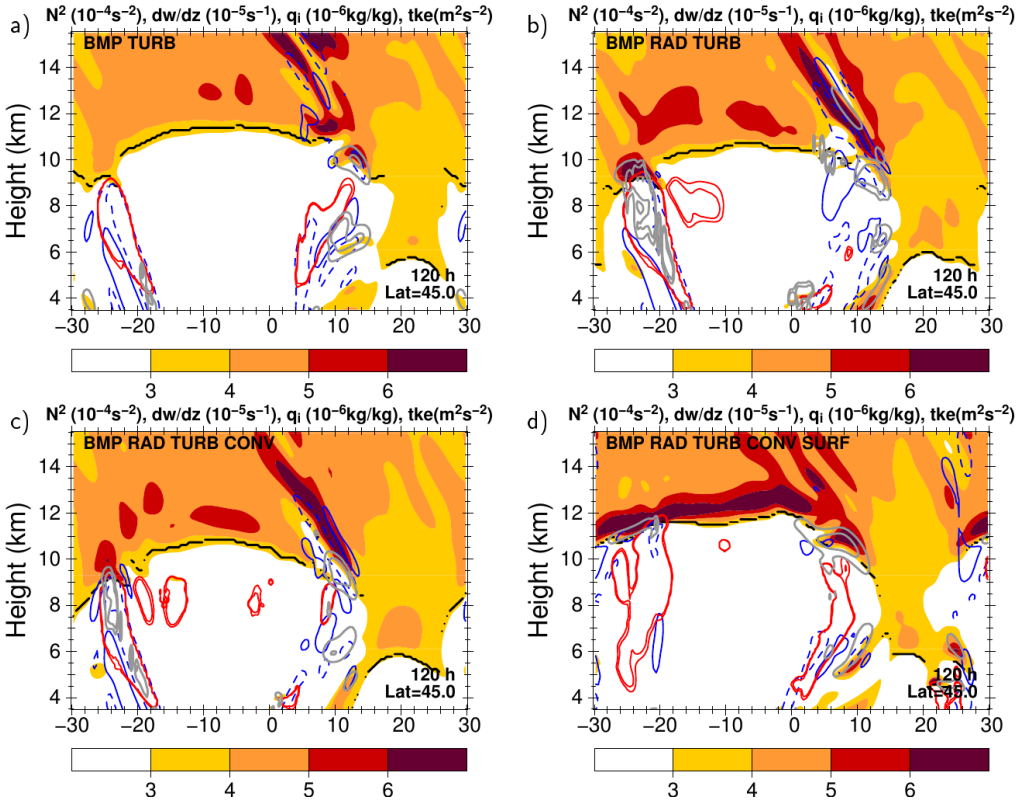

Figure A: As Figure 13 in the manuscript but at 120 h after model start.

Reply to Anonymous referee #3

The authors appreciate the valuable comments on the manuscript which led to a significant improvement. Referee comments are given in bold, the answers in standard font. Changes to the text are in italics.

Generally, we note that we revised most of the figures based on suggestions from the three referees. We also changed some of the acronyms of our experiments. Moreover, we included three more figures (new Figures 9, 15, and 16 in the revised manuscript) and based on questions and comments from Sebastian Schemm and George Craig we included a new section (Section 5 in the revised manuscript) in which results from LC2 experiments are discussed.

Specific comments

In Fig. 6, comparison between RAD and BMP is very interesting. As authors mentioned, both RAD and BMP show large ΔN2 values near the tropopause, while only RAD shows significant PV change near the tropopause. BMP show minimal change in PV, and this strongly supports authors idea that BMP's contribution on ΔN2 is largely due to upward motion (which is likely forced well below the tropopause). Further contrasting the two experiments in the text (around beginning paragraph in P21510) may be beneficial.

We extended the discussion around Fig. 6. Especially, we explicitly note that the altitude of the maximum diabatic PV change is closely related to the altitude where the water vapor gradient changes significantly below and across the tropopause. We further related this PV change to results given in another study (Chagnon et al., 2013) and we explained more specifically why there is hardly a change in PV evident in the domain mean for BMP. This is because in BMP the changes in PV do not occur always at the same altitude relative to the tropopause and occur on relatively small scales. In contrast, in RAD the PV change occurs on larger scales and almost on the same altitude (relative to the tropopause) at the respective time steps.

Related to Fig. 9, the early increase of N2 in BMP RAD TRUB CONV SURF experiment is interesting, but is it only attributable to radiation process? This could also be due to direct effect of enhanced upward motion (mass flux could be interpreted this way too). Could you clarify which one contribute more? If this is not straightforward, mentioning the both possibilities of radiation and updraft (direct effect) may lead the discussion to be a more balanced.

In lines 5-12 on page 21513 of the discussion paper we state that convective processes are most responsible for the earlier increase in N^2 in BMP RAD TURB CONV SURF. This is further supported by Fig. 9e (in the revised manuscript Fig. 10e) where we show the temporal evolution of the cloud base mass flux which serves as an indicator for convective activity.

First paragraph in P21514 (and Fig. 11): The initial importance of updraft and time behavior of TIL seems interesting. However, this paragraph and figures are complex and difficult to understand unless read it several times. For example, Fig 11 has 12 panels, but not all the figures are necessary for the discussion. Further simplification will be helpful for readers (maybe comparison of two contrasting experiments, BMP vs RAD?).

Thanks for pointing this out. We rephrased the corresponding paragraph on page 21514. However, we would like to keep the number of sub-panels for all simulations of the second part of our discussion (section 4). We think the full set of panels is useful for the reader to follow our discussion. We want to point out that the convergence of the vertical wind due to the large scale flow or small scale disturbances is of further importance for the formation and maintenance of the TIL during the life cycles.

Technical comments

P21505 L7: The abbreviation QADI sounds somewhat misleading. Although the saturation adjustment process is the most simple one, it gives enough latent heating as authors shows in Fig. 5b. In that sense, it is far from adiabatic process.
We changed QADI to BMP SATAD.

P21506 L11: BMP, RAD) → '('BMP, RAD) or may rephrase as "we compare results from the first four life cycle experiments (BMP, RAD, TURB, and REF)
We changed the sentence as suggested.

P21509 L7: "which increases the convergence of isentropic surfaces" the vertical gradient of isentropic surfaces"?
We rephrased the sentence to:
“Consequently, also the air above is slightly lifted, thereby increasing the vertical gradient of potential temperature, resulting in enhanced static stability above the tropopause.”

P21509 L12: "Fig.6a and Fig.6b" do not match with Fig. 6; maybe Fig.6 (left panels) and Fig.6 (right panels)?
Correct, changed accordingly to left and right panels.

P21514 L25: feedback feedback → feedback
Corrected as suggested.

P21517 L14: "sharpening" is sometimes used for stronger TIL; this may be misleading. Could you rephrase this?
We removed this part of the sentence.

P21517 L27: relative → relatively
Corrected as suggested.

Table 1: Experiment names are confusing if you break it into two lines. Putting indent for the second line could be helpful.
Thanks for pointing this out. We changed some of the long acronyms and now use shorter ones. In one case two lines where still necessary (BMP RAD NOCRF) where we used an indent at the beginning of the line.

Figure 13: This figures are somewhat redundant. Showing just one good example may be clearer.
The redundancy is reduced by showing Fig. 10 (new Fig. 11) at 120 hrs as suggested by George Craig, so Figure 13 (new Fig. 14) is at least unique at 144 hrs after simulation start. We want to keep the number of sub-panels to show that this feature is not only related to one specific combination of physical processes but always evident when the turbulence parameterization is turned on.

P21524 Fig1 caption: 0.002 is too small, maybe typo?
Correct, this should be 0.02.

References:
Chagnon, J. M. Gray, S. L., and Methven, J.: Diabatic processes modifying potential vorticity in a North Atlantic cyclone, Q. J. Roy. Meteor. Soc., 139, 1270–1282, doi:10.1002/qj.2037, 2013.